Aalborg Universitet

Physical Layer Parameter and Algorithm Study in a Downlink OFDM-LTE Context

Rom, Christian

[Link to publication from Aalborg University](#)

Physical Layer Parameter and Algorithm Study in a Downlink OFDM-LTE Context

Christian Rom

A dissertation accepted by the Faculty of Engineering, Science and Medicine of Aalborg University in fulfilment of the requirements for the degree of Doctor of Philosophy.

AALBORG UNIVERSITY

Radio Access Technology section
Department of Electronic Systems
Aalborg University
Denmark

June 2008

Dedicated to

my beloved parents.

Physical Layer Parameter and Algorithm Study in a Downlink OFDM-LTE Context

Christian Rom

Abstract

This Ph.D. is made in cooperation between Infineon Technologies Denmark, and the Radio Access Technologies (RATE) section at the Department of Electronic Systems. The development of the LTE standard has been based on new increased requirements, with high demands for spectral efficiency, reduced system and terminal complexity, cost and power consumption. This leads to investigate the duality between physical layer parameter and baseband receiver algorithm design in this Ph.D. thesis. More specifically the work has been focused on physical layer parameters and baseband algorithms design for OFDM in a downlink LTE context. The study is based on an accurate baseband matrix-vector model of the received signal. The model is useful to separate two different cases: a Cyclic Prefix (CP) length larger than the radio channel maximum excess delay, and a CP shorter than the maximum excess delay. The LTE baseband parameter design has been investigated with an emphasis on optimal CP length. In the case of a CP length larger than the maximum excess delay, an in-depth survey of linear Pilot Assisted Channel Estimation (PACE) algorithms has been conducted leading to the development of a novel unified modeling for fair comparison of PACE algorithms. The effect of virtual subcarriers as well as non-sample-spaced channel model is studied, showing that DFT based algorithms are only useful at low SNR values, but are subject to the leakage effect as the SNR increases (above 10dB). A clear dependency between a-priori information considered at the receiver and performance is established. To avoid the leakage effect only two algorithm types are useful: robust wiener filters

and interpolators using exact channel tap delay knowledge. A methodology for pilot pattern design has lead to a pilot scheme proposal for the downlink of LTE. Results are characterized without error correction coding in terms of uncoded BER, SINR and mean squared error estimates, and with error correction coding in terms of packet error rate and spectral efficiency. In the case of a CP length shorter than the maximum excess delay, interference cancelation techniques were investigated to cope with insufficient guard interval length, leading to the development of a novel algorithm: the Low-Complex-Interference-Cancelation (LCIC) algorithm.

Overall in this work, it has been shown that signal processing effort spent in the UE can increase the system spectral efficiency. If effort is spent on accurate tap delay estimation, much lower frequency direction pilot spacing can be used. In the same manner, the CP length can be reduced by using the proposed interference cancelation schemes.

Keywords: OFDM, LTE, Cyclic Prefix, Pilot Scheme, Channel Estimation, Interference Cancelation.

Dansk resumé

Dette Ph.D. er blevet udført i samarbejde med et lokalt firma, Infineon Technologies Denmark, og RATE sectionen i Institut for Elektroniske Systemer. Ønsket om at have et mobilt bredbånd som kan suportere stadige forøget data transmissions hastigheder samt øger spektral effektiviteten, har styret telekommunications standarder fra GSM, UMTS, HSPA og nu til den kommende LTE. Denne Ph.D. tese har fokuseret på det fysiske lags parameter design samt baseband algoritme design for OFDM i en downlink LTE kontekst. Studiet er baseret på en njagtig baseband matrix-vektor modelering af det modtaget signal. Parameter design er blevet undersøgt med speciel fokus på den optimale CP længde og pilot skema design. En dybdegående nutidig undersøgelse af kanal estimerings algoritmer er blevet udført og munder ud i udviklingen af en ny entydig modellering for at kunne udføre en fair sammenligning af kanal estimerings algoritmer. En klar afhængighed mellem a-prori information antaget i modtageren og performance er etableret. Til slut, undersøges interferens ophævelses tekniker for at kunne klare korte CP længder. En ny algoritme er udviklet: LCIC. Overordnet set, er det blevet påvist at digital signal processering i UE kan øge system spektral effektivitet. Hvis processerings kraft bliver brugt på nøjagtig estimering af tap forsinkelser kan der bruges væsentlig mindre pilot frekvens mellememrum. På samme måde, kan CP længden reduceres ved at udføre smart interferens ophævelses tekniker.

Declaration

The work in this thesis is based on research carried out at the "Institut for Elektroniske Systemer" at Aalborg University, in the Radio Access Technology (RATE) section, Denmark. No part of this thesis has been submitted elsewhere for any other degree or qualification. Some of the the work carried out is based on joint research. The parts with joint effort will be specified out. A large Link Level matlab based simulator was developed together with my fellow Ph.D. students: Na Wei, Akhilesh Pokhariyal and Basuki E. Priyanto. The work conducted in channel estimation has been largely carried out in cooperation with my former student and now colleague Carles Navarro Manchón, same goes for the work on interference cancelation carried out with my other former student and now colleague Guillaume Monghal.

Acknowledgements

Notation and Abbreviations

Scalar Symbols

α_{tti}: number of OFDM symbols in a TTI block

α_{ceb}: number of OFDM symbols in a channel estimation block

N_t: Number of CIR taps

N_g: number of samples for the CP

N_u: number of Used (active) subcarriers

N_{fft}: number of input and output samples of the transmitter FFT

N_{ofdm}: number of samples per OFDM symbol including the CP

N_p: number of pilots subcarriers

$N_{o,slot}$: number of OFDM symbols per slot

$N_{o,sec}$: number of OFDM symbols per second

α_f: the number of OFDM symbols in a frame

P_{ceb} number of pilots in 1 CEB

k_{mod}: number of bits per data symbol

s: outer iteration index

$\mathbf{S}$: maximal number of outer iterations

t: continuous time index

f: continuous frequency index

n: sample index

Δ_f: subcarrier spacing

k: subcarrier index

m: OFDM symbol index

T_g: Cyclic Prefix duration

T_{med}: maximum Excess Delay duration

T_u: duration of basic OFDM symbol without CP

T_{ofdm}: OFDM symbol duration with CP

T_f: LTE Frame duration

T_{slot}: LTE Slot duration

T_s: receiver sample time

f_k: baseband frequency of subcarrier k

F_s: baseband sampling frequency

$\mathbf{l}_{m,p}[n]$: n^{th} sample of the time varying CIR at the mth transmitted OFDM symbol

V : velocity

$g(t, \tau)$: continuous complex baseband CIR

$\alpha_i(t)$: time variant attenuation factor of the ith CIR tap

$\tau_i(t)$: time variant i^{th} CIR tap propagation delay

$\theta_i(t)$: time variant phase value of the ith CIR tap

f_c : Tx signal carrier frequency

r_g : ACF of CIR

r_h : Spaced-time spaced-frequency correlation function

S_h : Fourier Transform of the CIR ACF

t_{cor} : Coherence time

$(\Delta f)_c$: Coherence bandwidth

B_D : Doppler spread

f_d : Doppler frequency

C: bias function for SINR evaluation

N_p: number of pilots in 1 OFDM symbol with pilot information

N_e: number of Eigenvalues

L_{total}: performance loss in dB differing from the optimal receiver

L_{pilot}: performance loss in dB due to pilot overhead

L_{algo}: performance loss in dB due to channel estimation error

L_{ici}: performance loss in dB due to ICI from doppler distortion

b_i: LCIC matrix-row band index

$\mathbf{I}$: LCIC band Length

Vectors

b: data bits

d: transmitted data symbol

s: conceptual transmitted time OFDM signal

s: baseband transmitted OFDM signal

$\mathbf{s}_m$: m^{th} baseband transmitted OFDM signal

ψ_k: orthogonality function of subcarrier k

r: received signal on TTI level

$\mathbf{r}_m$: received signal on OFDM symbol level

w: AWGN on TTI level

$\mathbf{w}_m$: AWGN on OFDM symbol level

g: sample spaced CIR vector

$\mathbf{g}_m$: sample spaced CIR for the mth OFDM symbol

h: channel transfer function vector

$\mathbf{h}_m$: channel transfer function vector for the mth OFDM symbol

g : non sample spaced CIR vector **d**: data symbol vector on TTI level

$\mathbf{d}_m$: data symbol vector for the mth OFDM symbol

z: received signal after FFT on TTI level

$\mathbf{z}_m$: received signal after FFT on OFDM symbol level

y: received signal after channel CTF matching on TTI level

$\mathbf{y}_m$: received signal after channel CTF matching on OFDM symbol level

$\mathbf{g}_m$: CIR vector assumed constant during transmission of 1 OFDM symbol

Matrices

$\mathbf{\Psi}$: IDFT and CP matrix on TTI level

$\mathbf{\Psi}_m$: IDFT and CP matrix for the mth OFDM symbol

H: channel convolution matrix on TTI level

H0: channel convolution matrix on OFDM symbol level generating ICI

H1: channel convolution matrix on OFDM symbol level generating ISI

$\mathbf{R_{xx}}$: autocorrelation matrix of vector $\mathbf{x}$

$\mathbf{C0}_m$: ISI matrix

$\mathbf{C1}_m$: CTF + ICI matrix

F: DFT matrix

I: identity matrix

C : Wiener filter matrix

D: transmitted symbols matrix

Mathematical Notation

The notations used throughout this paper are:

$\forall$	:	for all
$\in$	:	membership
$(\cdot)^*$	:	complex conjugate
$(\cdot)^H$	:	hermitian transpose of a matrix or vector
$|\cdot|$	:	absolute value
$\lceil\cdot\rceil$	:	lowest integer value which is not smaller
		than the argument
$\lfloor\cdot\rfloor$	:	rounds the argument to the nearest integer
		greater than or equal to the argument
$\mathrm{tr}\{\cdot\}$	:	trace operator
$\mathbf{diag}\{\mathbf{x}\}$	:	diagonal matrix with elements of $\mathbf{x}$ in the diagonal
$\mathrm{E}\{\cdot\}$	:	expectation operator
$\mathcal{F}\{\cdot\}$	:	Fourier transform operator
$csgn\{\cdot\}$	:	symbol hard decision operator
$\Longleftrightarrow$	:	equivalence
$\gg$	:	much larger that
$\ll$	:	much lower that
$\mathbf{x}[k]$	:	the kth element of a vector $\mathbf{x}$
$\mathbf{X}[n,k]$	:	the nth row and k^{th} column element of
		matrix $\mathbf{X}$
$\hat{\mathbf{x}}$	:	estimate of $\mathbf{x}$
$\mathbb{N}$	:	natural numbers
$\mathbb{Z}$	:	integer numbers
$\mathbb{C}$	:	complex numbers

Bold upper-case letters are used for matrices and bold lower-case letters are used for vectors.

June 18, 2008

Abbreviations

3GPP	:	third Generation Partnership Project
ACF	:	Auto-Correlation Function of the CIR
ACK	:	Acknowledgement
ARQ	:	Automatic Repeat-request
AWGN	:	Additive White Gaussian Noise
BS	:	Base Station
BER	:	Bit Error Rate
BLAST	:	Bell Labs Layered Space-Time
CP	:	Cyclic Prefix
CMAC	:	Complex Multiply Accumulate
CEB	:	Channel Estimation Block
CIR	:	Channel Impulse Response
CRC	:	Cyclic Redundancy Check
CQI	:	Channel Quality Indicator
DDA	:	Decision Directed Algorithm
DDCE	:	Decision Directed Channel Estimation
DL	:	Downlink
DTX	:	Discontinuous packet Transmission
DVB-H	:	Digital Video Broadcast Handheld
DVB-T	:	Digital Video Broadcast Terrestrial
ECR	:	Effective Code Rate
EDGE	:	Enhanced Data Rates for GSM Evolution
EGC	:	Equal Gain Combining
FDD	:	Frequency Division Duplex
FDLA	:	Frequency Division Link Adaptation
FDM	:	Frequency Division Multiplexing
FEC	:	Forward Error Correcting Codes
FFT	:	Fast Fourier Transform
GSM	:	Global System for Mobile communications

GPRS	:	General Packet Radio Service
HARQ	:	Hybrid Automatic Repeat-request
HSDPA	:	High-Speed Downlink Packet Access
HSUPA	:	High-Speed Uplink Packet Access
ICI	:	Inter Carrier Interference
IC	:	Interference Cancelation
IR	:	Incremental Redundancy
ISI	:	Inter Symbol Interference
ISDB	:	Integrated Services Digital Broadcasting
LCIC	:	Low Complexity Interference Cancelation (scheme)
LE	:	Linear Equalizer
LS	:	Least Squares
LTE	:	Long Term Evolution
MCS	:	Modulation and Coding Set
MBMS	:	Multimedia Broadcast Messaging Service
MBWA	:	Mobile Broadband Wireless Access
MED	:	Maximum Excess Delay
MMSE	:	Minimum Mean Square Error
MRC	:	Maximum Ratio Combining
MS	:	Mobile Station
NACK	:	Negative Acknowledgement
OFDM	:	Orthogonal Frequency Division Multiplexing
OFDMA	:	Orthogonal Frequency Division Multiplexing Access
PSAM	:	Pilot Symbol-Assisted Modulation
PACE	:	Pilot Assisted Channel Estimation
PDP	:	Power Delay Profile
QAM	:	Quadrature Amplitude Modulation
QPSK	:	Quadrature Phase Shift Keying
RATE	:	Radio Access Technologies (section at AAU)

RAT	:	Radio Access Technology
RRM	:	Radio Resource Management
RU	:	Resource Unit
SAW	:	Stop and Wait
SEL	:	Spectral Efficiency Loss
SISO	:	Single Input Single Output
SFC	:	Space Frequency Coding
SFN	:	Single Frequency Network
STE	:	Single Tap Equalizer
TDD	:	Time Division Duplex
TFRC	:	Transport Format and Resource Combination
T-DMB	:	Terrestrial Digital Multimedia Broadcasting
UMTS	:	Universal Mobile Telecommunications System
UTRA	:	UMTS Terrestrial Radio Access
UE	:	User Equipment
UTRA	:	UMTS Terrestrial Radio Access
UTRAN	:	UMTS Terrestrial Radio Access Network
WCDMA	:	Wideband Code Division Multiple Access
WiMAX	:	Worldwide Interoperability for Microwave Access
WLAN	:	Wireless Local Area Network
WSS	:	Wide Sense Stationary

Contents

List of Figures

List of Tables

Chapter 1

Introduction

1.1 Background

Many different wireless technologies exist on the market or are planned to be rolled out within the next years. One can distinguish roughly between "mobile" and "static/nomadic" wireless technologies, where the main difference is that the latter doesn't support handover between access points. The second generation (2G) and third generation (3G) of mobile phones support "mobility", whereas the "nomadic" technologies are more oriented towards providing broadband packet-data access, such as fixed Wimax 802.16-2004 [14]. Yet the "nomadic" technologies are outside the scope of this work. The "mobile" 2G technologies such as GSM, GPRS and EDGE are giving theoretical downlink peak data rates of respectively 9,6 kbit/s, 80 kbit/s and 236,8 kbit/s, whereas the "mobile" 3G technologies such as WCDMA and HSDPA are giving theoretical downlink peak data rates of respectively 384 kbit/s and 14,4 Mbit/s. These will potentially go up to 42 Mbit/s with the second phase of HSDPA (HSPA Evolved) being specified in the upcoming 3GPP release 7. In a longer time frame perspective a fourth generation (4G) of mobile phones will arise. This 4G is officially not defined, but is estimated to become a high data rate technology supporting inter-Radio Access Technology (inter-RAT) handover with more than 100 Mbit/s for outdoor and 1 Gbit/s for indoor downlink data rates. In Figure 1.1 an overview over the different wireless technologies, existing and planned, is given. The different 2G and 3G wireless technologies can be situated. Combining

mobility with high data rates seems to be a great challenge for the evolution of the different standards. 4G is in this figure a future standard that will meet this challenge.
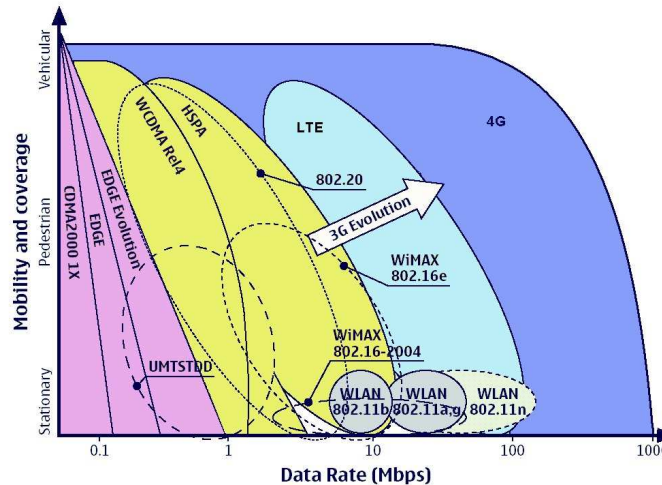
Figure 1.1: Throughput that can be delivered by the different wireless standards

With the latest 3GPP standards such as HSDPA and HSDPA, the radio-access technology will be competitive for several years. However with upcoming standards such as mobile Wimax 802.16e-2005 [15] and to ensure long term competitiveness for 10 years and beyond, a Long-Term Evolution (LTE) of the 3GPP Radio Access Network (RAN) has been considered. LTE will be the bridge technology allowing to evolve towards a 4th Generation of mobiles. The LTE standardization work has been developed in the mindset of meeting a set of initial requirements from [2]. They emphasize the need for signalling reduction thereby reducing the number of physical layer settings. Also spectrum efficiency is to be improved significantly, as well system and terminal complexity, cost and power consumption to be reduced. Different UE "types/capabilities" shall be used to capture different complexities versus performance tradeoffs. From these requirements a good tradeoff in the design of system parameters and the receiver algorithms must be found.

On one hand a general trend of wireless technologies is that they tend to support higher peak and average data rates for the User Equipment (UE). On the other hand the evolution of CPU speed has been roughly following Moore's Law. This law states that the number of transistors that can be stored in a Integrated Circuit

for minimum component cost doubles every 24 months [17]. However the size of a single transistor can't be reduced indefinitely, and will be limited by the atomic size of approximately 0,1 nm. Moore's Law is therefore bound to break and CPU speed evolution will slow down. As the need for higher transmission data rates doesn't seem to slow down, and with the growth of CPU speed slowing down, the need for efficient baseband signal processing algorithms will strongly increase.

After considering the trends of the LTE requirements and the evolution of Moore's law, a key aspect of this thesis will be how to design new system parameters and receiver algorithms in a way that requirements are fulfilled and receivers feasible.

1.2   Purpose of LTE

3GPP LTE is the name of a project within the 3GPP which aim is to enhance the UMTS standard and to deal with future requirements. These future requirements will need improvements of several key areas such as: efficiency, operator costs, better and new services, usage of available spectrums and better integration with other standards and will result in release 8 of the 3GPP standards. When presenting LTE a broad question arises: "What is the purpose of LTE?".

In this section we will attempt to answer to this question without too many technical details. The purpose of LTE is to develop a set of specifications that will be the basis of a framework for the evolution of the 3GPP radio-access technology. These should allow a high data rate, low latency and packet optimized radio access technology. In the following, the different goals of LTE relevant to this Ph.D. thesis will be listed:

- **Flexible/scalable transmission bandwidth**. It will go from 1,25 MHz up to 20 MHz in order to allow a flexible technology cohabitation with other standards. This will imply that the different algorithms should be flexible, adaptive and optimized for the different proposed bandwidths.

- **High peak data rates: 100 Mbps in downlink**. In this case it will require low complexity algorithms as the available computational complexity at the

UE per received bit will be low.

- **Increased cell edge bitrate maintaining site locations as in WCDMA**. This will be a vital consideration for the operator. There is no interest in increasing the amount of expensive base stations to cover a given area.

- **Improved spectrum efficiency**. The improvement should be of 2 to 4 times the one of Release 6 HSPA. Higher order modulation schemes (16QAM and 64QAM) as well as spatial multiplexing MIMO are required to achieve these requirements.

- **Reduced Radio-access network latency**. Possibility of latency below 10 ms. When looking at the physical layer, this goal has influence on the available estimation and data detection time, setting some tight requirements for algorithm implementation.

- **Reasonable system and terminal complexity, cost and power consumption**. This will result in many tradeoff decisions when looking at the parameter design and algorithmic choices to be made.

- **System optimized for low mobile speed but should also support high mobile speeds**. For a slowly fading radio channel the performance should be maximized without penalizing the functionality at high speeds.

1.3 Goals and Limitations

1.3.1 Goals

The goals of this Ph.D. thesis are set within the context of a "generic OFDM baseband model" with application to a " specific LTE scenario". In this way the analytical results can be extended to other OFDM based systems, and the practical results will show the applicability of the generic models and solutions to LTE. The goals of this thesis are several. First the impact of key physical layer parameters on system performance should be studied namely the CP length and the pilot scheme design.

Secondly the impact of these key parameter on receiver algorithm design should be investigated in several channel scenarios.

In order to achieve these goals several steps need to be carried out, among which are careful system modeling, simulator development, realistic simulations as well as algorithm investigation. To achieve the desired goals, each of the above steps are guided by key questions in the following.

First, within an analytical context, we would like to know "what is a good choice of OFDM baseband matrix-vector model?" More specifically the mathematical assumptions behind the modeling should be elaborated. From these assumptions a generic discrete model should be derived describing the baseband signal from the point of transmission until reception, including the effects of the multipath channel and gaussian noise.

When these models are established, the simulation context should be elaborated starting with understanding "how have the key OFDM physical layer parameters have been chosen in LTE?". A simulator environment supporting the 3GPP LTE parameters should be developed. This will enable us to answer to " what will the baseline LTE performance be in terms of Spectral Efficiency?"

The analytical modeling as well a performance of an OFDM system strongly depends on the physical channels models considered, as well as the length of the Cyclic Prefix. Therefore before undergoing an in depth algorithmic study in this thesis, we will try to answer "how shall the Cyclic Prefix length be chosen?". This will present an interesting tradeoff between transmission overhead and multi-path robustness.

Once the modeling and the simulation scene is established, the in depth algorithmic study can follow. When dealing with PACE and the classical signal model, we would like to know "how performance is affected by different OFDM channel estimation algorithms? What will be the most efficient tradeoffs between these algorithms in a LTE-OFDM context?". The scope of this study will be focused on linear algorithms. The introduction of virtual subcarriers as well as the leakage effect, due to non-sample-spaced PDP, is considered in an algorithm comparison. From performance results as well as a complexity study, solutions for practical implementation

will be suggested for LTE.

A choice of channel estimation algorithms will then set the baseline to determine "how the pilot scheme and spacing shall be chosen for LTE?" Time and frequency direction pilot spacing will be considered. Theoretical results derived from the Nyquist sampling theorem will be compared to practical performance results.

Considering the advanced novel signal model, we will then study "what is the effect of a longer impulse response than the CP length on Spectral Efficiency and how well can interference cancelation compensate for a short CP length?". When the CIR is longer than the CP the classical OFDM signal model is no longer accurate and the one tap equalizer is insufficient. Usage of classical Multiuser Detection (MUD) algorithms such as the Zero Forcer (ZF) or Minimum Mean Square Error (MMSE) approaches are computationally prohibitive. Therefore the special case of OFDM with Inter Carrier Interference (ICI) and Inter Symbol Interference (ISI), will be studied carefully and the equalization process will be enhanced with specific interference cancelation schemes.

1.3.2 Limitations

To narrow down the scope of the thesis and in order to focus in depth on the given topics, a few limitations have been established for the given work. They are given by:

- Performance evaluation will mainly be carried out using the downlink LTE settings given by the frame structure type 1 in FDD mode defined in 3GPP TS 36.211 [3].

- The focus of this thesis limits the study to FDD where all subframes are available for downlink transmission.

- Specific channel power delay profiles defined in the appendix A will be used for monte-carlo simulations.

- Single Input Single Output (SISO) antenna constellation is considered in all chapters.

- The modeling assumes perfect synchronization or the received signal in time and frequency domains.

- The PACE algorithms studied assume a Cyclic Prefix (CP) length longer than the maximum excess delay of the PDP and and a constant channel during the duration of 1 OFDM symbol

- The performance results are all single user results assuming one user having full usage of all downlink bandwidth available. Thereby no OFDMA or resource sharing is considered.

1.4 Methodology

During this thesis a pragmatic methodology has been adopted in order to achieve the goals. The strategy behind attacking the different posed problems has been based on an iterative approach. The methodology adopted can be summarized in the following order:

1. A state of the art is established from an extensive survey in the field of investigation.

2. The assumptions and limitations of the problems are clearly stated.

3. A mathematical matrix-vector model of the received OFDM signal is derived with the desired level of modeling detail.

4. A performance study of state of the art solutions is conducted within the area chosen.

5. A solution or new improved scheme is proposed.

6. A performance comparison of the proposed solution is carried out with the state of the art reference(s).

This process can then be iterated increasing the level of detail of the OFDM received signal model or changing the initial assumptions. Thereby the experience acquired during the first iteration can be used to refine the second iteration.

1.5 Outline and Organization of the Thesis

This thesis consists of 9 chapters and 3 appendices. The two main topics dealt with are parameter design and algorithm investigation. As these two topics depend on each other, and, at the same time are strongly influenced by the LTE system requirements, they are dealt with in an alternate order.

Chapter 1 gives an introduction to the thesis consisting of several sub-topics. A general technical background of the content, relevant LTE 3GPP specifications, goals and limitations will help in defining the thesis with a given scope and aim. A stress on the methodology used is followed by an outline, a list of publications and a list of inventions filed during this thesis.

Chapter 2 mainly covers OFDM basics, as well as an in depth modeling of the signal from transmitter to receiver side. The modeling work ends up with two relevant signal models: A classical, well known interference-free model, and a novel generic advanced model taking ISI an ICI into consideration.

Chapter 3 describes the two simulators developed during this work. The first simulator focuses on delivering quick simulations results as it doesn't have any outer receiver features such as error control coding. This first simulator will give MSE, uncoded BER and SINR results. The author has developed the core of this simulator, namely the Tx/Rx modules, the channel models and convolution. Much effort has also been spent on receiver algorithms and parameter design together with the authors former Master students Guillaume Monghal and Carles Navarro Manchón as illustrated in their respective master thesis [51] and [52]. A second link level UTRA-LTE simulator has been developed jointly with other Ph.D. students: W. Na, A. Pokhariyal and B.E. Prianto. Basic performance in terms of spectral efficiency of different modulation schemes is carried out in a 10MHz scenario. Validation of both simulators is given in appendix B.

Chapter 4 is an independent CP length study aimed at an LTE configuration. The dual nature of the CP (cancels interference but introduces system overhead) is discussed and the optimal CP length is elaborated for different channel and parameter conditions.

Chapter 5 presents the Pilot Assisted Channel Estimation (PACE) problematic

for OFDM. The nature and statistics of the radio channel are discussed and a channel estimation strategy proposed for LTE. This strategy will guide the structure and content of chapter 6 and of chapter 7.

Chapter 6 is the most extensive of this thesis and focuses on frequency direction PACE for OFDM. An extensive state-of-art is made from previous research. The lacks of previous comparisons are stressed and a generic unified formulation is developed to conduct a novel fair comparison of algorithms. Results show a clear relationship between a-priori information considered at the Rx side, and the performance obtained. Two algorithms are recommended for LTE: the robust wiener filter [78] and the true parametric wiener filter [75].

Chapter 7 investigates different pilot patterns and pilot densities for LTE. From the PACE strategy defined in chapter 5 a pilot spacing design method is proposed to determine which efficient scheme to be used in LTE.

Chapter 8 proposes to shorten the CP length used in OFDM by means of optimized interference cancelation techniques. A iterative, reduced complexity algorithm with fast convergence rate and tractable complexity is developed: the LCIC algorithm.

Chapter 9 concludes the thesis work and elaborates on possible future research topics.

1.6   Publications and Invention disclosures

The following articles have been published during the Ph.D. study:

- C. Rom, T.B. Sørensen, P.E. Mogensen and B. Vejlgaard, "Impact of Cyclic Prefix length on OFDM system Capacity", *Proceedings of the WPMC'05* Vol.3, pp. 1871-1875, 18-22 September 2005

- C. Rom, C. N. Manchón, T.B. Sørensen, P.E. Mogensen and Luc Deneire, "Analysis of Time and Frequency Domain PACE Algorithms for OFDM with Virtual Subcarriers" *Personal, Indoor and Mobile Radio Communications, 2007 IEEE 18th International Symposium* Sept. 2007 Pages: 1-5

- C. Rom, C. N. Manchón, T.B. Sørensen, P.E. Mogensen and Luc Deneire, "Unification of Frequency direction Pilot-symbol Aided Channel Estimation (PACE) for OFDM," *10th International Symposium on Wireless Personal Multimedia Communications* Vol.XX, pp. xxxx-xxxx, 03-06 September 2007

- G. Monghal, Y. Malidor, C. Rom and T.B. Sørensen, "Low Complexity Interference Cancellation applicable to OFDM with a Short Cyclic Prefix", *Proceedings of the WPMC'05* Vol.2, pp. 1032-1035, 18-22 September 2005

- A. Veiverys, V.P. Goluguri, Y. Le Moullec, C. Rom, O. Olsen, P. Koch, "A Generic Hardware-Accelerated OFDM System Simulator", IEEE Norchip 2005, 21-22 November 2005, Oulu, Finland

- B.E. Priyanto, C. Rom, C.N. Manchón, T.B. Sørensen, P.E. Mogensen, "Effect of Phase Noise on Spectral Efficiency for UTRA Long Term Evolution" *Personal, Indoor and Mobile Radio Communications, 2006 IEEE 17th International Symposium* Sept. 2006 Pages:1 - 5

- N. Wei, A. Pokhariyal, C. Rom, B.E. Priyanto, F. Frederiksen, C. Rosa, T.B. Sørensen, T. Kolding and P.E. Mogensen, "Baseline E-UTRA Downlink Spectral Efficiency Evaluation" *Proceedings of 2006 IEEE 64th Vehicular Technology Conference* 2006

The following inventions have been submitted to Infineon Technologies during the Ph.D. study:

- Low Complexity Interference Cancellation scheme for Orthogonal Frequency Division Multiplexing receivers, April 2005

- Aufwandsgüstige Kanalschätzung mit hoher Güte für Merhträgerfunksysteme (OFDM), April 2006

- Wireless communications system using pre-equalisation based on terminal location estimates, June 2006

- Threshold-Based Channel Tracking for Enhanced Noise Reduction in OFDM, July 2006, accepted for Patent

June 18, 2008

Chapter 2

OFDM modelling

OFDM (Orthogonal Frequency Division Multiplexing) has shown many interesting properties for wireless data transmission such as spectral efficiency, low complex transceivers and robustness over time dispersive channels. Also, OFDM has been chosen to be the downlink multiple access scheme in LTE. The purpose of this chapter is to give some general information regarding OFDM basics, including its definition, signal generation, CP insertion, parameter relationships, reception and signal properties and the advantages and disadvantages of this modulation scheme. A generic discrete matrix-vector analytical model of the received signal will be derived, which can be simplified into the classical model used for PACE OFDM.

2.1 OFDM basics

OFDM is a technology that has been shown to be well suited to the mobile radio environment for high rate and multimedia services. A worldwide convergence has occurred and OFDM has appeared as an emerging technology in many standards. Examples of commercial OFDM systems include WLANs such as the 802.11a/g [8] [9] [10] amendment to Wi-Fi, Digital Audio Broadcast (DAB) systems [11], Digital Video Broadcast TV systems such as DVB-T [12], DVB-H [13], T-DMB and ISDB-T, the IEEE 802.16 WiMAX Wireless MAN [14] [15], the IEEE 802.20 or Mobile Broadband Wireless Access (MBWA) system and the Flash-OFDM system. Much research has been done in the field of OFDM based physical layer [18] [19] [20], and

it can be classified as a mature research topic.
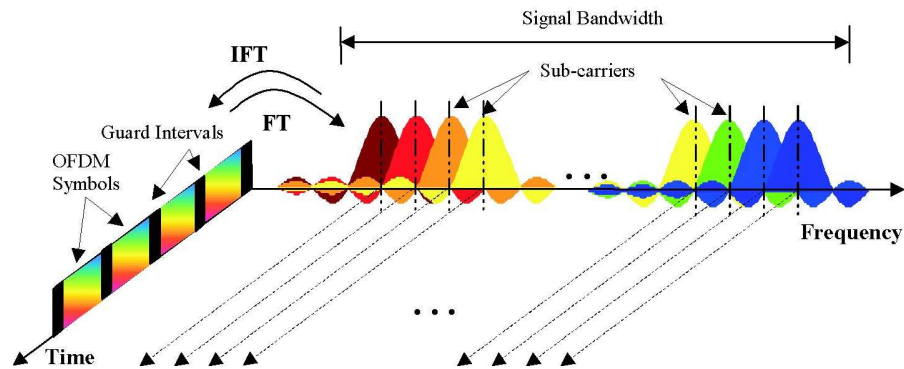
Figure 2.1: Time-frequency representation of a transmitted OFDM signal [3]

Definition: This technique is based on the well-known technique of Frequency Division Multiplexing (FDM). The OFDM technique transmits data over multiple carriers (from now on called subcarriers) that contain the information stream. These sub-carriers are orthogonal to each other in both time and frequency domains. However to compensate for radio channel multipath transmission delays, a guard time, called Cyclic Prefix (CP) is usually added to each OFDM symbol to combat the resulting interference as suggested in [3]. This technique, illustrated in figure 2.1, transforms a frequency-selective wide-band channel into a group of non-selective narrowband channels, which make CP-OFDM robust against large delays of the signal due to multipath.

Signal Generation: In this study information bits are linearly modulated into data symbols using for example Quadrature Phase Shift Keying (QPSK) or Quadrature Amplitude Modulation (QAM). The modulated symbols are then transmitted over closely spaced orthogonal subcarriers. The orthogonality is generated through the use of orthogonality functions, equally spaced in frequency, that are synchronously applied to the modulated data symbols. The transmitted baseband signal, as illustrated in figure 2.2, is then given by:

$$s_m(t) = \sum_{k=0}^{N_u-1} d_{m,k}\psi_k(t), \qquad (2.1)$$

where, $\psi_k(t) = \frac{1}{\sqrt{T_u}}e^{j2\pi f_k t}$ is the basic orthogonality function applied to the kth subcarrier. In classical literature these functions are also named tones at frequency f_k. N_u and T_u are respectively the number of used subcarriers and the OFDM symbol duration and $d_{m,k}$ the transmitted data symbol for the kth subcarrier and m^{th} OFDM symbol.
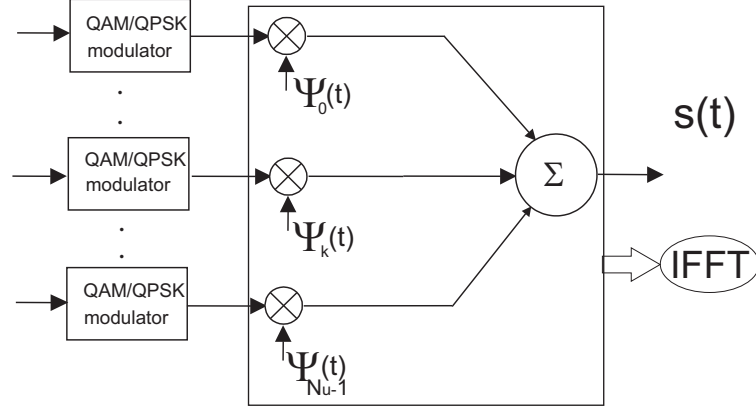
Figure 2.2: Principle of OFDM baseband signal generation

An advantage of OFDM is that the modulation of the orthogonality functions can be performed using an IFFT thereby significantly reducing the computational complexity required for a large transmission bandwidth.

Cyclic Prefix insertion   When transmitted over a multi-path channel, the OFDM signal is subject to Inter Symbol Interference (ISI) and Inter Carrier Interference (ICI) caused by the time-dispersive channel. A guard interval is therefore inserted prior to the useful OFDM symbol as seen in figure 2.3. In order to maintain orthogonality between subcarriers and their delayed replicas, the last N_g samples are copied at the beginning of each OFDM symbol. The orthogonality function is extended and becomes:

$$\psi_k(t) = \begin{cases} \frac{1}{\sqrt{T_u}}e^{j2\pi f_k(t+T_u)} & -T_g \leq t < 0, \\ \frac{1}{\sqrt{T_u}}e^{j2\pi f_k t} & 0 \leq t < T_u, \\ 0 & \text{otherwise} \end{cases}$$

At the receiver a matched filter is applied to retrieve the useful signal energy.
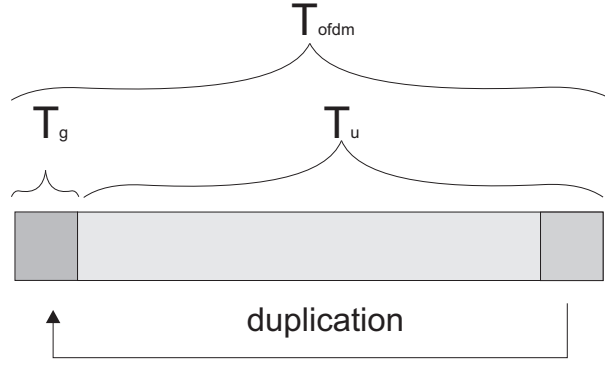
Figure 2.3: Cyclic Prefix insertion

This is done by integration with the complex conjugated orthogonality function:

$$\int_0^{T_u} \psi_k(t)\psi_{k'}^*(t)\mathrm{d}t = \begin{cases} 1 & k = k', \\ 0 & k \neq k'. \end{cases}$$

If delayed versions of the signal are received then for the replica delayed by τ:

$$\int_0^{T_u} \psi_k(t-\tau)\psi_{k'}^*(t)\mathrm{d}t = \begin{cases} 1 & k = k', \tau \leq T_g \\ \rho & k = k', \tau > T_g \\ 0 & k \neq k', \tau \leq T_g \\ \rho' & k \neq k', \tau > T_g. \end{cases}$$

This means that the kth orthogonality function is robust against correlation with any k'^{th} other orthogonality function as long as the maximum excess delay of the channel T_{med} is smaller than the CP duration T_g. When the delays are larger than T_g, the orthogonality is destroyed and a non zero output results.

Parameter relationships   When looking at OFDM without the insertion of a guard period, a classical design tradeoff lies in the relationship between subcarrier width Δ_k and OFDM symbol time T_u (in this case $T_g = 0$, $T_u = T_{ofdm}$), which is given by:

$$\Delta_k = \frac{1}{T_u}. \tag{2.2}$$

Two main channel distortion sources are the multipath delay spread, usually statistically characterized by the RMS delay spread τ_{rms} and the Doppler spread characterized by the coherence time t_{cor} (related to the Doppler frequency $f_d = \frac{1}{t_{cor}}$). In

order to have robustness against excess delays, one would need:

$$T_u \gg \tau_{rms}. \tag{2.3}$$

On the other hand in order to limit ICI due to fast fading:

$$T_u \ll t_{cor}. \tag{2.4}$$

The classical OFDM approach to determine T_u and Δ_k is a tradeoff between the UE speeds and the delay spreads supported. However when a CP is inserted and $T_g > T_{med}$, then the loss of orthogonality of subcarriers due to multipath spread is completely canceled. This leaves a large freedom of design of parameters in CP-OFDM, where mostly the subcarrier spacing versus supported Doppler frequencies needs to be considered. Note that the subcarrier spacing will indirectly affect the SEL loss due to CP overhead an can therefore not be indefinitely large.

Pros and cons of OFDM In the following, the main advantages and disadvantages of OFDM will be stated. Among the advantages of OFDM the next can be highlighted:

- Low complex equalizer at signal reception. When the CP length is longer than the maximum excess delay, and the effect due to Doppler distortion is negligible, the optimal equalization in SISO, only needs one complex operation per subcarrier [18] [19].

- Easy combination with MIMO enabling high spectral efficiencies.

- Adapts easily to varying mobile wireless channels through convenient choice of CP length, number of subcarriers and FFT length.

- Flexible bandwidth scalability allowing an easier cohabitation with other previously installed communication systems.

- Robust against narrowband interference as only a few subcarriers will be affected.

Among the disadvantages of OFDM can be highlighted:

June 18, 2008

- Peak-to-Average Power Ratio (PAPR) problematic.

- Sensitivity to synchronization.

- Reduced spectral efficiency due to CP.

2.2   Generic Analytical Matrix-vector model

This subsection will give a discrete-time description of the OFDM signal from transmission to reception at baseband level. In a first step a **"novel generic model"** is developed. It is generic in the sense that the assumptions are broad and few limitations are made. The signal is considered time variant at a resolution of the receiver sampling time T_s and the maximum excess delay of the CIR is shorter than the useful OFDM symbol time T_u. The model is also generic in the sense that different levels of modeling are targeted: frame level, OFDM symbol level and sample level.

Generic model:

A block diagram of the downlink baseband OFDM system is given in Fig.2.4. The bold vectors are expressed in matrix-vector notation in three levels:

- Frame level being the starting point and showing the relationship between the data transmitted through the physical channel and the data decoded at the receiver.

- OFDM symbol level showing the details of a symbol by symbol transmission.

- Sample level will be the lowest level providing an accurate tool for investigation and implementation enhancements.

The developed mathematical model will then follow the data flow of the transmission block diagram. The data bits to be transmitted are sent in blocks, and expressed by a vector:

$$\mathbf{b} = (\mathbf{b}[0], \mathbf{b}[1]...\mathbf{b}[n]...\mathbf{b}[\alpha_f k_{mod}(N_{fft} - 1)]), \qquad (2.5)$$

June 18, 2008
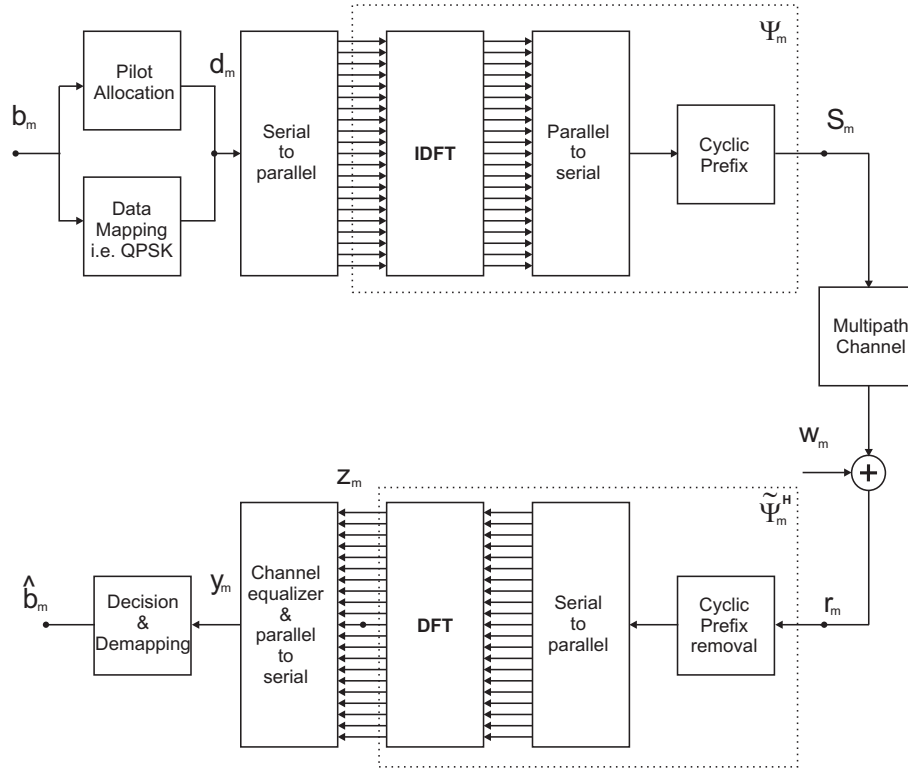
Figure 2.4: Block diagram of the OFDM system

where α_f is the number of OFDM symbols in a frame, k_{mod} is the number of bits per data symbol (i.e. for QPSK $k_{mod} = 2$, 8PSK $k_{mod} = 3$) and N_{fft} is the number of input symbols per DFT or, expressed from an implementation point of view, N_{fft} is the IFFT/FFT size.

Transmitted symbol at frame level: The transmitted frame with dimension $(\alpha_f \times N_{ofdm})$ is expressed by:

$$\mathbf{s} = \mathbf{\Psi} \mathbf{d}, \tag{2.6}$$

where $\mathbf{d}$ is the vector of transmitted data symbols on frame level with dimensions $(\alpha_f \cdot N_{fft})$ with:

$$\mathbf{d} = [\mathbf{d}_0^T \mathbf{d}_1^T ... \mathbf{d}_m^T ... \mathbf{d}_{\alpha_f - 1}^T]^T. \tag{2.7}$$

$\mathbf{\Psi}$ is a matrix that covers the IDFT and Cyclic Prefix (CP) effect on frame level. N_{ofdm} is the number of samples per OFDM symbol and depends the number of

CP samples N_g and the number of used subcarrier samples N_u. The dimensions of $\boldsymbol{\Psi}$ are $(\alpha_f \cdot N_{ofdm}) \times (\alpha_f \cdot N_{fft})$ and will be further explained in the symbol level subsection. We have:

$$\boldsymbol{\Psi} = \left\{ \begin{array}{ccccc} \boldsymbol{\Psi}_0 & 0 & \dots & & 0 \\ 0 & \ddots & & & \\ \vdots & & \boldsymbol{\Psi}_m & & \vdots \\ & & & \ddots & 0 \\ 0 & & \dots & 0 & \boldsymbol{\Psi}_{\alpha_f-1} \end{array} \right\}. \tag{2.8}$$

Transmitted OFDM symbol at symbol level: The mth transmitted OFDM symbol is expressed as follows:

$$\mathbf{s}_m = \boldsymbol{\Psi}_m \mathbf{d}_m \tag{2.9}$$

where $\boldsymbol{\Psi}_m$ is a sub-matrix of dimension $(N_{ofdm} \times N_{fft})$. It performs an IDFT of the input symbol sequence $\mathbf{d}_m$ and adds a redundant CP of size N_g. We have the relation: $N_{ofdm} = N_{fft} + N_g$.

$$\boldsymbol{\Psi}_m = (\boldsymbol{\Psi}_{m,0}^T \boldsymbol{\Psi}_{m,1}^T ... \boldsymbol{\Psi}_{m,k}^T ... \boldsymbol{\Psi}_{m,N_{fft}-1}^T) \tag{2.10}$$

$\boldsymbol{\Psi}_{m,k}^T$ is the kth orthogonality vector.

Having the relationship $f_k = k \frac{F_s}{N_{fft}}$, a convenient expression with CP is given by:

$$\boldsymbol{\Psi}_{m,k}[n] = \frac{1}{\sqrt{N_{fft}}} e^{j2\pi k(\frac{n-N_g}{N_{fft}})}, \tag{2.11}$$

with, $\boldsymbol{\Psi}_{m,k} = (\boldsymbol{\Psi}_{m,k}[0], \boldsymbol{\Psi}_{m,k}[1], ... \boldsymbol{\Psi}_{m,k}[N_{ofdm}-1])$, and $\mathbf{d}_m = (\mathbf{d}_m[0], \mathbf{d}_m[1], ... \mathbf{d}_m[N_{fft}-1])$ is a vector containing N_{fft} data symbols to be transmitted in the mth OFDM symbol, where f_k is the kth sub-carrier frequency, F_s is the sampling frequency. Some of the elements of $\mathbf{d}_m$ could be set to zero, thereby allowing the model to include virtual subcarriers.

Without CP we have:

$$\mathbf{s}_m = \boldsymbol{\Psi}_m \mathbf{d}_m \iff \mathbf{s}_m = IDFT\{\mathbf{d}_m\} \tag{2.12}$$

since

$$\boldsymbol{\Psi}_{m,k}[n] = \frac{1}{\sqrt{N_{fft}}} e^{j2\pi f_k \frac{n}{F_s}}. \tag{2.13}$$

Transmitted OFDM symbol at sample level: Each baseband transmitted sample can be expressed as:

$$\mathbf{s}_m[n] = \sum_{k=0}^{N_{fft}-1} \boldsymbol{\Psi}_{m,k}[n]\mathbf{d}_m[k], \tag{2.14}$$

where each subcarrier is multiplied with the corresponding data symbol, and then the product is summed for each subcarrier sample.

Received signal at frame level: The received signal vector $\mathbf{r}$, of dimension $(\alpha_f \times N_{ofdm})$ during the transmission of a full frame, can be expressed as:

$$\mathbf{r} = \mathbf{Hs} + \mathbf{w}, \tag{2.15}$$

where, $\mathbf{H}$ is the channel convolution matrix of dimensions $(\alpha_f \cdot N_{ofdm}) \times (\alpha_f \cdot N_{ofdm})$ expressed as:

$$\mathbf{H} = \left\{ \begin{array}{cccccc} \mathbf{H0}_0 & 0 & \ldots & & & 0 \\ \mathbf{H1}_0 & \mathbf{H0}_1 & 0 & & & \\ 0 & \mathbf{H1}_1 & \ddots & & & \vdots \\ & 0 & & \ddots & & \\ \vdots & & & \mathbf{H0}_{\alpha_f-2} & 0 \\ 0 & & & \mathbf{H1}_{\alpha_f-2} & \mathbf{H0}_{\alpha_f-1} \end{array} \right\}. \tag{2.16}$$

$\mathbf{H0}_m$ and $\mathbf{H1}_m$ are matrices of dimension $(N_{ofdm} \times N_{ofdm})$ and will be defined in the following, $\mathbf{s}$ is the transmitted frame of dimension $(\alpha_f \times N_{ofdm})$ and $\mathbf{w}$ is the Additive White Gaussian Noise (AWGN) vector of same dimension $(\alpha_f \times N_{ofdm})$, with $\mu_{\mathbf{w}} = \mathrm{E}\{\mathbf{w}\} = 0$ and $\mathbf{R}_{\mathbf{ww}} = \mathrm{E}\{\mathbf{ww}^H\} = \sigma_{\mathbf{w}}^2\mathbf{I}$.

Received signal at OFDM symbol level: The received signal vector $\mathbf{r}_m$, of dimension (N_{ofdm}), at symbol level can be expressed as:

$$\mathbf{r}_m = \mathbf{H1}_{m-1}\mathbf{s}_{m-1} + \mathbf{H0}_m\mathbf{s}_m + \mathbf{w}_m. \tag{2.17}$$

Given that the maximum length of the impulse response is limited to N_{ofdm} samples, the sub-matrices $\mathbf{H0}_m$ and $\mathbf{H1}_m$ are defined as:

$$\mathbf{H0}_m = \begin{Bmatrix} \mathbf{l}_{m,0}[0] & 0 & \cdots & & 0 \\ \mathbf{l}_{m,1}[0] & \mathbf{l}_{m,0}[1] & & & \\ & \mathbf{l}_{m,1}[1] & 0 & & \vdots \\ \vdots & & \ddots & & \\ & \vdots & & \mathbf{l}_{m,0}[N_{ofdm}-2] & 0 \\ \mathbf{l}_{m,N_{ofdm}-1}[0] & \mathbf{l}_{m,N_{ofdm}-2}[1] & \cdots & \mathbf{l}_{m,1}[N_{ofdm}-2] & \mathbf{l}_{m,0}[N_{ofdm}-1] \end{Bmatrix} \tag{2.18}$$

$$\mathbf{H1}_m = \begin{Bmatrix} 0 & \mathbf{l}_{m,N_{ofdm}-1}[1] & \mathbf{l}_{m,N_{ofdm}-2}[2] & \cdots & \mathbf{l}_{m,1}[N_{ofdm}-1] \\ 0 & 0 & \mathbf{l}_{m,N_{ofdm}-2}[2] & & \mathbf{l}_{m,2}[N_{ofdm}-1] \\ & & 0 & & \vdots \\ \vdots & & \ddots & & \\ & & & & \mathbf{l}_{m,N_{ofdm}-1}[N_{ofdm}-1] \\ 0 & & \cdots & & 0 \end{Bmatrix}. \tag{2.19}$$

$\mathbf{l}_{m,p}[n]$ is the pth discrete sample-spaced complex tap coefficient at sample instant n of the mth OFDM symbol.

Received signal at OFDM sample level: One way of representing the multi-path effect is done through a time representation of the arrival of the transmitted symbols for all the resolvable paths. A visualization of this channel convolution is shown in Fig.2.5. One can observe the same signal arriving at different delays, some within the timing of the CP others arriving later than the duration of the CP.

At sample level the received signal can be expressed as:

$$\begin{aligned} \mathbf{r}_m[n] &= \sum_{p=0}^{n} \mathbf{l}_{m,p}[n-p]\mathbf{s}_m[n-p] \\ &+ \sum_{i=n+1}^{N_{ofdm}-1} \mathbf{l}_{m-1,i}[N_{ofdm}+n-i]\mathbf{s}_{m-1}[N_{ofdm}+n-i] \end{aligned} \tag{2.20}$$

It is noted that equation 2.20 assumes that the delays are smaller than an OFDM symbol length.
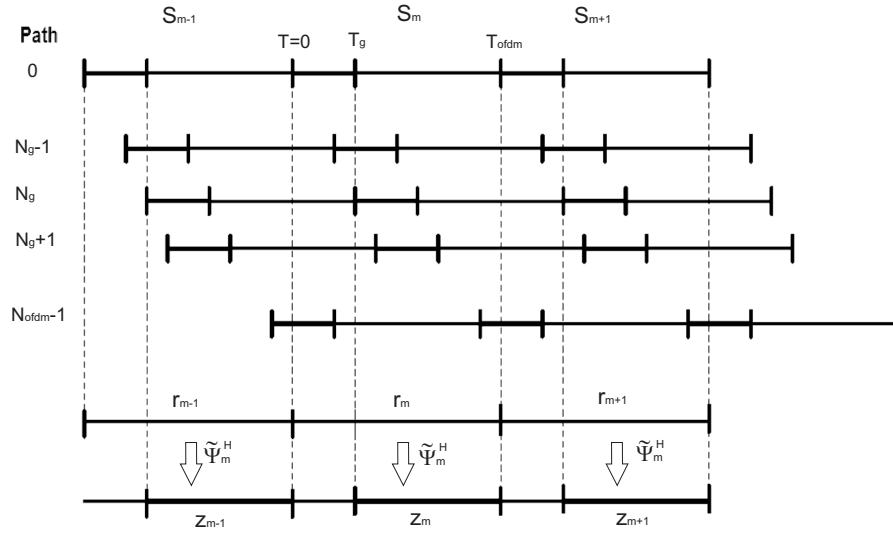
Figure 2.5: Channel convolution with transmitted signal

Output signal of DFT at the receiver at frame level: From Fig.2.5, it can be seen that the region of the received signal that is used for the DFT assumes a perfect synchronization and starts at $n = N_g$ sample. The output signal after the DFT and CP removal at the receiver can be expressed as:

$$\mathbf{z} = \tilde{\boldsymbol{\Psi}}^H \mathbf{r} = \tilde{\boldsymbol{\Psi}}^H (\mathbf{H} \mathbf{s} + \mathbf{w}), \tag{2.21}$$

where,

$$\tilde{\boldsymbol{\Psi}}^H = \left\{ \begin{array}{ccccc} \tilde{\boldsymbol{\Psi}}_0^H & 0 & \cdots & & 0 \\ 0 & \ddots & & & \\ \vdots & & \tilde{\boldsymbol{\Psi}}_m^H & & \vdots \\ & & & \ddots & 0 \\ 0 & & \cdots & 0 & \tilde{\boldsymbol{\Psi}}_{\alpha_f - 1}^H \end{array} \right\}. \tag{2.22}$$

The submatrices $\tilde{\boldsymbol{\Psi}}_m^H$ will be defined in the following.

Output signal of DFT at the receiver at OFDM symbol level: After each received OFDM symbol, the CP part of the signal is removed and a DFT is performed on the received signal. A matrix $\tilde{\boldsymbol{\Psi}}_m^H$ will perform both operations and is

defined as:

$$\tilde{\mathbf{\Psi}}_{m,k}^H[n] = \begin{cases} \mathbf{\Psi}_{m,n}^H[k] & \text{if } n > N_g, \\ 0 & \text{else.} \end{cases}$$

The output of the DFT can then be expressed as:

$$\mathbf{z}_m = \tilde{\mathbf{\Psi}}_m^H \mathbf{r}_m = \tilde{\mathbf{\Psi}}_m^H(\mathbf{H1}_{m-1}\mathbf{s}_{m-1} + \mathbf{H0}_m\mathbf{s}_m + \mathbf{w}_m), \qquad (2.23)$$

where, $\tilde{\mathbf{\Psi}}_m^H$ is equal to $\mathbf{\Psi}_m^H$ with the CP elements set equal to zero. Multiplying the data to be transmitted by $\mathbf{\Psi}_m^H$ is equal to perform an IDFT and to add a CP. Multiplying the received signal with $\tilde{\mathbf{\Psi}}_m^H$ is equal to remove the CP and perform a DFT.

It is then possible to describe the received OFDM signal at symbol level in a more intuitive way. The impact of the time and frequency selective physical channel is given by one single equation:

$$\mathbf{z}_m = \mathbf{C1}_{m-1}\mathbf{d}_{m-1} + \mathbf{C0}_m\mathbf{d}_m + \tilde{\mathbf{\Psi}}_m^H\mathbf{w}_m \qquad (2.24)$$

with,

$$\begin{aligned} \mathbf{C1}_{m-1} &= \tilde{\mathbf{\Psi}}_m^H\mathbf{H1}_{m-1}\mathbf{\Psi}_{m-1} \\ \mathbf{C0}_m &= \tilde{\mathbf{\Psi}}_m^H\mathbf{H0}_m\mathbf{\Psi}_m \end{aligned}$$

The effects of the ISI ($\mathbf{z}_{\text{ISI},m}$) and the ICI ($\mathbf{z}_{\text{ICI},m}$) can then be separated from the desired signal ($\mathbf{z}_{\text{S},m}$) by:

$$\mathbf{z}_m = \mathbf{z}_{\text{ISI},m} + \mathbf{z}_{\text{ICI},m} + \mathbf{z}_{\text{S},m} + \tilde{\mathbf{\Psi}}_m^H\mathbf{w}_m. \qquad (2.25)$$

We have:

$$\begin{aligned} \mathbf{z}_{\text{ISI},m} &= \mathbf{C1}_{m-1}\mathbf{d}_{m-1}, \\ \mathbf{z}_{\text{ICI},m} &= \mathbf{C0}_{\text{ICI},m}\mathbf{d}_m, \qquad (2.26) \\ \mathbf{z}_{\text{S},m} &= \mathbf{C0}_{\text{S},m}\mathbf{d}_m, \end{aligned}$$

where,

$$\mathbf{C0}_{\text{ICI},m}[k',k] = \begin{cases} \mathbf{C0}_m[k',k] & \text{if } k' \neq k, \\ 0 & \text{if } k' = k, \end{cases}$$

and

$$\mathbf{C0}_{\text{S},m}[k',k] = \begin{cases} 0 & \text{if } k' \neq k, \\ \mathbf{C0}_m[k',k] & \text{if } k' = k. \end{cases}$$

Output signal of DFT at the receiver at sample level: At sample level the signal after the DFT can be expressed as follows:

$$\mathbf{z}_m[k'] = \sum_{k=0}^{N_{ofdm}-1} \mathbf{C1}_{m-1}[k',k]\mathbf{d}_{m-1}[k] + \mathbf{C0}_m[k',k]\mathbf{d}_m[k] + \tilde{\boldsymbol{\Psi}}_{m,k'}^H[k]\mathbf{w}_m[k], \quad (2.27)$$

with each element of the correlation matrices given as:

$$\mathbf{C0}_m[k',k] = \sum_{n=0}^{N_{ofdm}-1} \tilde{\boldsymbol{\Psi}}_{m,k'}^*[n] \sum_{i=0}^{n} \mathbf{l}_{m,i}[n-i]\boldsymbol{\Psi}_{m,k}[n-i], \qquad (2.28)$$

and

$$\begin{aligned}
\mathbf{C1}_m[k',k] &= \sum_{n=0}^{N_{ofdm}-2} \tilde{\boldsymbol{\Psi}}_{m,k'}^*[n] \\
&\quad \cdot \sum_{i=n+1}^{N_{ofdm}-1} \mathbf{l}_{m-1,i}[N_{ofdm}+n-i]\boldsymbol{\Psi}_{m-1,k}[N_{ofdm}+n-i].
\end{aligned} \qquad (2.29)$$

2.3   Classical Analytical Matrix-vector model

The previous general model can be brought into a more commonly used model by assuming that the CIR is stationary during the transmission time of an OFDM symbol and that the maximum excess delay is shorter than the CP length. These assumptions allow a major simplification leading to the standard OFDM model encountered for most OFDM-based publications such as [26] [27] and [28].

The received signal after the DFT can be simplified to:

$$\mathbf{z}_m = \mathbf{C0}_{\mathrm{S},m}\mathbf{d}_m + \mathbf{w}_m. \qquad (2.30)$$

By introducing the Channel Transfer Function (CTF) vector $\mathbf{h}_m = \mathbf{F}\mathbf{g}_m$, where $\mathbf{F}$ is a DFT matrix of dimension $(N_{fft} \cdot N_{fft})$ and $\mathbf{g}_m$ is the CIR vector of dimension $(N_{fft} \cdot 1)$, we have the relationship:

$$\mathbf{C0}_{\mathrm{S},m}[k,k] = \mathbf{h}_m[k]. \qquad (2.31)$$

The received signal after DFT can the be rewritten as:

$$\mathbf{z}_m = \mathbf{D}_m\mathbf{h}_m + \mathbf{w}_m, \qquad (2.32)$$

and at sample level gives:

$$\mathbf{z}_m[k] = \mathbf{D}_m[k,k]\mathbf{h}_m[k] + \mathbf{w}_m[k]. \qquad (2.33)$$

The discrete signal after the one tap equalizer at sample level is then:

$$\mathbf{y}_m[k] = \frac{\mathbf{z}_m[k]}{\hat{\mathbf{h}}_m[k]}, \tag{2.34}$$

with $\hat{\mathbf{h}}_m[k]$ being the CTF estimate at the m^{tf} OFDM symbol and k^{tf} subcarrier.

Thereby only one operation per subcarrier is needed to equalize the signal after the CP removal and DFT. This feature is especially attractive for large bandwidths and high throughput signals as the complexity per subcarrier remains constant and minimized.

In the generic model, $\mathbf{l}_{m,p}$ is a discrete channel tap coefficient, yet, in this classical model a few notational difference will be noted. As in the generic model, we assume the OFDM signal to be transmitted over a normalized multipath Rayleigh fading channel with a Channel Impulse Response (CIR) given by:

$$g(\tau, t) = \sum_{i=0}^{N_t-1} a_i(t)\delta(\tau - \tau_i) \tag{2.35}$$

with

$$\sum_{i=0}^{N_t-1} \mathrm{E}\{|a_i(t)|^2\} = 1 \tag{2.36}$$

where $a_i(t)$ are the different wide sense stationary, uncorrelated complex Gaussian random path gains at time instant t, with their corresponding time delays τ_i and N_t being the number of paths. For the sake of simplicity, it is assumed that the variations of the channel response over the duration of an OFDM symbol are negligible and therefore the time index of $a_i(t)$ will be removed in the rest of this chapter. Furthermore the maximum path delay τ_{N_t-1} is assumed to be smaller than the CP duration of the signal, thus avoiding inter-symbol and inter-subcarrier interference.

2.3.1 Baseband Model in Full Bandwidth

The OFDM signal is generated by performing an IFFT on the modulated symbols to be transmitted, thus mapping each of them on a different subcarrier. When the number of symbols transmitted in each OFDM block equals the size of this IFFT, all subcarriers in the system are occupied with modulated symbols. In the following, this scenario will be referred to as Full Bandwidth. In this case, the received signal

after CP removal and FFT can be described as:

$$\mathbf{y} = \mathbf{D}\mathbf{h} + \mathbf{w} \tag{2.37}$$

where $\mathbf{D} \in \mathbb{C}^{N_{fft} \times N_{fft}}$ is a diagonal matrix with the complex modulated transmitted symbols, $\mathbf{h} \in \mathbb{C}^{N_{fft}}$ is the Channel Transfer Function (CTF) vector and $\mathbf{w} \in \mathbb{C}^{N_{fft}}$ is a vector with zero-mean Additive White Gaussian Noise (AWGN) of variance σ_w^2. N_{fft} denotes the FFT size.

The CTF at the subcarrier k is related to the CIR by:

$$\mathbf{h}[k] = \sum_{i=0}^{N_t-1} a_i e^{-j2\pi \frac{\tau_i}{\tau_s} \frac{k}{N_{fft}}} \tag{2.38}$$

where $(k \in \mathbb{Z}, \frac{-N_{fft}}{2} \le k \le \frac{N_{fft}}{2} - 1)$, and τ_s is the receiver sampling time. This operation can be expressed in matrix notation as:

$$\mathbf{h} = \mathbf{T}\mathbf{a} \tag{2.39}$$

where $\mathbf{T} \in \mathbb{C}^{N_{fft} \times N_t}$ and $\mathbf{a} \in \mathbb{C}^{N_t}$ are given by:

$$\mathbf{T}[k, i] = e^{-j2\pi \frac{k}{N_{fft}} \frac{\tau_i}{\tau_s}} \tag{2.40}$$

$$\mathbf{a}[i] = a_i \tag{2.41}$$

with $(\forall \{k, i\} \in \mathbb{Z}^2, \frac{-N_{fft}}{2} \le k \le \frac{N_{fft}}{2} - 1, 0 \le i \le N_t - 1)$.

From a receiver point of view, however, it might be more appropriate to express the CTF as a function of the equivalent sample-spaced CIR (SS-CIR) vector $\mathbf{g} \in \mathbb{C}^{N_{fft}}$, namely:

$$\mathbf{h} = \mathbf{F}\mathbf{g} \tag{2.42}$$

with the DFT matrix $\mathbf{F} \in \mathbb{C}^{N_{fft} \times N_{fft}}$ given by:

$$\mathbf{F}[k, n] = e^{-j2\pi \frac{nk}{N_{fft}}} \tag{2.43}$$

where $(n \in \mathbb{Z}; 0 \le n \le N_{fft} - 1)$.

From (2.39) and (2.42), the relationship between $\mathbf{g}$ and $\mathbf{a}$ can be found to be:

$$\mathbf{g} = \frac{1}{N_{fft}} \mathbf{F}^H \mathbf{T}\mathbf{a} = \mathbf{L}\mathbf{a} \tag{2.44}$$

where

$$\mathbf{L}[n,i] = \frac{1}{N_{fft}} \frac{\sin(\pi \frac{\tau_i}{\tau_s})}{\sin(\frac{-\pi}{N_{fft}}(n - \frac{\tau_i}{\tau_s}))} e^{-j \frac{\pi}{N_{fft}}((N_{fft}-1)\frac{\tau_i}{\tau_s}+n)} \tag{2.45}$$

$\mathbf{L} \in \mathbb{C}^{N_{fft} \times N_t}$ is the leakage matrix, and represents how the complex gain a_i of each channel path is mapped to the SS-CIR.

2.3.2 Baseband Model in Partial Bandwidth

Due to some spectral constraints, many multicarrier systems make use of only a subset of $N_u < N_{fft}$ subcarriers, leaving unused the $N_{fft} - N_u$ remaining ones, usually placed at the edges of the transmission bandwidth. The latter are the so-called virtual subcarriers, and this scenario will be referred to as Partial Bandwidth. In such a context, the received signal at the used subcarriers can be described by:

$$\mathbf{y}_u = \mathbf{D}_u \mathbf{h}_u + \mathbf{w}_u = \mathbf{D}_u \mathbf{F}_u \mathbf{g} + \mathbf{w}_u \tag{2.46}$$

where the CTF at the used subcarrier positions $\mathbf{h}_u \in \mathbb{C}^{N_u}$ is:

$$\mathbf{h}_u = \mathbf{F}_u \mathbf{g} \tag{2.47}$$

$\mathbf{D}_u \in \mathbb{C}^{N_u \times N_u}$ is a diagonal matrix with the transmitted symbols at the used subcarriers, $\mathbf{w}_u \in \mathbb{C}^{N_u}$ is the AWGN vector corresponding to the used subcarriers, and $\mathbf{F}_u \in \mathbb{C}^{N_u \times N_{fft}}$ is a subset of $\mathbf{F}$ with $\mathbf{F}_u[k,n] = \mathbf{F}[k,n]$ for $\frac{-N_u}{2} \leq k \leq \frac{N_u}{2} - 1$.

2.3.3 Received Signal at Pilot Subcarriers

In order to make channel estimation possible at the receiver, N_p pilot symbols are transmitted in some predefined subcarrier positions $\{p_m, 0 \leq m \leq N_p - 1\}$. The received signal in these pilot subcarriers can be then written as:

$$\mathbf{y}_p = \mathbf{D}_p \mathbf{h}_p + \mathbf{w}_p = \mathbf{D}_p \mathbf{F}_p \mathbf{g} + \mathbf{w}_p \tag{2.48}$$

where the CTF at the pilot positions $\mathbf{h}_p \in \mathbb{C}^{N_p}$ is:

$$\mathbf{h}_p = \mathbf{F}_p \mathbf{g} \tag{2.49}$$

$\mathbf{D}_p \in \mathbb{C}^{N_p \times N_p}$, $\mathbf{h}_p \in \mathbb{C}^{N_p}$, $\mathbf{F}_p \in \mathbb{C}^{N_p \times N_{fft}}$ and $\mathbf{w}_p \in \mathbb{C}^{N_p}$ are subsets of the corresponding matrices defined in the previous section, i.e, $\mathbf{D}_p[m,m] = \mathbf{D}_u[p_m, p_m]$, $\mathbf{h}_p[m] = \mathbf{h}_u[p_m]$, $\mathbf{F}_p[m,n] = \mathbf{F}_u[p_m, n]$ and $\mathbf{w}_p[m] = \mathbf{w}_u[p_m]$.

2.4   Conclusion

In this chapter, different properties of OFDM have been described. A novel **generic analytical model** has been derived, taking into consideration the effects of ICI and ISI on the received signal. This model is used for further investigations on optimal CP length studies in chapter 4, and for an interference cancelation study in chapter 8. The model is developed on three levels of accuracy: frame level, OFDM symbol level and sample level, allowing to get an intuitive overview as well as high parametric resolution.

When making the classical assumptions of channel stationarity during the transmission of 1 OFDM symbol as well as a CP length larger than the CIR length, one can simplify the generic model into a **classical analytical model**. This model is used mainly for channel estimation study in chapters 5 and 6.

The main outcome of this chapter will become clearer in these upcoming chapters, with the possibility of applying solutions on different levels of modeling.

Chapter 3

Simulator context and LTE baseline performance

3.1 Introduction

Once the analytical background has been established, we will look closer at the simulation context used for generating performance results in this thesis. Two simulators were developed to generate the different performance investigations of this thesis. First, a link simulator named **L1-EUTRA simulator** was developed together with three other Ph.D. students in order to have a common tool for monte carlo simulations for downlink LTE. The extensive software developed includes the majority of the 3GPP LTE link chain processing modules. This goes from the generation of transport blocks, CRC attachment, code block segmentation, channel coding, interleaving, constellation mapping, IFFT and CP addition for the signal generation; then generating a multipath radio channel with AWGN, receiving the signal and performing the opposite operations of the transmitter to obtain performance measures such as BER and BLER. Secondly, another simulator named **uncoded OFDM simulator** was developed for faster result generation as channel coding is not included and as the radio channel model is based on block fading. Both simulators show identical behavior in terms of uncoded BER but with a large simulation time gain for the uncoded OFDM simulator. The LTE parameters used for the simulator are discussed with a focus on their practical design in a unicast SISO context.

Finally a baseline performance evaluation is given for the chosen settings at 10MHz bandwidth.

This chapter will first present the two simulators in section 3.2 with an emphasis on the L1-EUTRA link simulator and only highlighting the difference for the uncoded OFDM simulator. A description and discussion of the key physical layer parameters adopted for DL LTE will the be elaborated in section 3.3. This will then set the baseline performance context in section 3.4 and a conclusion will finalize this chapter in section 3.5.

3.2   Simulation tools

3.2.1   L1-EUTRA link simulator

The block diagram of the link chain used in the performance evaluation is depicted in Figure 3.1. As shown, the left side models the BS transmitter, and the right side models the Mobile Station (MS) receiver. The link adaptation module operates as follows: it selects a Transport Format and Resource Combination (TFRC) for transmission on the basis of Channel Quality Indication (CQI) measurement from the MS. The TFRC decision is passed to the Transport Block Generator which generates a packet of the requested size. It is followed by Cyclic Redundancy Check (CRC) encoding. Then depending on the packet size and the maximum code block size, the packet is divided into several blocks before being fed to the channel encoder. The UTRA release 7 Turbo coding is used in this study. According to the code rate requirement, the output coded bits are punctured/repeated by the rate matcher (approximately from 1/6 to 1/1). The coded and interleaved bits are modulated, and for QAM modulation, a QAM re-mapping is performed [41]. The purpose is to put the systematic bits at more reliable constellation points as this can improve the decoder performance. The modulated symbols are space-time processed according to the selected MIMO scheme. For each spatial channel, an IFFT is applied and the cyclic prefix is added. At receiver side, the MS basically performs the reverse operations. If the CRC decoder determines the data packet to be error free, an acknowledgement (ACK) is signalled back to the BS, otherwise, the soft bits remain

in the UE buffer, and a negative acknowledgement (NACK) is signalled back. Upon reception of a NACK, the BS performs fast L1 retransmission of the data packet.
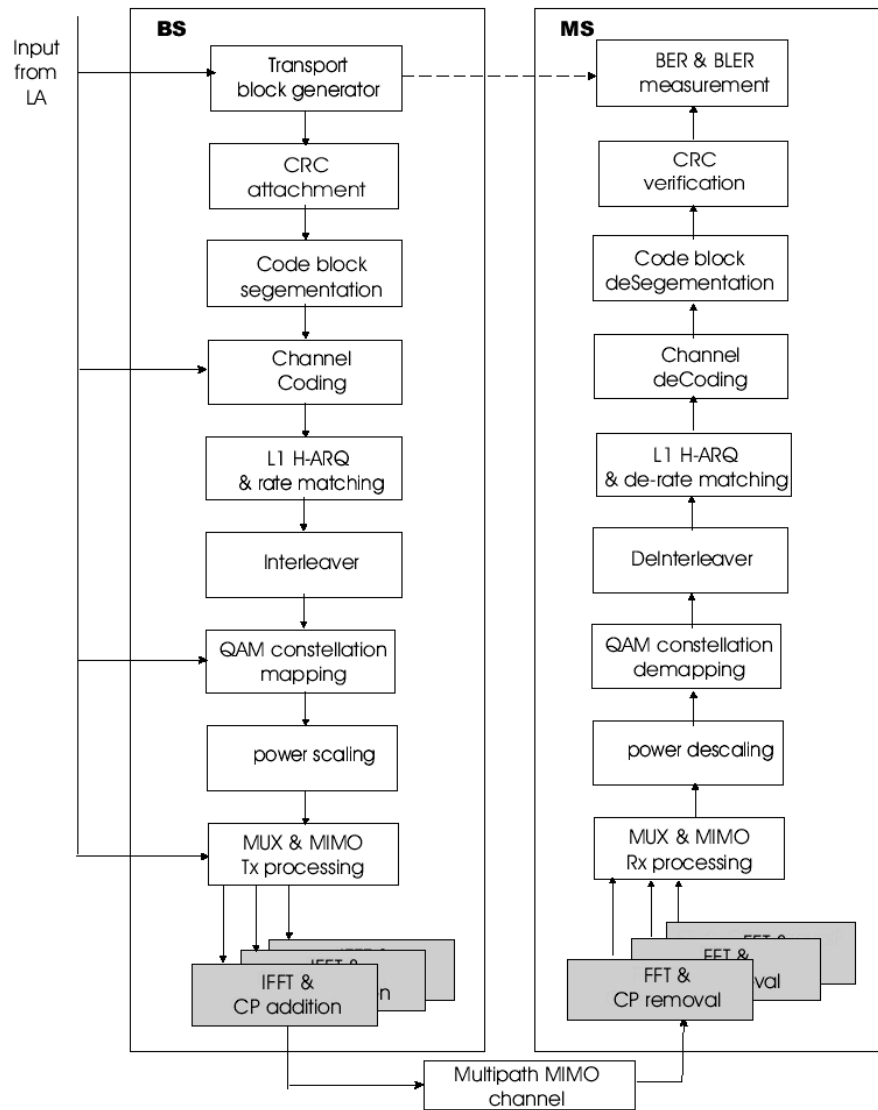
Figure 3.1: Block diagram of the link level chain

The simulator supports different MIMO configurations and reception algorithms in both transmission and reception. For diversity MIMO the Space Frequency Coded (SFC) Alamouti scheme [42] is implemented and for multi-stream MIMO the Vertical Bell Laboratories -Layered -Space Time (V-BLAST) scheme [43] is implemented. The MIMO channel used is based on the implementation in [45]. Here, the spatial correlation-based stochastic MIMO model has been used [37]. To ensure that the correlation properties in the frequency domain are realistic, different Power Delay

Profiles (PDP) from COST 259 [46] and ITU-R M.1225 [16] will be used in this study. Antennas are assumed to be uncorrelated. Note that for the further chapters of this thesis only the SISO antenna configuration will be used. Different channel estimation algorithms, as well as pilot schemes are also implemented and will be further elaborated in chapters 6 and 7. The PER and spectral efficiency results provided by this simulator will be given for different Sinal to Noise Ratio (SNR) values, where SNR is defined as the ratio between the received signal power and the noise power. No errors are assumed in the transmission of ACK/NACK messages. Further, the channel estimation is assumed to be ideal for the baseline results. To allow for processing and propagation delays, the retransmission scheme is based on the stop and wait (SAW).

3.2.2 Uncoded OFDM simulator

The second simulator was developed with the intention of obtaining results at a highly reduced simulation time. It closely follows the block diagram of figure 2.4 where all modules related to channel coding are removed, namely: TFRC, CRC attachment, HARQ, Interleaving, Link Adaptation. Also the MIMO module is removed as not needed for the study. As the data of consecutive transmitted OFDM symbols, is uncorrelated, the channel model is assumed to be uncorrelated block fading. By this is meant that for each transmitted OFDM symbol a new CIR with uncorrelated Rayleigh taps is generated. This setup allows the simulation time to be strongly reduced for generation of uncoded Bit Error Rate (BER) and Mean Squared Error (MSE) results.

The advantages of this simulator are its large flexibility in parameter settings allowing to go beyond the settings of specified for LTE and its increased simulation speed as results converge quickly because of the uncorrelated block fading. Thereby more investigations for comparative results can be run before making a wiser selection of parameter settings and algorithms to be run in the L1-EUTRA link simulator.

3.2.3 Simulator comments

The previous subsections described the functionality of the simulators used. However in this thesis not all of these functionalities where in the scope of investigation. I.e. the H-ARQ and the MIMO schemes are only given as performance guidelines and are not studied further. Channel estimation and interference cancelation results will be given in the corresponding chapters, however in the baseline performance these are not considered.

3.3 OFDM parameters in LTE

3.3.1 UTRA backward compatibility

One of the first requirements set to Evolved UTRA has been the possibility of dual-mode usage together with UTRA. Therefore a backward compatibility with the radio-frame length of 10 msec has been necessary. Previously in conventional dual-mode GSM/UMTS modems, clocking has been using 2 different time bases requiring multiple clocks and clock generation circuitry. Also clock synchronization circuitry must also be added inside of the dual-mode modem to allow the sharing of information between clock domains. This creates latency in the information transferred, more power consumption and additional die-area. In order to avoid these problems a sampling frequency of 3.84 MHz in a 2,5 MHz transmission bandwidth is chosen for LTE. To ensure flexibility and efficient use of bandwidth with other Radio Access Technologies (RAT), other transmission bandwidths that are either integer multiple or fractions of the initial 2,5 MHz bandwidth are also given. These can be seen in table 3.1.

Table 3.1: Different bandwidths and sampling frequencies in LTE

Transmission BW	1,25 MHz	2,5 MHz	5 MHz	10 MHz	20 MHz
Sampling frequency	1,92 MHz	3,84 MHz	7,68 MHz	15,36 MHz	30,72 MHz

The frame structure used in this thesis has been limited to Type 1 specified in [5] and can be seen in Figure 3.2. It is applicable to both FDD and TDD mode and consists of 20 slots of 0,5ms, where a subframe is defined as two consecutive slots.

One radio frame, T_f=10 ms

One slot, T_{slot} = 0.5 ms

| #0 | #1 | #2 | #3 | .... | #18 | #19 |

One subframe
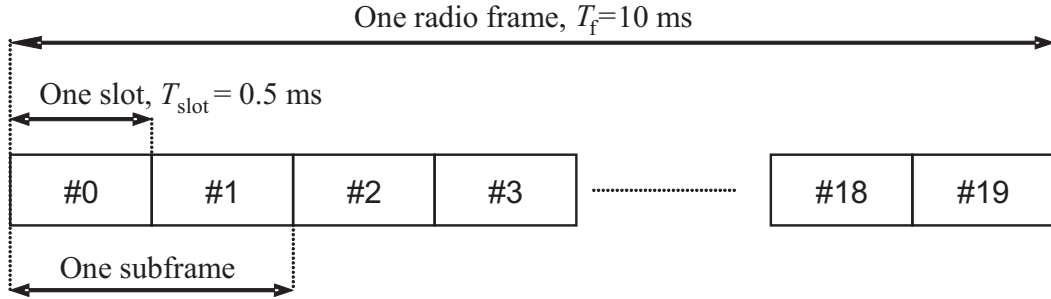
Figure 3.2: LTE frame structure type 1

The transmitted signal in each slot is described by a resource grid of N_u subcarriers and $N_{o,slot}$ OFDM symbols. The quantity N_u depends on the downlink transmission bandwidth configured in the cell. The number of OFDM symbols in a slot $N_{o,slot}$ depends on the cyclic prefix length and subcarrier spacing configured. In this study the CP length will be fixed to $T_g = 4,69\mu s$, the subcarrier spacing $\Delta_f = 15kHz$ and thereby $N_{o,slot} = 7$.

3.3.2   Subcarrier spacing and OFDM symbol time

The two main factors that influence the subcarrier spacing design are the Doppler effect due to the mobility of the UE and the phase noise generated by the fluctuations in the frequency of the local oscillators of the Base Station (BS) and the UE. An overview over the maximum Doppler frequencies perceived, as a function of UE speed for different carrier frequencies can be seen in table 3.2. The subcarrier spacing Δ_f is related to the OFDM symbol duration length (without CP) T_u by:

$$T_u = \frac{1}{\Delta_f}. \tag{3.1}$$

When increasing the subcarrier spacing the robustness against ICI generated by high velocity or phase noise increases, however the duration of the OFDM symbol diminishes, increasing the sensitivity to channel delay spread. Therefore the design

of the subcarrier spacing for OFDM, without a CP covering the entire excess delay, is a tradeoff between sensitivity to Doppler frequency or to delay spread of the physical channel.

Table 3.2: Perceived maximum Doppler frequencies at different speeds and carrier frequencies

Fc	V = 30 kmph	V = 300 kmph	V = 500 kpmh
900 MHz	25,0 Hz	250 Hz	410 Hz
2000 MHz	55,6 Hz	556 Hz	926 Hz
2600 MHz	72,2 Hz	722 Hz	1203 Hz

From a Radio Resource Management (RRM) point of view, it is important to keep signaling complexity low. This is especially true when considering the basic transmission unit, Physical Resource Block (PRB), allocation and management. Typically a RU will consist of several joint subcarriers and these will therefore need to be of fixed size as design constraint, in order to minimize the signalling complexity. The subcarrier spacing has therefore to be constant for all bandwidths. Also the FFT size used should be a power of two ($N_{fft} = 2^n, n \in \mathbb{N}$, i.e. $N_{fft} = 128, 256, 512, 1024, 2048$) due to FFT implementation advantages.

Only few combinations are then left when keeping the subcarrier spacing fixed. For example when choosing the sampling frequency of 3,84 MHz, the FFT lengths of 128, 256 and 512 would respectively lead to a subcarrier spacing of 30 kHz, 15 kHz and 7,5 kHz. Other choices of FFT sizes would lead to higher or lower subcarrier spacings. A basic OFDM rule of thumb, as given in [7] is that the ratio between the maximum Doppler frequency and the subcarrier spacing should be of 10 to 20 in order to support high speeds. The study also shows that when wider than 10 kHz, the influence of phase noise is small compared to the other impairments. It follows naturally that the 15 kHz is a compromise solution to the choice of subcarrier spacing, leading to a factor 14,5 times the maximum Doppler frequency of table 3.2. The parameters chosen can bee seen in table 3.3.

Table 3.3: FFT sizes for the different bandwidths

Transmission BW	1,25 MHz	2,5 MHz	5 MHz	10 MHz	20 MHz
FFT size	128	256	512	1024	2048
Subcarrier spacing	15 kHz				

3.4   Baseline performance

3.4.1   Achievable peak rates in DL LTE

In the following, we propose to give a realistic estimate of the achievable maximum peak rates, just from reading the LTE specifications and assuming optimal transmission conditions. At the moment of writing this Ph.D. thesis, the standardization process is still ongoing and some of the parameters and settings given in the following might vary from the ones that will be used ultimately. In the 3GPP TS36 series, the LTE physical layer is specified. LTE proposes a flexible bandwidth usage (supporting 1.25, 2.5, 5, 10 and 20 MHz) leading to a scalable number of used subcarriers $N_u \in \{76, 151, 301, 601, 1201\}$. In the case of the generic downlink frame structure proposed in TS36.211 [5], where a subframe is of duration 1 ms and contains 14 OFDM symbols, the number of OFDM symbols per second $N_{o,sec}$ is then 14000. A high spectral efficiency is then obtained with the use of MIMO schemes and especially spatial multiplexing where the maximum number of streams $N_{stream} \in \{1, 2, 4\}$ mainly depends on the available antenna configuration and antenna correlation. The high peak rates will then be achieved with the 20MHz bandwidth and by combining the mentioned techniques with higher order modulation such as QPSK, 16QAM and 64QAM where the number of bits per data symbols is $N_{mod} \in \{2, 4, 6\}$. The transmitted data is encoded with a Turbo encoder which leads to additional redundancy. A subset of suggested ECRs is given by $O_{ecr} \in \{ 1/6, 1/3, 1/2, 2/3, 3/4, 4/5, 5/6\}$. Practical issues such synchronization and channel estimation require presence of pilot data giving a pilot loss factor of $O_{pilot} \in \{0.9524\ 0.9048\ 0.8571\}$ corresponding respectively to a loss of 4.76 %, 9.52 % and 14.29 %. This pilot loss depends on the different MIMO and MBMS settings.

Finally a protocol signalling and together with CP loss $O_{sig} = 0.70$ of 30% is also considered.
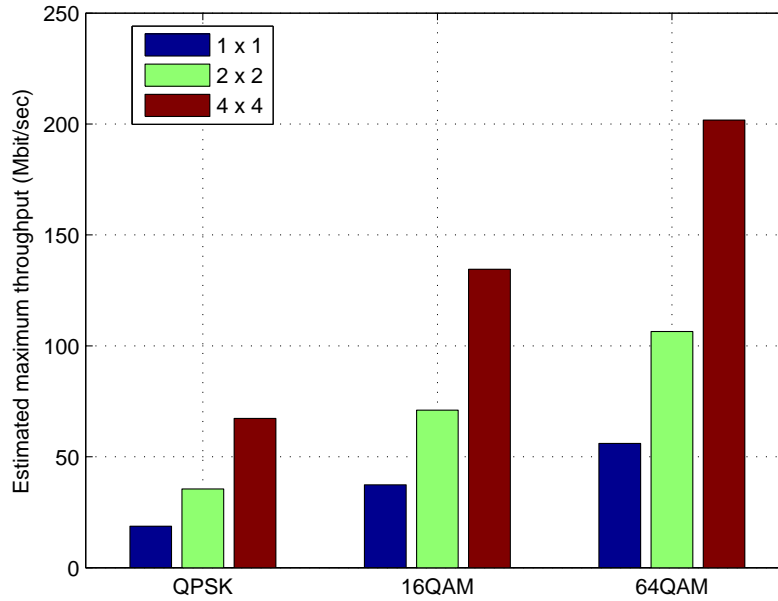
Figure 3.3: Maximum deliverable throughput in LTE for different physical layer configurations

The throughput can then be expressed as:

$$\text{Throughput} = (N_{o,sec} \cdot N_u \cdot \text{N}_{mod} \cdot \text{N}_{stream}) \cdot \text{O}_{pilot} \cdot \text{O}_{ecr} \cdot \text{O}_{sig}. \qquad (3.2)$$

The different estimated maximum achievable throughputs in LTE are given in Figure 3.3 for a 20MHz bandwidth, for three MIMO scenarios and given an efficient code rate of 5/6. These numbers should be seen as the "best case" feasible scenario. By "best case" is meant the highest effective code rate with a PER of 0, and by feasible is meant calculations including most overhead that is present in both physical layer and signalling. From the observed numbers it can be concluded that the LTE peak rate objectives of 100 Mbit per second will only be achieved with multistream MIMO combined with higher order modulation (at least 16QAM).

3.4.2 Baseline performance

Now that the achievable peak rates in DL LTE have been described, some baseline spectral efficiency results will be given. The L1-EUTRA simulator is used for this performance analysis. The parameter settings used are the ones from section 3.3 for a 10 MHz scenario. No overhead due to pilot symbols is considered here as the degradation due to channel estimation is not studied in the baseline performance. This degradation will however be largely studied in later chapters. The set of Modulation and Code Schemes (MCS) chosen is given on table 3.4. The turbo decoder implementation has been verified against results in [14]. The uncoded BER performance of the link simulator has also been verified for different modulation formats. Throughput results have also been compared to the ones from other companies in appendix B.

Table 3.4: Used set of MCS

Modulation	ECR
QPSK	1/6, 1/3, 1/2, 2/3
16QAM	1/2, 2/3, 3/4
64QAM	3/4, 4/5

In figure 3.4, the spectral efficiency, defined as useful throughput over bandwidth, of different modulation and code sets without HARQ, in a SISO antenna configuration is plotted versus SNR. The bandwidth is set to 10 MHz and the channel model is the Typical Urban [46].

The spectral efficiency versus SNR when using HARQ is shown in figure 3.5 for 3 MCS using Incremental Redundancy (IR). Including HARQ increases performance for all SNRs except when the PER is null. In this case there is no gain to achieve, as no retransmissions are needed. The individual curves without HARQ have the characteristic steep slope due to the Turbo Codes employed. When using HARQ the BLER degradation is more gradual and the classical staircase curve is observed with a correspondence between the number of average packet transmissions and the different steps.
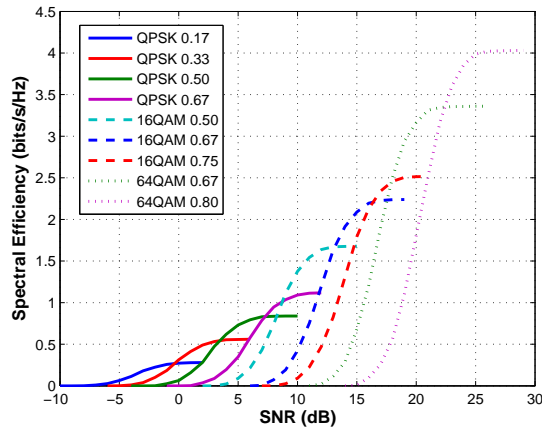
Figure 3.4: **without HARQ**   Figure 3.5: **HARQ** vs. **no HARQ**
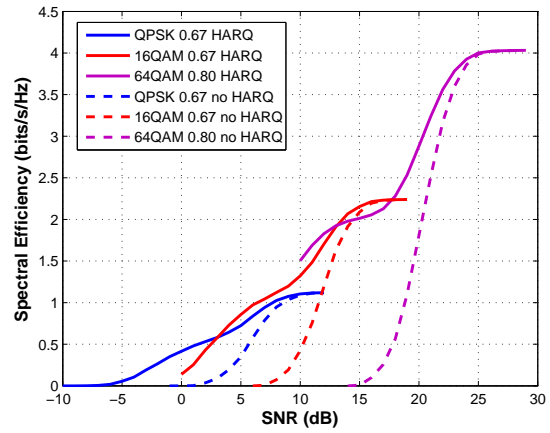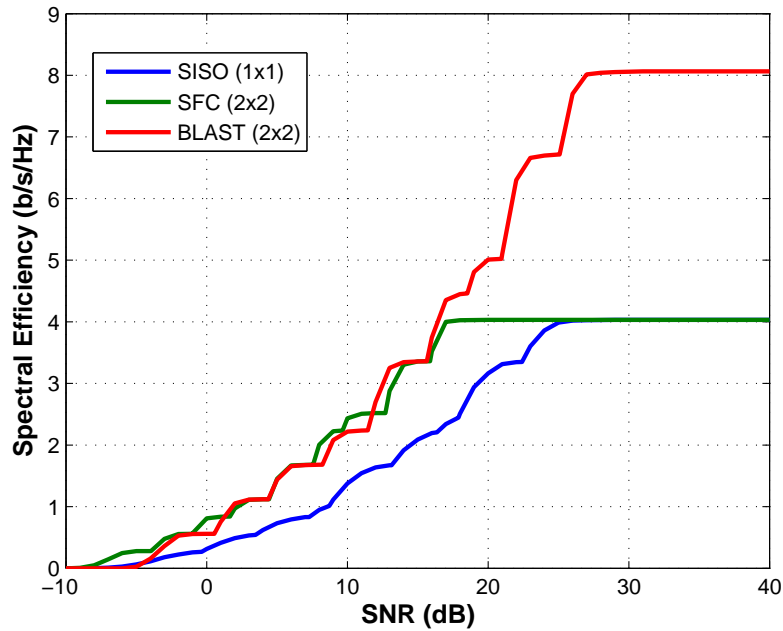
Figure 3.6: Maximal Spectral Efficiency for different MIMO schemes **without HARQ** in a 10 MHz bandwidth

In Figure 3.6, the spectral efficiency for the different antenna configuration and reference MIMO schemes are shown for comparison. Three performance curves are included. All curves represent the maximal achievable performance from adapting to the best MCS set for a given average SNR. The first curve represents the SISO

case from figure 3.4. The second one is based on single data stream Alamouti [42] SFC scheme with a 2 by 2 antenna configuration. The third curve represents a dual stream, 2 by 2 antenna configuration, BLAST scheme. At SNR below 17dB, both dual antenna schemes have similar performance with a gain of 5-7 dB over the SISO performance. At SNR above 17dB the SFC performance is saturated and converges towards the one from SISO. The BLAST performance however, gains from the dual stream transmission where the spectral efficiency is doubled at SNR above 28 dB, compared to the two other single stream schemes performance curves.

3.5 Conclusion

In this chapter the simulator context and LTE baseline performance have been presented. The two simulators that will be used for the rest of this thesis have been described. These are the L1-EUTRA link simulator for DL LTE and the uncoded OFDM simulator. The L1-EUTRA was developed to generate accurate link results according to 3GPP requirements and was verified by comparing performance against official results from other companies. Thereby the obtained SISO simulation chain results have been verified. The uncoded OFDM simulator only generates BER, MSE and SINR results, but simulation time is greatly reduced as no FEC is included and the simulated radio channel is based on block fading.

The physical layer parameters adopted for DL LTE have been described and the reasoning behind their choice and design has been explained. With these parameters, baseline performance for 10 MHz was outlined for key reference scenarios. First the maximum achievable peak rates were given for different antenna configurations and modulation schemes (QPSK, 16QAM and 64QAM). In the same manner, spectral efficiency results for different SNR values were presented showing the advantages of using HARQ and MIMO schemes. More specifically the 2 by 2 antenna Alamouti SFC and BLAST schemes advantages against simple 1 by 1 antenna SISO configuration were drawn to light.

For the rest of this thesis the investigations carried out will however be restricted to the SISO 1 by 1 antenna scenario without the use of HARQ.

Chapter 4

On Cyclic Prefix Length

4.1 Introduction

A CP is generally inserted in OFDM transmission. It is an additional redundant guard period that efficiently combats interference resulting from the multipath nature of the physical channel. If the CP length is larger than the length of the Maximum Excess Delay (MED), all multipath energy resulting from delayed versions of the signal is constructively recovered [20] [21]. The CP has no influence on the interference resulting from mobility and the resulting Doppler shift [22]. Therefore, arbitrarily, the Doppler spectrum is considered flat in this subsection. The introduction of CP has the drawback of reducing the overall system capacity in an irreversible manner. This reduction can be expressed through the Spectral Efficiency Loss (SEL): $SEL = \frac{T_g}{T_{ofdm}}$, with T_g being the CP length, T_u the useful symbol length and $T_{ofdm} = T_g + T_u$ the total OFDM symbol length. It can be see that the SEL does not only depend on T_g but also on T_u . If T_g is fixed, the SEL diminishes when T_u is increased. During this study T_u will be fixed to a few chosen values inspired from previous studies [53], [54] for generic results and the LTE parameters for more specific LTE results. On the other hand, as CP covers more and more of the PDP length it reduces the SINR, thus enhancing the overall BLER performance of the system. The other advantage when the CP length is larger than the MED is that interference free reception can be achieved with a Single Tap Equalizer (STE) [55]. From a complexity point of view this STE has interesting properties and is there-

fore adopted in the following. System level CP length studies have previously been conducted but without focusing precisely on variation of PDP. In [56] for instance, CP length was studied in connection with synchronization.

Efficient adaptive CP length has recently been proposed by Lim [57] . The drawback of such a solution is increased signalling overhead. In this chapter we conduct a study giving insight on the choice of an optimal CP length. We also evaluate and propose different fixed CP lengths and compare them to the proposed values of LTE in [5]. In section 4.2 an analytical method for evaluating SINR in OFDM is given leading to an evaluation of CP length in section 4.3. Finally we conclude in 4.4.

4.2   SINR evaluation

In the following, an analytical method for evaluating SINR, inspired from [22] and [56], is presented. This method gives an intuitive understanding of the effects of T_g, T_u, T_{ofdm}, the PDP and SNR on the received SINR. The method is then verified by a statistical evaluation.

A general SINR formulation is given by:

$$SINR = \frac{P_s}{P_i + \sigma_{\mathbf{w}}^2} \tag{4.1}$$

Where P_s is the "useful" signal power, P_i is the interference power, and $\sigma_{\mathbf{w}}^2$ is the variance of the white gaussian noise. All powers are expressed per subcarrier.

Analytical SINR evaluation

In this section the "useful" signal and the interference signal are both calculated from a given PDP and a weighting function called "bias function" seen on Figure 4.1. This function was first used in [22] and extended to use timing offset in [56]. The synchronicity assumption leads to the following definition:

$$C(\tau) = \begin{cases} 0, & \tau < 0 \\ 1, & 0 \leq \tau < T_g \\ \frac{T_u - (\tau - T_g)}{T_u}, & T_g \leq \tau < T_{ofdm} \\ 0, & T_{ofdm} \leq \tau \end{cases}$$
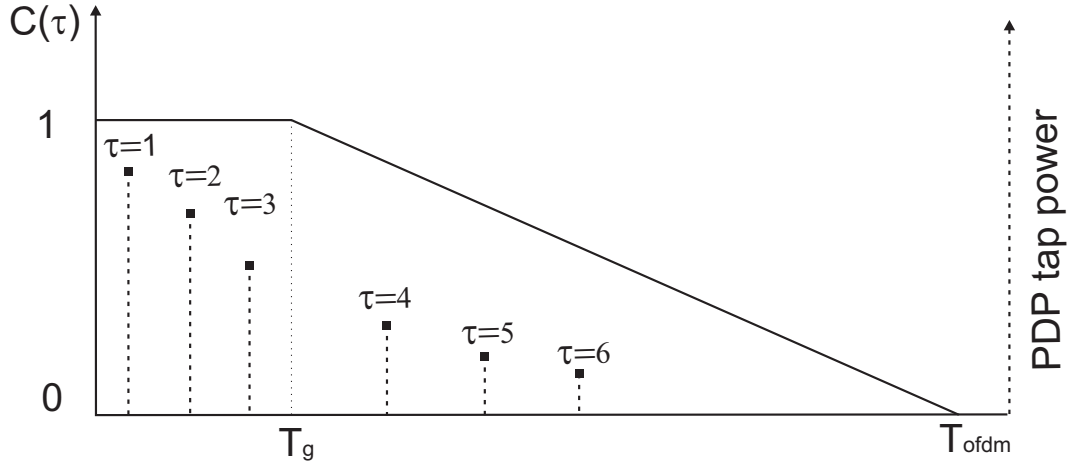
Figure 4.1: Dual axis illustration of the weight function and an example PDP

We assume the channel PDP to have N_t taps with power $\mathrm{E}\{|a_i(t)|^2\}$ at the ith tap at delay τ_i. According to equation 2.36, the channel is normalized in the following way:

$$\sum_{i=0}^{N_t-1} \mathrm{E}\{|a_i(t)|^2\} = 1$$

When removing the time indexing we have the expression: $\mathrm{E}\{|\mathbf{a}[i]|^2\} = \mathrm{E}\{|a_i(t)|^2\}$. The power of the "desired" signal is given by:

$$P_s = \sum_{i=0}^{N_t-1} C(\tau_i)^2 \mathrm{E}\{|\mathbf{a}[i]|^2\} \tag{4.2}$$

The interference is given by:

$$P_i = \sum_{i=0}^{N_t-1} (1 - C(\tau_i)^2) \mathrm{E}\{|\mathbf{a}[i]|^2\} \tag{4.3}$$

Monte Carlo verification

The Monte Carlo based verification method is evaluated on the signal $\mathbf{z}_m$ after the FFT at the receiver. The "desired" signal is given by:

$$\mathbf{z}_s[k] = \mathbf{C0}_m[k,k]\mathbf{d}_m[k] \tag{4.4}$$

The power of the "desired" signal per subcarrier is then estimated by:

$$P_s[k] = \mathrm{E}\{|\mathbf{z}_s[k] - \mathrm{E}(\mathbf{z}_s[k])|^2\} \tag{4.5}$$

The interference per subcarrier is given by:

$$\mathbf{z}_i[k] = \mathbf{z}_m[k] - (\mathbf{z}_s[k] + \mathbf{w}_m[k]) \tag{4.6}$$

The power of the interfering signal per subcarrier is then estimated by:

$$P_i[k] = \mathrm{E}\{|\mathbf{z}_i[k] - \mathrm{E}(\mathbf{z}_i[k])|^2\} \tag{4.7}$$

During the simulations the variance of the white gaussian noise is assumed known. It is noted that analytical method and the verification simulations give exactly the same SINR results with a margin of error determined by the confidence interval due to the finite length of the Monte Carlo simulations. The Analytical approach is therefore adopted in the rest of this work for SINR calculation.

Channel Profiles considered

The strategy behind the choice of profiles has been to select PDPs with different maximum excess delay lengths: short, medium and long. These are divided in two categories: the ones coming from known standards and the ones that are based on an exponential decaying function. The standardization based are the three ITU-R M.1225 [16] profiles given in table A.1 and the Hilly Terrain from the COST 259 project [46] in table A.2, and are given in appendix A. The exponential decaying PDPs characteristics are given in table 4.1. τ_{rms} is the Root Mean Square (RMS) delay spread of the considered profile, and τ is the considered tap delay.

Table 4.1: Exponential decaying channel PDP's considered

Profile Name	Tap Spacing (ns)	τ_{rms} (ns)
E100	40	100
E630	160	630
E3000	640	3000
E4000	1000	4000

SINR results

As the focus of this study is to give insight on the choice of an optimal CP length, the impact on the received SINR is studied. Figure 4.2 shows the SINR power
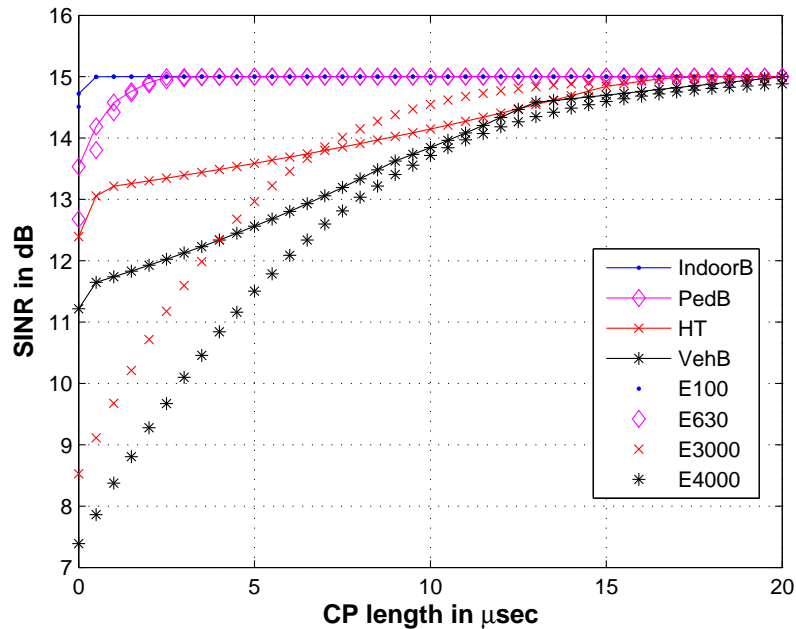
Figure 4.2: SINR at receiver as a function of the CP length, Eb/No=15dB, $T_u = 66,67\mu s$

in dB as as a function of T_g. T_u is fixed to $66,6\mu sec$. The different previously proposed PDP's are chosen for the results and it can be seen by inspection that the τ_{rms} doesn't fully describe the impact of the PDP on the SINR. For example, when looking at the pair of profiles with equal τ_{rms} such as Pedestrian B and the E630, the SINR obtained are different. Generally, when comparing the exponential decaying PDP's with the ITU and COST profiles, a clear difference in SINR levels can be linked to the clustering of the channel power taps. This is especially true for the HT profile and the E3000 or the VehB and the E4000. For all curves the maximum SINR corresponds to the received SNR and is obtained when T_g exceeds the maximum excess delay. In Figure 4.3 similar results are obtained for 30db SNR. It can be seen that the overall SINR is increasing together with the SNR, implying an larger CP length sensitivity.

June 18, 2008
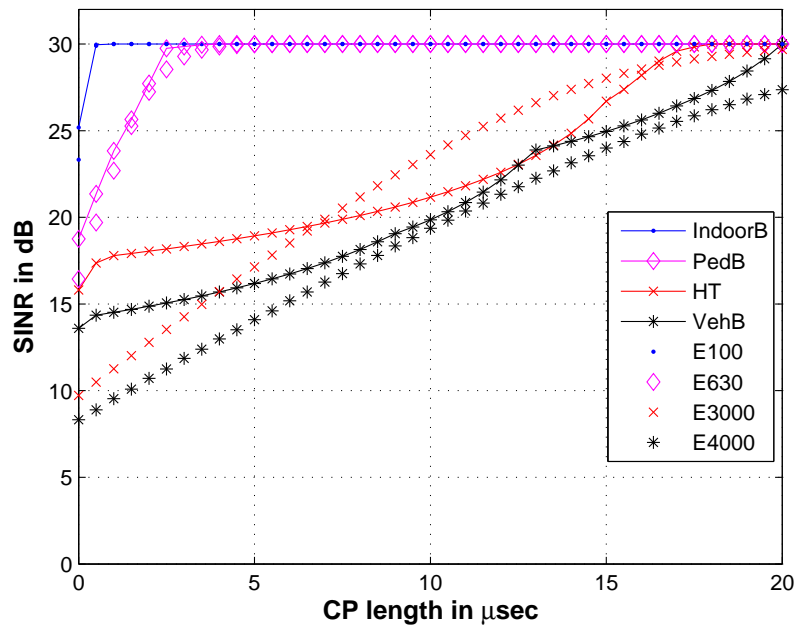
Figure 4.3: SINR at receiver as a function of the CP length, Eb/No=30dB, $T_u = 66,67\mu s$

4.3   On the "optimal" CP length

Maximizing the SINR increases the Bit Error Rate (BER) at the receiver, but at the same time when the CP length is extended, transmission time is lost in an irrecoverable manner. A System link level evaluation is therefore more appropriate to take account on both effects. In the following we use an approach similar to the one used in [56] where the SINR is mapped to capacity in Bit per Second per Hertz (b/s/Hz) through Shannons capacity theorem.

Capacity model

In order to account for a link adaptation loss α_{loss} following model model is proposed:

$$C(T_g) = (1 - SEL) \cdot log_2(1 + \alpha_{loss} \cdot SINR(T_g)). \tag{4.8}$$

Note that $SEL = \frac{T_g}{T_{ofdm}}$ and α_{loss} is a fixed loss from the Shannon limit and varies with the system settings. In this study we are limited to the SISO case and α_{loss} is respectively set to 0,4 where the latter corresponds to the degradation used in [58].

Simulation results
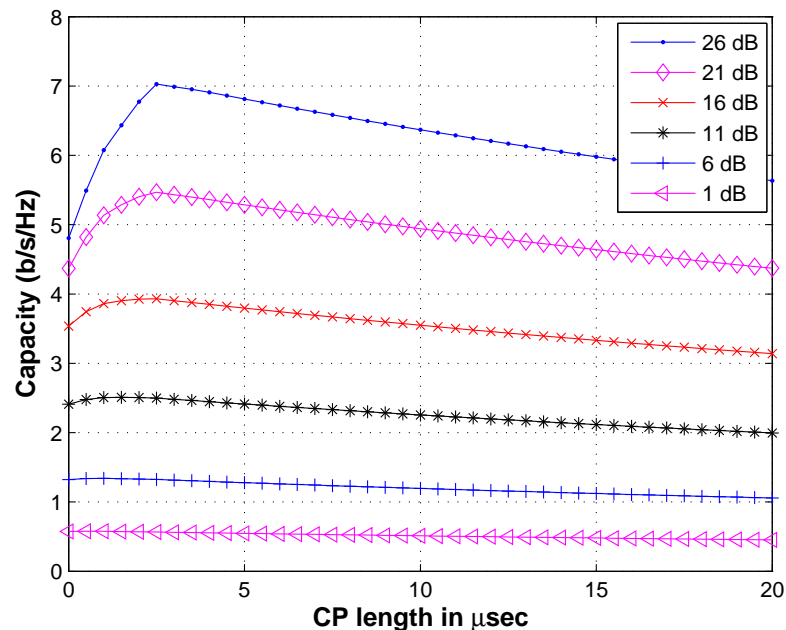
Figure 4.4: Influence of the received SNR on CP length. Capacity for different received signal powers, PDP= PedB $T_u = 66, 67\mu s$

The SINR defined previously in equation 4.1 depends on the "desired" SNR at the receiver. Note that the SNR is equal to the SINR when the CP length is larger than the maximum excess delay of the CIR. The impact of the SNR is studied in Figure 4.4. It is observed that the receiver is more sensitive to the CP length at high SNR, whereas at low SNR its impact is almost neglegible. I.e. at 26 dB there is a difference of 2,2 b/s/Hz for T_u varying between 0 an 2,5μs, whereas at 1 dB the variation is less than 0,1 b/s/Hz in the same interval. Therefore in the following only a high midrange SNR value of 16dB is considered.

The length of the "useful" OFDM symbol T_u is studied in Figure 4.5 where the capacity versus the CP length is plotted for T_u varying from 10μs to 160 μs and the PDP is PedB. It is noted that T_u only has little influence on the optimal CP length. However the longer T_u, the less sensitive the capacity is to a non optimal CP length (that is too short or too long). I.e. if $T_g = 8\mu s$ then with $T_u = 160\mu s$ the capacity is only reduced by 0,2 b/s/Hz from the maximum achievable performance. On the
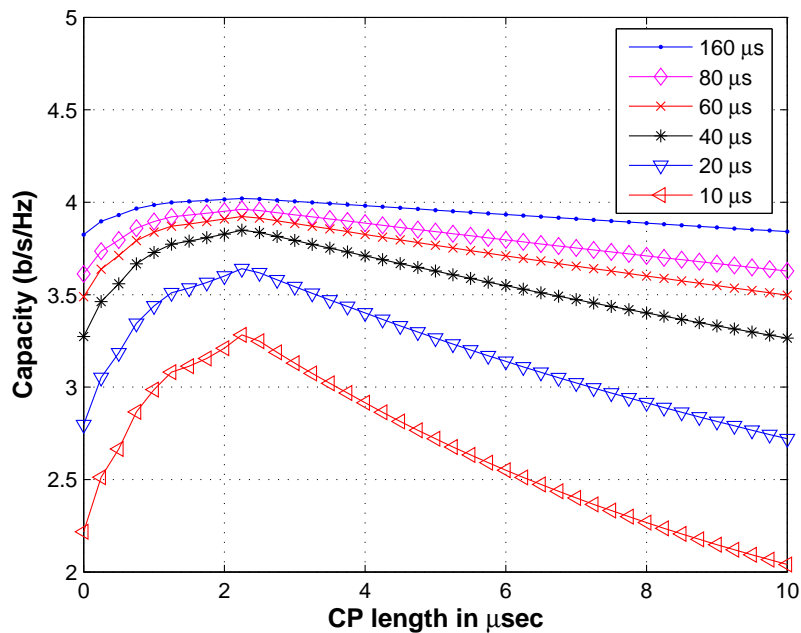
Figure 4.5: Influence of useful OFDM symbol length T_u on CP length T_g. Capacity for different received signal powers, PDP= PedB, Eb/No=16dB

other hand, with $T_u = 10\mu s$ the loss would be more than 1,0 b/s/Hz.

In Figure 4.6, the four exponentially decaying PDPs of table 4.1 are plotted. It is noted that the optimal CP length increases as τ_{rms} increases. This result has often been used as a design guideline in common literature. Yet when comparing HT [46] and VehB [16] of respectively τ_{rms} of 3000 and 4000 ns with their exponential decaying counterparts at same τ_{rms} , it is noted that the optimal CP length can significantly vary from profile to profile. I.e. for the HT PDP, the optimum T_g is 1,1μs, but for the E3000 PDP it is 9,8 μs. Hence linear dependency is not always true between optimal CP length and τ_{rms} and the entire PDP must be considered for proper evaluation.

Discussion

In order to avoid system signaling overhead to control a variable CP length, one single constant CP value is preferable. This length should give the best average performance. The highest capacity is achieved with a 1 path PDP and no CP.
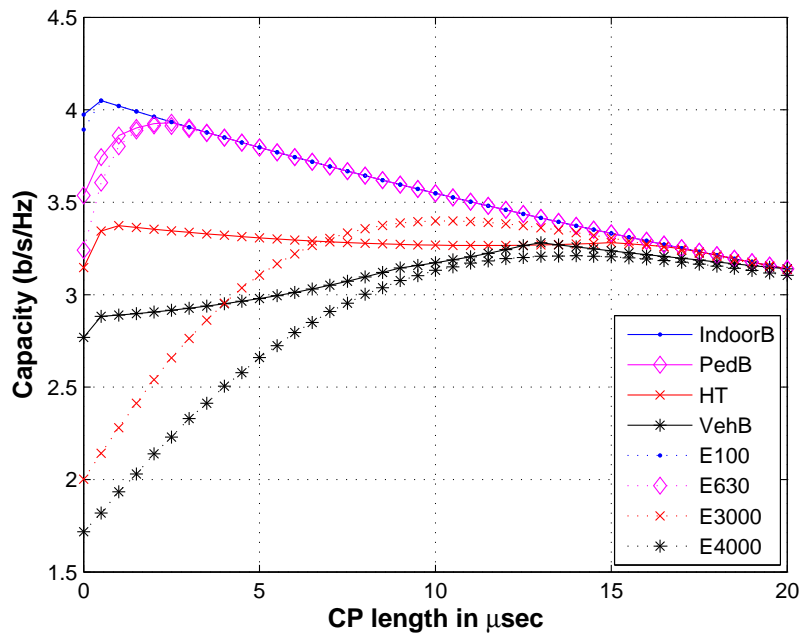
Figure 4.6: Influence of the PDP on CP length T_g. Capacity for different channel profiles, Eb/No=16dB

However, for a dispersive channel, a CP length not covering the full CIR will always lead to a loss. This loss can be divided in two components: the loss due to SEL and the loss due to self-interference. The choice of a single CP length will be a tradeoff between how much permanent SEL the system can accept and how much "worst-case interference" can be allowed. This tradeoff can be seen in Figure 4.7. We assume that the E4000 is the worst-case scenario. A CP length of 4 μs will give a capacity of 2,4 b/s/Hz whereas a CP length of 14,0 μs will perform better with a capacity of 3,2 b/s/Hz. According to the radio channel measurements of [56] τ_{rms} is smaller than 2,71 μs in 95 % of the time and in average would be of 0,5 μs to 0,9 μs. Therefore we recommend a CP length for the type of environment that is targeted. In most urban and indoor cases a length of 4 to 5 μs is more than sufficient especially when $T_g = 66.67$ μs. However when large delay spreads are present like the E3000 or E4000 the CP should be much longer and values of 14 to 16 μs should be adopted for optimal performance.
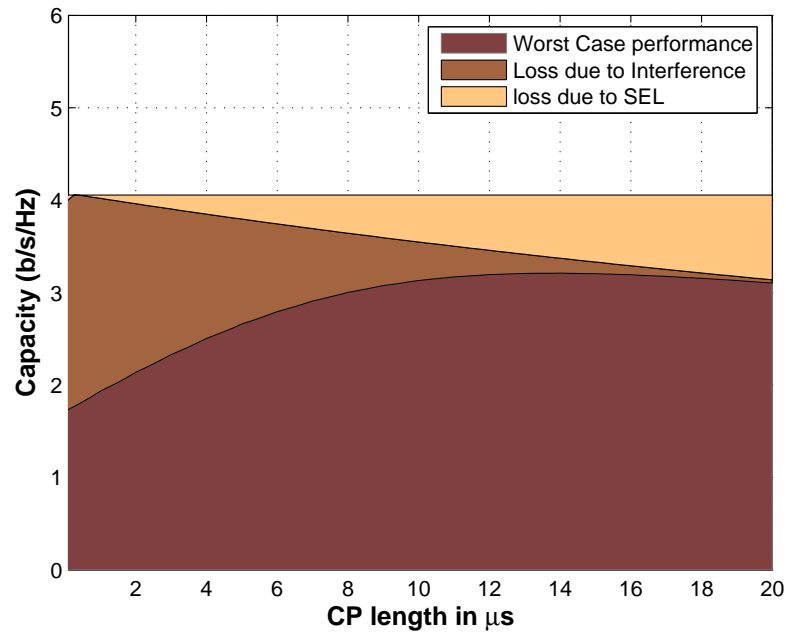
Figure 4.7: On the efficiency of the CP to cope with multipathT_g. , Eb/No=16dB, $T_u = 66, 67\mu s$, PDP= E4000

4.4 Conclusion

In this chapter we have studied the influence of CP length on SISO OFDM system capacity with LTE based parameters, when using a single tap equalizer in the receiver. The results showed that if only one CP length is to be chosen, then a good tradeoff value would be in the range 4 to 5 μs as high SNRs are mostly observed in Urban areas and the PDP lengths are not to large. This would still give relatively acceptable performance in long delay areas as the expected SNRs are lowered. Two different SINR models were proposed and proved to give same results. The influence of different parameters on the CP length design were analyzed.

First, it was shown in the study that the received SNR increased the sensitivity of the Capacity to the CP length. This can be interpreted as: Tx power and other cell interference affect the capacity. A higher Tx power will increase the sensitivity to a correct CP length and thereby increase the CP length. On the other hand, higher other cell interference will decrease the sensitivity to CP and its length could be reduced.

Secondly, it was shown that the duration of the useful OFDM symbol didn't impact the optimal CP length significantly. However it impacted the capacity loss due to a CP being too long or too short. Therefore the useful OFDM symbol should be as long as the system design allows.

In a third step, the RMS delay spread of a PDP turns out not to be a sufficient statistic to determine the optimal CP length. The whole PDP of the channel shall be considered. Large variations of optimal CP length can be observed for PDPs having equal RMS delay spread.

More areas remain for future study. Capacity analysis based on SINR analysis for different channel environments, was used as quality measure to determine the optimal CP length. A fixed loss from the shannon limit was adopted, yet larger and more detailed link simulation study could increase the accuracy of the results. Also the effect of MIMO techniques is also an important topic for further investigation in a LTE context. Finally interference cancelation techniques should be considered. Some of these techniques are treated in chapter 8 of this thesis.

Chapter 5

Channel Estimation in OFDM and LTE

5.1   Introduction

In the previous chapters the OFDM signal has been modeled at different levels and system parameter design has been studied. The simulation results assumed the Channel Transfer Function (CTF) to be known to the receiver for equalization. Thereby the results have been used for best-case performance evaluation. When more realistic results are desired and receiver algorithm design is considered, channel estimation needs to be studied. In a classical CP-OFDM receiver with coherent detection, the CTF needs to be estimated in order to compensate for channel distortion prior to demodulation. The accuracy of the estimator influences greatly the total system performance. Particularly the sensitivity is increased with higher order modulation schemes or higher SNR's. Channel estimation techniques can be separated in the ones operating on the frequency response of the OFDM symbol (signal after receiver FFT) and the ones employing time domain correlation algorithms. The latter will not be the scope of the study in this thesis. Among the algorithms operating on the spectrum of the received OFDM symbol, different strategies have been studied in literature.

Pilot based Channel Estimation (PACE), the most common technique, is based on Pilot Symbol-Assisted Modulation (PSAM) where known information to the

transmitter and receiver is inserted at given subcarriers. For each received pilot subcarrier the corresponding CTF value is estimated. Then, the CTF estimate for the information-carrying subcarriers, is derived from these pilot-based CTF estimates by means of interpolation between them such as [63], [66], [72], [73], [74] and [75].

Decision Directed Channel Estimation (DDCE) techniques, such as the ones described by Hanzo, in [26] are based on the concept of generating an initial *a posteriori* least-squares CTF estimate of remodulated subcarrier data symbols. This estimate is then enhanced through signal processing such as 1-D Minimum Mean Square Error (MMSE) [67], [68] or 2-D MMSE [78] estimator to give an improved *a posteriori* CTF estimate. This improved *a posteriori* CTF estimate is then used as an *a priori* channel estimate for the demodulation of the next times lot OFDM symbol. DDCE techniques such as [86] have been studied using channel predictors [80]. However such DDCE techniques suffer from some drawbacks that can prevent them from being used in real life receivers. These are mainly poor compatibility with frequency hopping schemes, discontinuous transmission and Frequency Domain Link Adaptation (FDLA). Also and increased complexity is observed compared to classical linear PACE techniques more especially in the case of MIMO transmission.

Different blind or semi-blind channel estimation techniques have also been studied as in [90], [91] and [92]. Although the pilot overhead is removed with these techniques, blind estimation suffer from the need for training period or very high computational complexity.

In this chapter the channel estimation problematic will be addressed. First applied to the generic PSAM OFDM scenario; then more specifically elaborated for LTE.

5.2 The physical radio channel model

5.2.1 General description and considerations

The radio propagation environment experienced by the signal transmitted from a BS to a MS clearly places the fundamental limitations on the performance of the

studied communication system. The radio wave propagation largely depends on the frequency band of transmission. In the case of LTE the carrier frequency will be of 2GHz order and therefore characterized as an Ultra High Frequency (UHF) [30]. In that case communication takes place via direct and reflected components of the radio wave. The wave propagation will be affected by reflections due to both ground, natural and man-made obstacles. Also diffraction over buildings and hilltops are to be taken into account.

When looking at received signal strength over time one can distinguish between long-term and short-term variations. The short term are classically described by the *multipath* fading phenomena. The long term variations are described as *slow fading* and correspond to gross variations in the terrain profile between BS and MS over the MS in motion. **In this thesis we restrict our work to short-term variations.**

Rayleigh distribution is usually a good approximation for the received signal envelope. However when a strong direct path is present, the distribution departs significantly from Rayleigh and can better be described by a Ricean distribution. **In this thesis for simplicity, we restrict our work to Rayleigh fading for each tap of the multipath CIR.**

Apart from the delay domain, signal fading description can also be done in the frequency domain. *Frequency-flat fading* is said to exist if all frequency components within the signal bandwidth behave similarly. *Frequency-selective fading* is said to exist if the signal considered occupies a bandwidth larger than the bandwidth over which spectral components are affected in a similar way. The extent of the correlation depends on the spread of the delays in time since the phase shift arise from the excess path delays. The bandwidth over which the spectral components are affected in a similar way is known as the *coherence bandwidth*.

A time-frequency characterization of the multipath phenomena is illustrated in Figure 5.1. The perceived channel is then described by a time varying Channel Impulse Response (CIR) and by a time varying Channel Transfer Function (CTF).
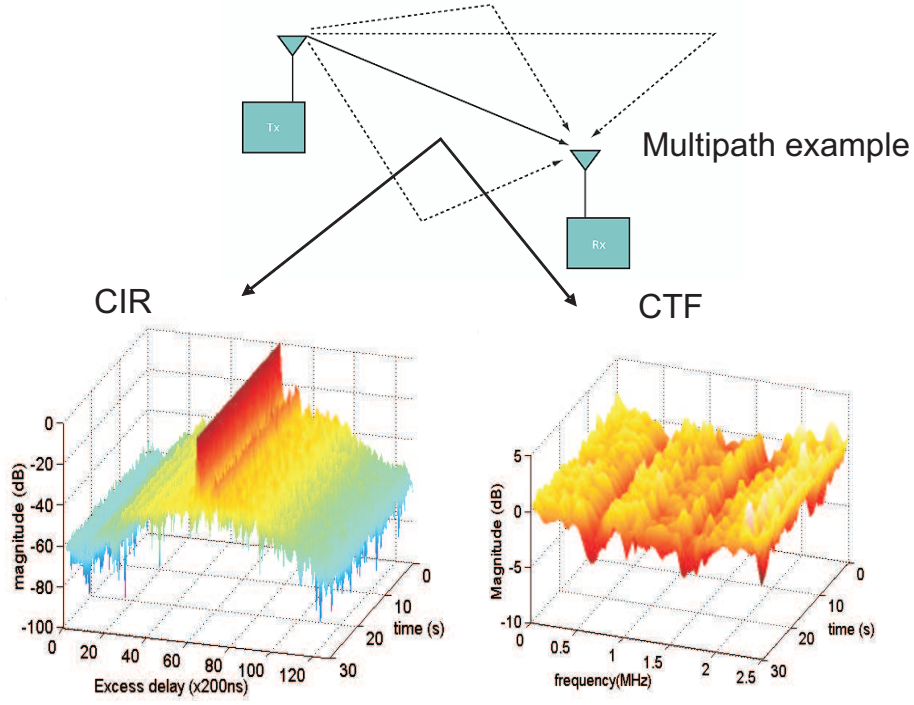
Figure 5.1: Example of the time varying multipath described by a time varying CIR and CTF

5.2.2 Stochastic approach

The convolution of the time varying multipath CIR with the transmitted OFDM signal has been described in section 2.2. Yet in this following sub-section a stochastic characterization of the multipath propagation will be given.

At a given receiver antenna, we observe the arrival of different attenuated and delayed versions of the transmitted signal du to multipath. The complex baseband CIR can then be expressed by:

$$g(t,\tau) = \sum_i \alpha_i(t)e^{-j2\pi f_c\tau_i(t)}\delta[\tau - \tau_i(t)] = \sum_i \alpha_i(t)e^{-j\theta_i(t)}\delta[\tau - \tau_i(t)] \qquad (5.1)$$

In this model, the attenuation factor $\alpha_i(t)$ has a corresponding i^{th} propagation delay $\tau_i(t)$. The phase value $\theta_i(t) = 2\pi f_c\tau_i(t)$ depends on the carrier frequency f_c which is in the order of 2GHz in this study. Small changes of tap delays $\tau_i(t)$ will result in large phase value variations. As stated earlier each tap of the CIR is modeled as a zero-mean Gaussian random process with respect to t, and the envelope $|g(t,\tau)|$ is Rayleigh distributed.

June 18, 2008

The different correlation functions and associated fourier transforms will be given in the following in order to describe statistically the radio channel as shown in [26].

Auto-Correlation Function (ACF) of the CIR: $r_g(\Delta t, \tau)$

The ACF can be expressed as:

$$r_g(\Delta t, \tau_1, \tau_2) = \mathrm{E}\{g(t, \tau_1), g^*(t - \Delta t, \tau_2)\} \tag{5.2}$$

This expression assumes that the CIR process is Wide-Sense-Stationary (WSS) [31], meaning that the mean value of the process is time invariant and its auto-correlation is only a function of the time difference Δt. If the amplitudes and phase shifts of the different time delays $\tau_1 \neq \tau_2$ are uncorrelated, it follows:

$$r_g(\Delta t, \tau_1, \tau_2) = r_g(\Delta t, \tau_1)\delta(\tau_1 - \tau_2) \tag{5.3}$$

The PDP is then given as $r_g(0, \tau) = r_g(\tau)$ giving the average power output channel for a given tap delay τ.

Spaced-time spaced-frequency correlation function: $r_h(\Delta t, \Delta f)$

The time variant CTF is denoted by $h(t, f)$ and is obtained by taking the Fourier transform of the CIR:

$$h(t, f) = \int_{-\infty}^{\infty} g(t, \tau)e^{-j2\pi f\tau} d\tau \tag{5.4}$$

The auto-correlation function of $h(t, f)$, namely $r_h(\Delta t, f_1, f_2)$, is then given as the Fourier transform of the auto-correlation function of the CIR taken with respect to τ:

$$\begin{aligned} r_h(\Delta t, f_1, f_2) &= \mathrm{E}\{h(t, f_1)h^*(t - \Delta t, f_2)\} = \mathcal{F}_{\tau \to f}\{r_g(\Delta t, \tau)\} \\ &= r_h(\Delta t, \Delta f), \end{aligned} \tag{5.5}$$

and is also known as the spaced-time spaced-frequency correlation function of the channel. Given the assumption of WSS it comes that this function is dependent on Δf rather than specific frequency values. For $\Delta t = 0$, which corresponds to considering the CTF's associated with a specific OFDM symbol, the ACF $r_h(\Delta t, \Delta f)$

simplifies to $r_h(0, \Delta f) = r_h(\Delta f)$, and which in turn is related to the multipath intensity profile by:

$$r_h(\Delta f) = \mathcal{F}_{\tau \to \Delta f}\{r_g(\tau)\} \tag{5.6}$$

A definition of the *coherence bandwidth* $(\Delta f)_c$ of the channel in the range $-(\Delta f)_c/2 \leq \Delta \leq (\Delta f)_c/2$ of frequencies over which the CTF exhibits significant correlation, can be given from this previous relationship. The coherence bandwidth is related to the multipath spread (maximum excess delay)by:

$$(\Delta f)_c \approx \frac{1}{T_{med}} \tag{5.7}$$

Fourier Transform of the CIR's ACF with respect to the multipath delay and space-time variables: $S_h(f_d, \Delta f)$

Further characterization of the channel is done by taking the Fourier transform of $r_h(\Delta t, \Delta f)$ with respect to the time difference:

$$S_h(f_d, \Delta f) = \mathcal{F}_{\Delta t \to f_d}\{r_h(\Delta t, \Delta f)\} \tag{5.8}$$

In the case of $\Delta f = 0$, this function simplifies to $S_h(f_d, 0) = S_h(f_d)$, known as the *Doppler power spectrum* of the channel. Analogously to the definition of the *coherence bandwidth* and the related multipath spread, we can define the *Doppler Spread* B_D of the channel as the range $-B_D/2 \leq f_d \leq B_D/2$ of frequencies over which $S_h(f_d)$ exhibits significant values. We can express it inverse as the *coherence time* as:

$$t_{cor} \approx \frac{1}{B_D}. \tag{5.9}$$

5.3 PACE principles

The following will be dealing with Pilot-symbol Aided Channel Estimation (PACE) in doubly selective physical channels in a downlink OFDM LTE context. Transmitting a radio signal over a multipath fading channel, the receiver signal will have unknown amplitude and phase variations. When using a classical OFDM receiver as described in [59], coherent demodulation needs a CTF estimate at each OFDM symbol. Coherent detection of the received signal requires accurate channel estimation

to be performed. When dealing with PACE a subset of transmitted subcarriers will be used as pilot symbols. From the known received pilots, initial estimates of the CTF at the pilot subcarriers can be obtained. However interpolation between the initial estimates is required to obtain the full CTF, giving also a channel estimate at the data subcarrier positions. These pilots will however occupy resources that could be used for data transmission. Such insertion impacts directly as spectral efficiency loss of a system. The idea is then to minimize the pilot overhead without significantly deteriorating the CTF estimate quality. One way of seeing the pilot spacing in time and frequency direction is a sample grid of the physical channel, which itself can be more or less selective. The optimum spectral efficiency would then be achieved by adapting the pilot spacing grid to the perceived physical channel conditions as shown in [60].

In the following a signal model will first be explained to introduce the initial CTF estimation at pilot positions. Then the optimum linear interpolator will be presented in the form of a two dimensional Wiener filter. Finally different pilot constellations will be discussed and the optimum constellation presented. This section will show the need for an algorithmic study for practical interpolators as well as pilot spacings in a LTE context elaborated in chapter 6 and chapter 7.

5.3.1 Signal model

When OFDM is ICI and ISI free it can be modeled as follows. Recalling equation 2.33 the signal after FFT is:

$$\mathbf{z}_m[k] = \mathbf{h}_m[k]\mathbf{d}_m[k] + \mathbf{w}_m[k],$$

with:

m: index for the considered OFDM symbol

k: index for the considered subcarrier

$\mathbf{h}_m[k]$: channel transfer function coefficient

$\mathbf{d}_m[k]$: transmitted symbol

$\mathbf{w}_m[k]$: AWGN contribution

The classical one tap equalizer from equation is also recalled:

$$\hat{\mathbf{d}}_m[k] = \frac{\mathbf{z}_m[k]}{\hat{\mathbf{h}}_m[k]}, \tag{5.10}$$

with:

$\hat{\mathbf{d}}_m[k]$: transmitted symbol estimate

$\hat{\mathbf{h}}_m[k]$: channel transfer function estimate
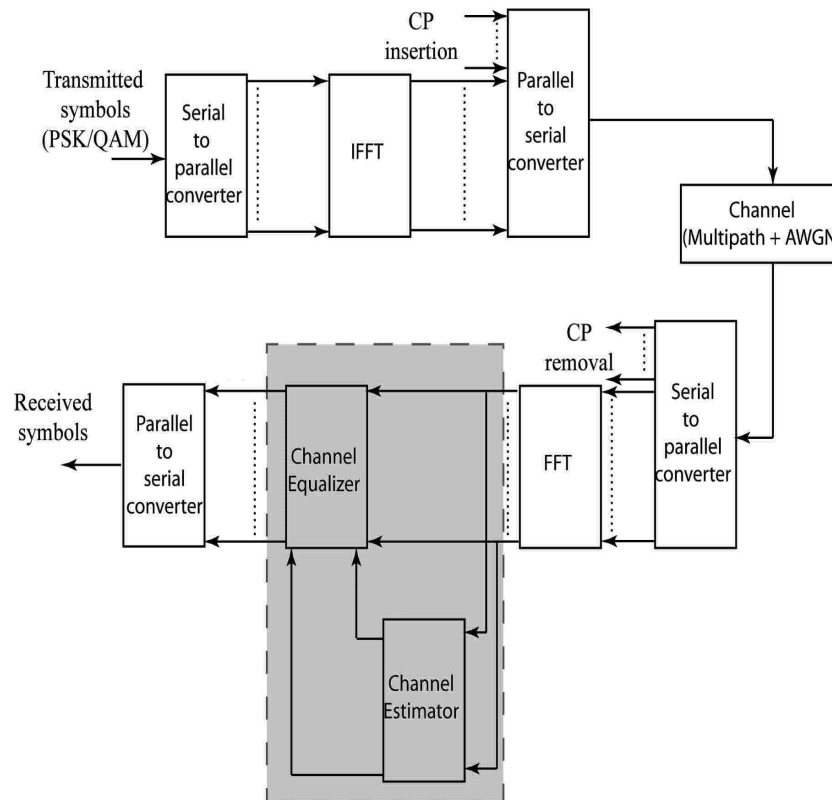
Figure 5.2: Simplified block diagram of a baseband OFDM transmitter receiver system

Figure 5.2 shows a simplified baseband block diagram of an OFDM transceiver. The receiver part dealing with channel estimation is highlighted in gray. It focuses on the signal after the CP has been removed and the FFT performed. The obtained CTF estimate is then used for the classical OFDM single tap equalizer.

5.3.2 The optimum linear 2D interpolation algorithm

The optimum linear interpolator in the Minimum Mean Square Error (MMSE) sense, has been derived for PACE by Hoeher in [63] with the 2-dimensional Wiener filter. This a result also valid in the case when the amount of pilot symbols available for interpolation is limited [84]. It follows that the channel estimates are computed from a block of OFDM symbols also called the *Channel Estimation Block* (CEB). The pilot of symbols will all contribute with an initial Least Squares (LS) estimate by:

$$\mathbf{h}_{CEB,ls}[n] = \frac{\mathbf{z}_m[k]}{\mathbf{d}_m[k]} \quad , \quad n = \lceil \frac{k}{\Delta p_f} \rceil + \lceil \frac{m}{\Delta p_t} \rceil \tag{5.11}$$

where, Δp_t and Δp_f are the pilot spacing in respectively the time and frequency direction, $\mathbf{h}_{CEB,ls}$ is the LS estimate vector of length $N_p = N_{pf} \cdot N_{pt}$, with N_{pf} and N_{pt} being the number of pilot subcarriers in respectively frequency and time direction. Not that the set m, k are chosen only for pilot subcarrier positions. The initial LS estimates of the channel at the pilot positions then lead to a MMSE estimate of the CTF expressed by:

$$\mathbf{h}_{CEB,mmse} = \mathbf{C}_{CEB}\mathbf{h}_{CEB,ls} \tag{5.12}$$

In this expression illustrated in figure 5.3, $\mathbf{h}_{CEB,mmse}$ is the MMSE CTF estimate for all subcarriers in the CEB, and $\mathbf{C}_{CEB}$ is the Wiener interpolation matrix of dimensions $((N_u\alpha_{ceb}) \cdot (N_p))$, where α_{ceb} is the number of OFDM symbols in one CEB. The MMSE finite length interpolation filter can be expressed by one matrix as derived in [26], by:

$$\mathbf{C}_{CEB} = \mathbf{R}_{\mathbf{h}_{CEB}\mathbf{h}_{CEB,ls}} \mathbf{R}_{\mathbf{h}_{CEB,ls}\mathbf{h}_{CEB,ls}}^{-1}, \tag{5.13}$$

with,

$$\begin{aligned} \mathbf{R}_{\mathbf{h}_{CEB}\mathbf{h}_{CEB,ls}} &= \mathrm{E}\{\mathbf{h}_{CEB}\mathbf{h}_{CEB,ls}^H\} \\ \mathbf{R}_{\mathbf{h}_{CEB,ls}\mathbf{h}_{CEB,ls}} &= \mathrm{E}\{\mathbf{h}_{CEB,ls}\mathbf{h}_{CEB,ls}^H\} \end{aligned} \tag{5.14}$$

The vector $\mathbf{h}_{CEB}$ contains the perfect channel values at all subcarrier positions. It is defined as $\mathbf{h}_{CEB}[n] = \mathbf{h}_m[k]$ with $n = k + mN_u$.

As previously stated the 2D wiener is the optimum linear solution. However as the amount of pilots grow the computational complexity of the interpolation filter
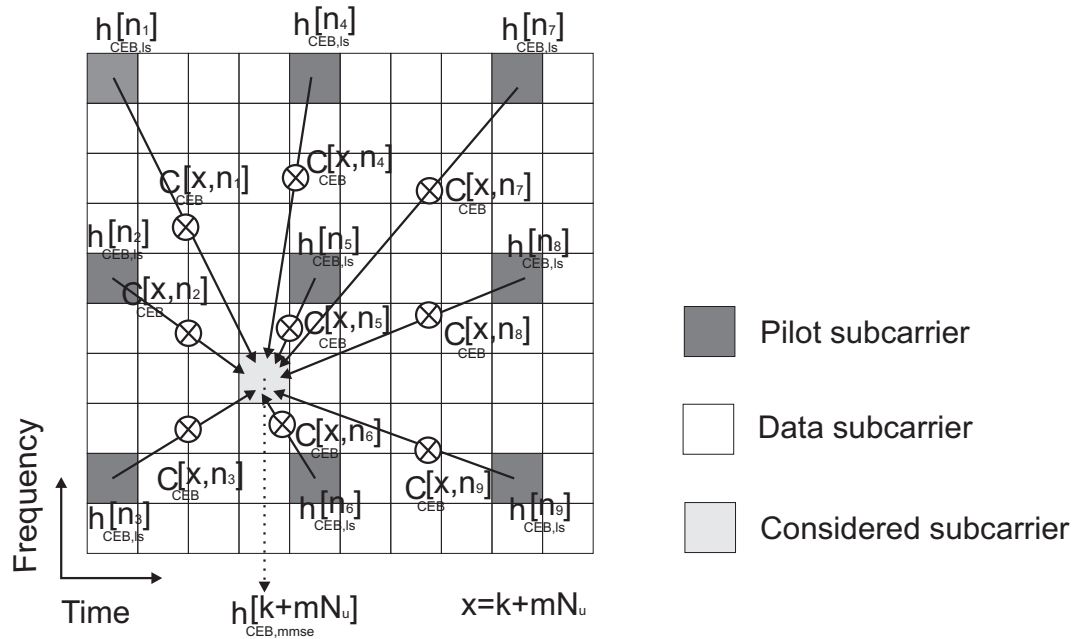
Figure 5.3: 2D FIR Wiener channel estimation for the mth CEB and n^{th} subcarrier

can by quite large. In [63] it was shown that two cascaded orthogonal 1-D filters are simpler to implement and show to be virtually as good as a true 2-D filter.

One major drawback of the presented optimum solution is that the knowledge of channel statistics is required. In a real receiver the channel characteristics will change over time and need therefore to be tracked as in [70] and re-estimated. Also the covariance matrix $\mathbf{R}_{\mathbf{h}_{CEB,ls}\mathbf{h}_{CEB,ls}}$ of dimensions $(N_p \times N_p)$ has to be inverted whenever the statistics of the channel vary significantly. Such an inverse can be computationally prohibitive and different techniques are employed to lower the overhead of the Wiener filter such as [68, 76, 77]. Many interpolation algorithms have been proposed and studied in literature for PACE OFDM such as [63,66–68,71–75,78,79]. However to the authors it was not clear which one to use and what are the reasons for choosing one solution rather than another. More specifically with the upcoming LTE release 8 standard it is not clear what algorithm shall be implemented in a UE terminal. A thorough comparative study is **needed** and will be conducted in chapter 6.

5.3.3 Pilot schemes

Performance of channel estimation in OFDM systems is strongly related to the pilot signal. The use of pilot subcarriers eases the estimation of the channel coefficients, and as the pilot density increases the constraints to the estimator decrease. However pilot information is pure overhead and can therefore directly be considered as spectral efficiency loss. If the interpolator used is the two dimensional Wiener filter, with unlimited pilots, the MSE of the CTF only depends on the pilot density and not the pilot pattern as shown in [84]. In practice the number of pilots available for interpolation is limited and the optimal Wiener solution is to complex due to large computational complexity. When classical simple interpolators such as linear interpolation, Spline, Lagrange [60] [62] are used with a finite amount of pilots it was shown in [84] that, for a given pilot density, the optimum pilot pattern that minimizes the MSE of the CTF estimate is the diamond structure. The different proposed pilot structures can be depicted in Figure 5.4 and 5.5.

In practical systems such as LTE, an diamond structure with equidistant pilots is not necessarily the most desired solution. When using a two times one dimensional "cascaded interpolators" approach, the Nyquist-Shannon sampling theorem [85] can be stated in both time and frequency direction.

When considering the time direction the minimum pilot spacing to avoid aliasing is given by the relationship:

$$\Delta pt_{min} = \lfloor \frac{1}{B_D T_s} \rfloor, \tag{5.15}$$

where B_D is the Doppler spectrum bandwidth and T_s is the sampling time.

When considering the frequency direction the minimum pilot spacing to avoid aliasing is given by the relationship:

$$\Delta pf_{min} = \lfloor \frac{1}{T_{med}\Delta_f} \rfloor, \tag{5.16}$$

where T_{med} is the length of the maximum excess delay and Δ_f is the subcarrier spacing.

Due to the variations of the channel time and frequency correlation characteristics, there is no single optimal pilot spacing to obtain for a system. An adaptive
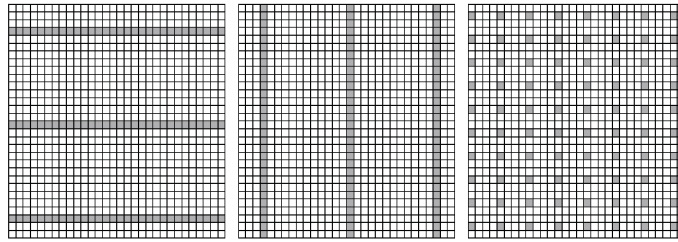
Figure 5.4: Classical pilot grids
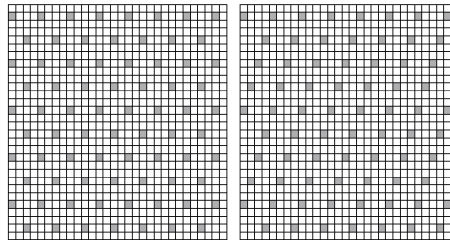
Figure 5.5: Diamond and diagonal pilot grids

pilot spacing would be preferred from a spectral efficiency point of view, however this would introduce an undesired signalling complexity and overhead. Also different practical considerations such as latency requirements and limited buffering in a UE receiver will influence the choice of pilot spacing. An in depth study of pilot scheme and constellation is **needed** in order to propose a pilot structure for LTE . Such a study will be conducted in chapter 7 and the results compared to the actual standardization choices made.

5.4   Conclusion

This chapter presented the technical background for the choice of PACE in many OFDM systems. Linear PACE presents numerous advantages compared to DDCE and blind channel estimation which make it a popular scheme. A stochastic description of the radio channel to be estimated was given, providing statistical indicators for system pilot design. The principle of pilot based channel estimation was presented, and more specifically the optimum linear Wiener filter elaborated. Also the optimal diamond pilot constellation scheme was presented. However it was also

shown that for a practical system such as LTE many considerations such as system signalling complexity, computational complexity and latency requirements had to be taken into account. This leads to a need for thorough algorithm investigation as well as pilot constellation and spacing studies which have respectively been carried out in chapter 6 and chapter 7.

Chapter 6

Frequency direction interpolation

In the 3GPPP LTE specifications [4] [5] no channel interpolation algorithms are dictated or recommended, leaving this issue open to the UE manufacturers. So far different studies have been done for other PACE OFDM based standards such as for the 802.11 or 802.16 families. Even though the algorithms studied in this chapter aren't directly novel, their behavior has not been studied previously in a LTE context.

In this chapter, "state-of-the-art" solutions for frequency direction PACE are evaluated by first performing a survey of Linear algorithms. The studied solutions are then reformulated in a discrete generic matrix-vector notation and classified according to their a priori assumptions on channel statistics. An analytical study is conducted leading to a generalized closed formulation. Performance is evaluated through Monte Carlo simulations. Finally, a complexity study evaluates the computational needs of the studied solutions.

6.1 Introduction

As stated in chapter 5 Hoeher showed in [63] that the two-dimensional interpolation problem of PACE could be solved by using two cascaded orthogonal one-dimensional filters, giving virtually no performance loss compared to the two-dimensional filter. The latency requirements of standards such as LTE or IEEE 802.16e limit the pilot span available for channel estimation in the time direction to a low number of

samples. This increases the importance of the frequency-direction interpolation, which is the focus of this chapter.

Much attention has been given to this topic showing that the performance trade-off of the algorithms depends on the relationship between the Power Delay Profile (PDP) properties and the frequency-domain pilot spacing. Deterministic approaches have, so far, been separated into time- and frequency-domain solutions. Deterministic time-domain solutions are: the Time-Domain Least Squares (TDLS) [66, 71], the Maximum Likelihood (ML) approach [72, 79] and the Noise Reduction Algorithm (NRA) [73]. Deterministic frequency-domain methods are Spline, Gaussian or Lagrange interpolation, and require higher pilot overhead to achieve an acceptable performance [74]. Bayesian approaches such as the Minimum Mean Squared Error (MMSE) estimator in time domain and/or frequency domain have been proposed in [63,66], with complexity reduction by Singular Value Decomposition (SVD) suggested in [68].

Different comparisons of these algorithms have been done. Van de Beek studies the TDLS versus the MMSE approach in a non-sample-spaced (NSS) channel [66], however he assumes a full bandwidth system with pilots in all subcarriers, thereby avoiding the leakage effect on the TDLS algorithm. Edfors compares a low rank reduction of the MMSE with a Discrete Fourier Transform (DFT) based implementation versus an SVD based [68] showing the superiority of the SVD for NSS channels. However the MMSE can be implemented with a low complex non-DFT based matrix, avoiding leakage, as shown by Yang [75]. Morelli compares the ML with the MMSE approach [79] using virtual subcarriers but uses a sample-spaced (SS) channel which favors the ML performance as no leakage is present.

In general, parameters such as the FFT size, number of virtual subcarriers, pilot spacing, PDP and whether the channel is sample-spaced or not, have a critical impact on formulation, performance and complexity of the studied algorithms. A clear overview is therefore difficult to achieve from literature, and a comprehensive comparison is needed.

The major contribution of this chapter is to provide a framework for the choice of a channel estimation algorithm for the upcoming PACE

OFDM-based standards. In this study we derive a uniform algorithm and Mean Squared Error (MSE) formulation, covering all studied algorithms and thereby facilitating a generic performance comparison. Three main effects will be studied: the impact of a priori knowledge in a full bandwidth system with a SS channel, the effect of virtual subcarriers and the effect of a NSS channel. Performance simulations are conducted in a LTE context. The importance of using an interpolation algorithm insensitive to the channel statistics at the receiver such as the Robust Wiener filter (RW) [78] is essential to avoid the leakage effect due to NSS channel used with DFT based solutions. However it will be demonstrated that knowledge of the exact CIR tap delay locations is a key parameter for low MSE results.

6.2 Classification of Channels estimation Algorithms

Why doing a classification of algorithms? What is the goal and the usefulness of such? The idea is to have a framework for a fair comparison of state of the art solutions. This would then help to choose a channel estimation algorithm in a system like LTE. On top of this, when new algorithms are developed, their evaluation is eased as well as comparison with the state of art solutions. A comparison by inspection would be sufficient to highlight the differences with the most similar solution and thereby give an intuitive performance difference.

So far, Hanzo et. al. has made a classification of various 2D-FIR Wiener related channel estimation approaches in [26]. These approaches use standard techniques known from literature of multidimensional signal processing. This classification describes complexity reduction techniques of the optimal 2D-FIR Wiener approach, where the most relevant are:

- Hoeher proposed to select a subset of nearest pilot channel estimates based on a derived metric [63, 64].

- Hoeher showed that "2 times 1D" interpolation should be used instead of "pure 2D" interpolation [63, 64].

- Edfors derived a low rank approximation technique with the aid of a Singular

Increasing A priori knowledge	Time domain algorithms	Frequency domain algorithms
None $\{\varnothing\}$	TD-LS	Linear Interpolation Polynomial, Lagrange, Spline Rw_1, Interpolation
Maximum Excess Delay $\{T_{med}\}$	ML	Rw_2
Signal To Noise Ratio $\{SNR\}$	NRA	Rw_3
PDP tap delays $\{\tau_0, \tau_1, ..., \tau_{Nt-1}\}$	ENRA	-
PDP tap Gains $\{|a_0|, |a_1|, ..., |a_{Nt-1}|\}$	TD-MMSE	FD-MMSE (Wiener)

Figure 6.1: Classification of Linear Frequency direction interpolation channel estimation algorithms in OFDM

Value Decomposition [68].

- Van de Beek et. al. proposed the use of a DFT instead of the unitary linear transform employed int the SVD-based filter [66].

More recently Tolochko focused his work on MMSE based algorithms with an emphasis on statistical parameter estimation in [69].

Despite the previous work, an in depth comparison, including time domain and frequency domain approaches, is not known to the author. Different limited comparisons have been made in several publications, such as in [66, 68, 75, 79], but in section 6.1, none of these comparisons give a clear overview over the existing linear solutions. Other non-MMSE based techniques should therefore also be considered. A broader classification is then needed, and will be carried out in the following. A priori knowledge together with a separation into time domain and frequency domain approaches will determine the "type" of algorithm considered. Figure 6.1 illustrates how the algorithms can be classified into time and frequency domain approaches, also the dependency of the studied algorithms on a priori information is brought to evidence.

6.3   Estimation Algorithms

All the different channel estimators are based on an initial Least Squares (LS) estimate of the channel response at pilot positions $\mathbf{h}_{ls} \in \mathbb{C}^{N_p}$, which is obtained as:

$$\mathbf{h}_{ls} = \mathbf{D}_p^{-1}\mathbf{y}_p = \mathbf{h}_p + \mathbf{D}_p^{-1}\mathbf{w}_p \qquad (6.1)$$

It is assumed that the pilot symbols are M-PSK modulated with unit power, so that the noise in the LS estimate $\mathbf{D}_p^{-1}\mathbf{w}_p$ has the same statistical properties as $\mathbf{w}_p$. Furthermore, the number of pilot symbols N_p, is assumed to be larger than the normalized maximum excess delay of the channel, $\frac{\tau_{N_t-1}}{\tau_s}$.

In the following, two scenarios are considered:

Case 1   A SS-CIR scenario, where it is assumed that the delays τ_i are sample spaced on the same grid as the receiver and all $\frac{\tau_i}{\tau_s}$ are integer values.

Case 2   A NSS-CIR scenario, where it is assumed that the delays τ_i are not
sample spaced on the same grid as the receiver and some $\frac{\tau_i}{\tau_s}$ are not integer
values.

6.3.1   Sample-Spaced Channel

In a SS scenario, $\forall i \; \frac{\tau_i}{\tau_s} \in \mathbb{N}$, and the leakage matrix $\mathbf{L}$ reduces to:

$$\mathbf{L}[n, i] = \begin{cases} 1, & n = \frac{\tau_i}{\tau_s} \\ 0, & \text{otherwise} \end{cases} \tag{6.2}$$

and, consequently, the SS-CIR vector becomes:

$$\mathbf{g}[n] = \begin{cases} \alpha_i, & n = \frac{\tau_i}{\tau_s} \\ 0, & \text{otherwise} \end{cases} \tag{6.3}$$

In such conditions only N_t out of the N_{fft} elements of $\mathbf{g}$ will be non-zero. This
observation can be used to reduce the signal subspace dimension of $\mathbf{g}$ depending on
the a priori knowledge at the receiver. Using a generic notation, the CTFs at used
and pilot subcarriers can, respectively, be expressed as:

$$\mathbf{h}_u = \mathbf{F}_{ux}\mathbf{g}_x \tag{6.4}$$

$$\mathbf{h}_p = \mathbf{F}_{px}\mathbf{g}_x \tag{6.5}$$

where $\mathbf{g}_x \in \mathbb{C}^{N_x}$ is a subset of N_x elements of $\mathbf{g}$ including all the non-zero samples,
and $\mathbf{F}_{ux} \in \mathbb{C}^{N_u \times N_x}$ and $\mathbf{F}_{px} \in \mathbb{C}^{N_p \times N_x}$ are subsets of, respectively, $\mathbf{F}_u$ and $\mathbf{F}_p$ with
the columns corresponding to the elements included in $\mathbf{g}_x$. The exact definition of
these matrices and vectors will depend on the estimator used, specifically on the
a priori information about the channel that the estimator assumes. The different
studied algorithms can be written in the following generic formula:

$$\mathbf{h}_{est} = \mathbf{F}_{ux}\mathbf{g}_{est} = \mathbf{F}_{ux}\mathbf{M}_{est}\mathbf{h}_{ls} \tag{6.6}$$

which will be specified for each estimator next.

Time-Domain Least Squares

The TDLS estimator was studied in [66, 71]. This estimator assumes no a priori
knowledge of the channel, and estimates $N_x = N_p$ samples of $\mathbf{g}$, corresponding to

$\mathbf{g}_p[n] = \mathbf{g}[n]$ for $0 \leq n \leq N_p - 1$. The formulation of TDLS is:

$$\mathbf{h}_{tdls} = \mathbf{F}_{up}\mathbf{g}_{tdls} = \mathbf{F}_{up}\mathbf{F}_{pp}^{-1}\mathbf{h}_{ls} \tag{6.7}$$

where $\mathbf{F}_{pp} \in \mathbb{C}^{\mathrm{N}_p \times \mathrm{N}_p}$ and $\mathbf{F}_{up} \in \mathbb{C}^{\mathrm{N}_u \times \mathrm{N}_p}$ correspond, respectively, to $\mathbf{F}_{pp}[m, n] = \mathbf{F}_p[m, n]$ and $\mathbf{F}_{up}[k, n] = \mathbf{F}_u[k, n]$ for $0 \leq n \leq N_p - 1$. For the TDLS estimator, then, $\mathbf{M}_{est} = \mathbf{F}_{pp}^{-1}$. Note that $\mathbf{F}_{pp}$ is always invertible due to the Vandermonde structure of the DFT matrix [71]; however, in a Partial Bandwidth scenario, this matrix can become ill-conditioned depending on the number of virtual subcarriers.

Maximum Likelihood

The ML estimator, proposed in [72, 79], assumes that the receiver knows the CIR length, i.e, the last channel CIR tap's delay τ_{N_t-1}, and only estimates the $N_x = N_s = \frac{\tau_{N_t-1}}{\tau_s} + 1$ first samples of the SS-CIR, corresponding to $\mathbf{g}_s[n] = \mathbf{g}[n]$ for $0 \leq n \leq N_s - 1$. The ML estimator is expressed as:

$$\mathbf{h}_{ml} = \mathbf{F}_{us}\mathbf{g}_{ml} = \mathbf{F}_{us}(\mathbf{F}_{ps}^H\mathbf{F}_{ps})^{-1}\mathbf{F}_{ps}^H\mathbf{h}_{ls} \tag{6.8}$$

where $\mathbf{F}_{ps} \in \mathbb{C}^{\mathrm{N}_p \times \mathrm{N}_s}$ and $\mathbf{F}_{us} \in \mathbb{C}^{\mathrm{N}_u \times \mathrm{N}_s}$ correspond, respectively, to $\mathbf{F}_{ps}[m, n] = \mathbf{F}_p[m, n]$ and $\mathbf{F}_{us}[k, n] = \mathbf{F}_u[k, n]$ for $0 \leq n \leq N_s - 1$. In this case, $\mathbf{M}_{est} = (\mathbf{F}_{ps}^H\mathbf{F}_{ps})^{-1}\mathbf{F}_{ps}^H$. Similarly to the case of the TDLS estimator, the matrix $\mathbf{F}_{ps}$ is always of full column rank (for $N_p \geq N_s$), implying that $\mathbf{F}_{ps}^H\mathbf{F}_{ps}$ is of full rank. However, in the presence of virtual subcarriers this matrix can become ill-conditioned, as for the TDLS estimator. In appendix C.3 more details on the properties of $\mathbf{F}_{ps}^H\mathbf{F}_{ps}$ are given.

Noise Reduction Algorithm

As a solution to the ill-conditioning problems of the previous estimators, a small value can be added to the diagonal of the matrix to be inverted [73], thus avoiding numerical instability. This is also known as Tikhonov regularization [81], a method to improve the conditioning of an ill-posed problem. This modification leads to the following expression of the NRA:

$$\mathbf{h}_{nra} = \mathbf{F}_{us}\mathbf{g}_{nra} = \mathbf{F}_{us}(\mathbf{F}_{ps}^H\mathbf{F}_{ps} + \gamma_{nra}\mathbf{I}_s)^{-1}\mathbf{F}_{ps}^H\mathbf{h}_{ls} \tag{6.9}$$

where $\mathbf{I}_s$ is the identity matrix of size N_s, and γ_{nra} is a positive scalar value. From (6.9), it follows that $\mathbf{M}_{est} = (\mathbf{F}_{ps}^H \mathbf{F}_{ps} + \gamma_{nra}\mathbf{I}_s)^{-1}\mathbf{F}_{ps}^H$. In a Full Bandwidth scenario with evenly spaced pilot subcarriers, it can be shown that the optimum value is $\gamma_{nra} = N_s \sigma_w^2$. Furthermore, the NRA with this value is equivalent to the robust Wiener filter estimator proposed in [68, 78], as it is proven in appendix C.1. The effect of variation of this value on MSE is given in appendix C.5.

Enhanced Noise Reduction Algorithm

The Enhanced Noise Reduction Algorithm (ENRA) differs from the NRA by only estimating the $N_x = N_t$ samples of $\mathbf{g}$ which are not null, i.e., $\mathbf{g}_t[n] = \mathbf{g}[\tau_n/\tau_s]$ for $0 \leq n \leq N_t - 1$. Therefore, the knowledge of the number of CIR taps and their corresponding delays is required. The estimator is given by:

$$\mathbf{h}_{enra} = \mathbf{F}_{ut}\mathbf{g}_{enra} = \mathbf{F}_{ut}(\mathbf{F}_{pt}^H \mathbf{F}_{pt} + \gamma_{enra}\mathbf{I}_t)^{-1}\mathbf{F}_{pt}^H \mathbf{h}_{ls} \qquad (6.10)$$

where $\mathbf{F}_{pt} \in \mathbb{C}^{N_p \times N_t}$ and $\mathbf{F}_{us} \in \mathbb{C}^{N_u \times N_t}$ correspond, respectively, to $\mathbf{F}_{pt}[m,n] = \mathbf{F}_p[m, \tau_n/\tau_s]$ and $\mathbf{F}_{ut}[k,n] = \mathbf{F}_u[k, \tau_n/\tau_s]$ for $0 \leq n \leq N_t - 1$. $\mathbf{I}_t$ denotes the identity matrix of size N_t. Hence, for the ENRA $\mathbf{M}_{est} = (\mathbf{F}_{pt}^H \mathbf{F}_{pt} + \gamma_{enra}\mathbf{I}_t)^{-1}\mathbf{F}_{pt}^H$. Analogously to the NRA, the value $\gamma_{enra} = N_t \sigma_w^2$ is optimum in a Full Bandwidth with equally spaced pilots scenario, and will be assumed in the following. It can be observed that this estimator corresponds to the one proposed in [75], when the CIR tap gains' average powers are not known and the CIR tap delays are sample-spaced.

Wiener Filter

The Wiener filter (WF) estimator minimizes the MSE of the estimate by making use of channel and noise correlation properties, and has been broadly treated in literature [63, 68, 75, 78]. It is classically formulated as:

$$\mathbf{h}_{wf} = \mathbf{R}_{\mathbf{h}_u \mathbf{h}_p}(\mathbf{R}_{\mathbf{h}_p \mathbf{h}_p} + \sigma_w^2 \mathbf{I}_p)^{-1}\mathbf{h}_{ls} \qquad (6.11)$$

where $\mathbf{R}_{\mathbf{h}_u \mathbf{h}_p} = \mathrm{E}\{\mathbf{h}_u \mathbf{h}_p^H\}$ is the correlation matrix of $\mathbf{h}_u$ and $\mathbf{h}_p$, $\mathbf{R}_{\mathbf{h}_p \mathbf{h}_p} = \mathrm{E}\{\mathbf{h}_p \mathbf{h}_p^H\}$ is the autocorrelation matrix of $\mathbf{h}_p$, and $\mathbf{I}_p$ is the identity matrix of size N_p. In the sample spaced case, these frequency correlation matrices become:

$$\mathbf{R}_{\mathbf{h}_u \mathbf{h}_p} = \mathbf{F}_{ut}\mathbf{R}_{\mathbf{g}_t \mathbf{g}_t}\mathbf{F}_{pt}^H \qquad (6.12)$$

$$\mathbf{R}_{\mathbf{h}_p \mathbf{h}_p} = \mathbf{F}_{pt} \mathbf{R}_{\mathbf{g}_t \mathbf{g}_t} \mathbf{F}_{pt}^H \tag{6.13}$$

where $\mathbf{R}_{\mathbf{g}_t \mathbf{g}_t} = \mathrm{E}\{\mathbf{g}_t \mathbf{g}_t^H\}$ is the autocorrelation matrix of $\mathbf{g}_t$. Inserting (6.12) and (6.13) in (6.11), and using the matrix relation $\mathbf{AB}^H(\mathbf{I} + \mathbf{BAB}^H)^{-1} = (\mathbf{A}^{-1} + \mathbf{B}^H\mathbf{B})^{-1}\mathbf{B}^H$ [25], leads to:

$$\mathbf{h}_{wf} = \mathbf{F}_{ut}\mathbf{g}_{wf} = \mathbf{F}_{ut}(\mathbf{F}_{pt}^H\mathbf{F}_{pt} + \sigma_w^2\mathbf{R}_{\mathbf{g}_t\mathbf{g}_t}^{-1})^{-1}\mathbf{F}_{pt}^H\mathbf{h}_{ls} \tag{6.14}$$

which is equivalent to the estimator proposed by Yang in [75] when considering sample spaced channels. For WF, $\mathbf{M}_{est} = (\mathbf{F}_{pt}^H\mathbf{F}_{pt} + \sigma_w^2\mathbf{R}_{\mathbf{g}_t\mathbf{g}_t}^{-1})^{-1}\mathbf{F}_{pt}^H$.

Note that when no information about the channel correlation is available, a robust sample-spaced design of the wiener filter is shown in [44]. To obtain this sample-spaced robust estimate $\mathbf{h}_{ssrw}$ it is assumed that the PDP is sample-spaced with N_s samples of equal mean power in all taps. In such conditions $\mathbf{F}_{ut} = \mathbf{F}_{us}$, $\mathbf{F}_{pt} = \mathbf{F}_{ps}$ and $\mathbf{R}_{\mathbf{g}_t\mathbf{g}_t} = \frac{1}{N_s}\mathbf{I}_s$. In [44] the authors proved that this robust WF estimate $\mathbf{h}_{ssrw}$ is fully equivalent to the NRA estimate $\mathbf{h}_{nra}$ given in (6.9). The mathematical derivations are given in appendix C.1.

Generic Formulation

When observing the expressions of the studied algorithms, a general formulation that covers all the cases can be given by:

$$\mathbf{h}_{est} = \mathbf{F}_{ux}\mathbf{g}_{est} = \mathbf{F}_{ux}(\mathbf{F}_{px}^H\mathbf{F}_{px} + \gamma_{est}\mathbf{C}_{\mathbf{est}})^{-1}\mathbf{F}_{px}^H\mathbf{h}_{ls} \tag{6.15}$$

An overview over the specific values taken by each element of (6.15) is given in Table 6.1.

MSE of the Estimators

The different studied estimators are all described by (6.6). It is then possible to evaluate their respective performance by using one single generic MSE expression. The MSE is calculated as:

$$\mathbf{MSE}\{\mathbf{h}_{est}[k]\} = \mathrm{E}\{|\mathbf{h}_u[k] - \mathbf{h}_{est}[k]|^2\} \tag{6.16}$$

Using (6.6), the MSE for the kth subcarrier becomes:

$$\mathbf{MSE}\{\mathbf{h}_{est}[k]\} = \mathbf{Q}[k, k] \tag{6.17}$$

June 18, 2008

Table 6.1: Generalization of the algorithms

Estimator	$\mathbf{F}_{ux}$	$\mathbf{F}_{px}$	γ_{est}	$\mathbf{C_{est}}$	$\mathbf{g}_x$	N_{est}
TDLS	$\mathbf{F}_{up}$	$\mathbf{F}_{pp}$	0	0	$\mathbf{g}_p$	N_p
ML	$\mathbf{F}_{us}$	$\mathbf{F}_{ps}$	0	0	$\mathbf{g}_s$	N_s
NRA	$\mathbf{F}_{us}$	$\mathbf{F}_{ps}$	$N_s\sigma_w^2$	$\mathbf{I}_s$	$\mathbf{g}_s$	N_s
ENRA	$\mathbf{F}_{ut}$	$\mathbf{F}_{pt}$	$N_t\sigma_w^2$	$\mathbf{I}_t$	$\mathbf{g}_t$	N_t
WF	$\mathbf{F}_{ut}$	$\mathbf{F}_{pt}$	σ_w^2	$\mathbf{R}_{\mathbf{g}_t\mathbf{g}_t}^{-1}$	$\mathbf{g}_t$	N_t

where

$$\begin{aligned}
\mathbf{Q} &= \mathbf{F}_{ux}[(\mathbf{I} - \mathbf{M}_{est}\mathbf{F}_{px})\mathbf{R}_{\mathbf{g}_x\mathbf{g}_x}(\mathbf{I} - \mathbf{F}_{px}^H\mathbf{M}_{est}^H) \\
&+ \sigma_w^2\mathbf{M}_{est}\mathbf{M}_{est}^H]\mathbf{F}_{ux}^H
\end{aligned} \tag{6.18}$$

Note that $\mathbf{R}_{\mathbf{g}_x\mathbf{g}_x} = \mathrm{E}\{\mathbf{g}_x\mathbf{g}_x^H\}$ depends on the a priori assumptions made by each estimator. The average MSE of the estimator can consequently be defined as:

$$\overline{\mathbf{MSE}}\{\mathbf{h}_{est}\} = \frac{1}{\mathrm{N}_u}\mathrm{tr}\{\mathbf{Q}\} \tag{6.19}$$

In a Full Bandwidth ($N_u = N_{fft}$) scenario with a constant pilot spacing $\Delta_p = \frac{N_{fft}}{N_p}$, the products between the DFT-based matrices become diagonal matrices, and it is easy to simplify (6.18). Under such conditions, the MSE of the estimate becomes independent on the subcarrier index k. For the estimators which do not assume any knowledge of the mean power of the CIR taps (TDLS, ML, NRA and ENRA), the MSE reduces to the generic expression:

$$\overline{\mathbf{MSE}}\{\mathbf{h}_{est,full}\} = \frac{\gamma_{est}^2 + N_{est}N_p\sigma_w^2}{(N_p + \gamma_{est})^2} \tag{6.20}$$

which, using the values in Table 1, leads to the following for each of the estimators:

$$\overline{\mathbf{MSE}}\{\mathbf{h}_{tdls,full}\} = \sigma_w^2 \tag{6.21}$$

$$\overline{\mathbf{MSE}}\{\mathbf{h}_{ml,full}\} = \frac{N_s}{N_p}\sigma_w^2 \tag{6.22}$$

$$\overline{\mathbf{MSE}}\{\mathbf{h}_{nra,full}\} = \frac{N_s\sigma_w^2}{N_p + N_s\sigma_w^2} \tag{6.23}$$

$$\overline{\text{MSE}}\{\mathbf{h}_{enra,full}\} = \frac{N_t\sigma_w^2}{N_p + N_t\sigma_w^2} \tag{6.24}$$

When the mean powers of each CIR tap are known, we have for the WF estimator:

$$\overline{\text{MSE}}\{\mathbf{h}_{wf,full}\} =$$
$$\sum_{i=0}^{N_t-1}\left\{\mathbf{R}_{\mathbf{g}_t\mathbf{g}_t}[i]\left(1 - N_p\frac{\mathbf{R}_{\mathbf{g}_t\mathbf{g}_t}[i]}{\sigma_w^2+N_p\mathbf{R}_{\mathbf{g}_t\mathbf{g}_t}[i]}\right)^2\right. \tag{6.25}$$
$$\left.+\sigma_w^2 N_p\left(\frac{\mathbf{R}_{\mathbf{g}_t\mathbf{g}_t}[i]}{\sigma_w^2+N_p\mathbf{R}_{\mathbf{g}_t\mathbf{g}_t}[i]}\right)^2\right\}$$

Observations

Different observations can be done for each algorithm:

i) For the TDLS estimator, no a priori channel knowledge is needed. The matrix to be inverted, $\mathbf{F}_{pp}$, is static, can be precalculated and stored in memory. If the matrix is ill-conditioned, the algorithm is not usable, otherwise the performance depends only on σ_w^2.

ii) For the ML estimator, knowledge of the CIR length N_s is needed. The matrix $\mathbf{F}_{ps}^H\mathbf{F}_{ps}$ is always of full rank, and can also be precalculated and stored in memory for different CIR lengths. When ill-conditioned it is also not applicable. It outperforms the TDLS estimator unless:
$$\{N_s = N_p\} \Rightarrow \{\mathbf{h}_{ml} = \mathbf{h}_{tdls}\}.$$

iii) For the NRA, knowledge of the CIR length N_s and σ_w^2 is needed. In the same way as for the ML approach, matrices can be precalculated and stored in memory. The ill-conditioning effect disappears and the NRA outperforms the ML estimator. As the SNR increases it follows that:
$$\{\sigma_w^2 \rightarrow 0\} \Rightarrow \{\mathbf{h}_{nra} \rightarrow \mathbf{h}_{ml}\}$$
$$(\{\sigma_w^2 \rightarrow 0\} \wedge \{N_s = N_p\}) \Rightarrow \{\mathbf{h}_{nra} \rightarrow \mathbf{h}_{tdls}\}.$$

iv) For the ENRA, exact tap delay and σ_w^2 knowledge is required. The matrix of size $(N_t \times N_t)$ to be inverted is dynamic and must therefore be computed each time a tap delay changes. The ENRA outperforms the NRA if $N_t < N_s$, otherwise:
$$\{N_t = N_s\} \Rightarrow \{\mathbf{h}_{enra} = \mathbf{h}_{nra}\}.$$

June 18, 2008

v) For the WF estimator, exact tap delay, mean tap power as well as σ_w^2 knowledge is required. The matrix dimensions are equal to the ones of the ENRA, requiring also an adaptive $(N_t \times N_t)$ matrix inversion. By inspection of (6.14) it follows that:

$$\{\sigma_w^2 \to 0\} \Rightarrow \{\mathbf{h}_{wf} \to \mathbf{h}_{enra}\}.$$
$$(\{N_t = N_s\} \wedge \{\sigma_w^2 \to 0\}) \Rightarrow \{\mathbf{h}_{wf} \to \mathbf{h}_{nra}\}.$$

A general comment is that there is no ill-conditioning effects when the full bandwidth of the FFT is used for data and pilot symbol transmission. The TDLS, ML and NRA estimators can be precomputed and stored in memory, whereas ENRA and WF will need to be adaptive to track the channel variability. In all cases $\mathbf{F}_{ux}$ and $\mathbf{F}_{px}$ can be implemented using a partial-input partial-output FFT [89], thereby significantly reducing the complexity of the required matrix multiplication. For the adaptive algorithms the size of the matrix to invert strictly depends on the number of CIR taps N_t and, for channels with a moderate number of CIR taps, is therefore easily computable on the fly. Generally speaking, the performance and complexity of the estimators will depend on the a priori channel information and noise variance knowledge considered at the receiver.

6.3.2   Non-Sample-Spaced Channel

In an NSS scenario, there is at least one CIR tap of the channel with a delay τ_i which is not an integer multiple of the sampling period τ_s. In this situation, the ith column of the leakage matrix $\mathbf{L}$ will have no null values for every element, i.e., $\mathbf{L}[n, i] \neq 0$ $\forall n$. As a consequence, the complex gain of the ith CIR tap will have a contribution on all the samples of the equivalent SS-CIR. Fig. 6.2 illustrates how NSS CIR taps are mapped to the equivalent SS-CIR for a simple example where $N_{fft} = 64$ and the channel is $g(\tau) = 0.8\delta(\tau - 0.5\tau_s) + 0.5\delta(\tau - 3.5\tau_s) + 0.3\delta(\tau - 7.5\tau_s)$. As can be seen, most of the power of each CIR tap is mapped to the surrounding samples in the SS-CIR. It is especially interesting how the last samples have significant amplitude, due to the leakage of the first channel CIR taps.
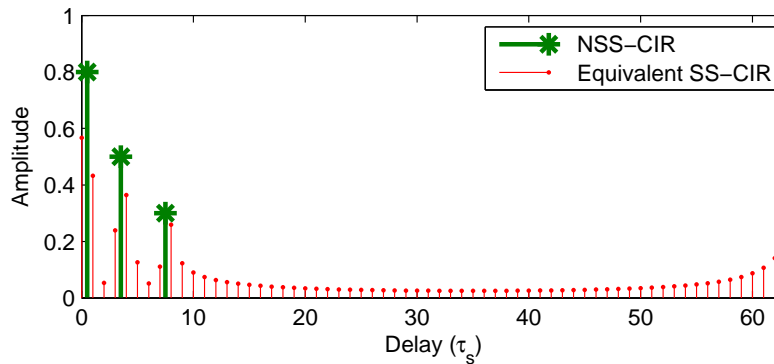
Figure 6.2: Leakage of the NSS-CIR taps to the equivalent SS-CIR

The estimators studied in the sample-spaced case rely on the fact that most of the samples of **g** are zero, and thus they can be canceled in the estimation problem. Obviously, this assumption does not hold any more in the NSS scenario, and the estimators must be modified accordingly. Due to the ill-condition problems of the TDLS and ML estimators, only NRA, ENRA and WF will be considered in the following.

Modified NRA

The NRA algorithm for SS channel is based on the knowledge of the CIR length, i.e., the maximum excess delay of the channel, so that every sample of **g** beyond this value is assumed to be zero. For the NSS scenario, however, the length of the SS-CIR is N_{fft} due to the leakage effect, which will cause a performance degradation if $N_p < N_{fft}$. This degradation will therefore appear in the Partial Bandwidth scenario where $N_p \leq N_u < N_{fft}$ or in the Full Bandwidth scenario if $\Delta_p > 1$. A tradeoff solution consists of estimating only the subset of samples of **g** which have the highest power. Since the actual CIR tap delays are unknown, the selection of the samples to estimate can only be approximated: it is expected that they will be concentrated at the beginning and at the end of the SS-CIR. Therefore, a suboptimal solution to the problem, provided that no knowledge of the actual channel CIR taps

is available, is given by the Modified NRA, (MNRA), which is formulated as:

$$
\begin{aligned}
\mathbf{h}_{mnra} &= \mathbf{F}_{um}\mathbf{g}_{mnra} \\
&= \mathbf{F}_{um}(\mathbf{F}_{pm}^H\mathbf{F}_{pm} + \gamma_{mnra}\mathbf{I}_m)^{-1}\mathbf{F}_{pm}^H\mathbf{h}_{ls}
\end{aligned}
\tag{6.26}
$$

where the matrix $\mathbf{F}_{um} \in \mathbb{C}^{N_u \times N_m}$ is defined as:

$$
\mathbf{F}_{um}[k, n] =
\begin{cases}
\mathbf{F}_u[k, n], & 0 \leq n \leq \lceil N_m(1 - \alpha) \rceil - 1 \\
\mathbf{F}_u[k, N_{fft} - N_m + n], & \lceil N_m(1 - \alpha) \rceil \leq n \leq N_m - 1
\end{cases}
\tag{6.27}
$$

and $\mathbf{F}_{pm} \in \mathbb{C}^{N_p \times N_u}$ is defined analogously with respect to $\mathbf{F}_p$. $\mathbf{I}_m$ is the identity matrix of size N_m. Furthermore, the parameter γ_{mnra} is selected to be $\gamma_{mnra} = N_m\sigma_w^2$, analogously to the sample-spaced case.

Two parameters shall be adapted depending on the PDP and σ_w^2: N_m representing the number of samples of the equivalent SS-CIR to estimate, and α representing the proportion of the estimated samples in the final part of the SS-CIR.

ENRA and Wiener Filter

When using the ENRA or the Wiener Filter estimator, it is assumed that the delays of the channel are perfectly known, so that there is no need to estimate the equivalent SS-CIR. Instead, the parameters to estimate are the complex gains a_i of each of the CIR taps, represented by the vector $\mathbf{a}$. The estimators can be rewritten for the NSS scenario as:

$$
\mathbf{h}_{enra} = \mathbf{T}_u\mathbf{a}_{enra} = \mathbf{T}_u(\mathbf{T}_p^H\mathbf{T}_p + \gamma_{enra}\mathbf{I}_t)^{-1}\mathbf{T}_p^H\mathbf{h}_{ls}
\tag{6.28}
$$

$$
\mathbf{h}_{wf} = \mathbf{T}_u\mathbf{a}_{wf} = \mathbf{T}_u(\mathbf{T}_p^H\mathbf{T}_p + \sigma_w^2\mathbf{R}_{aa}^{-1})\mathbf{T}_p^H\mathbf{h}_{ls}
\tag{6.29}
$$

where the matrices $\mathbf{T}_u \in \mathbb{C}^{N_u \times N_t}$ and $\mathbf{T}_p \in \mathbb{C}^{N_p \times N_t}$ are defined with respect to $\mathbf{T}$ in the same way as $\mathbf{F}_u$ and $\mathbf{F}_p$ with respect to $\mathbf{F}$. As in the SS case, $\gamma_{enra} = \sigma_w^2 N_t$, and $\mathbf{R}_{aa} \in \mathbb{C}^{N_t \times N_t}$ is the correlation matrix of the channel gains, i.e, $\mathbf{R}_{aa} = \text{diag}\{\text{E}\{|a_0|^2\}, \ldots, \text{E}\{|a_{N_t-1}|^2\}\}$ as we assume i.i.d. channel taps.

The formulation in 6.29 requires exact knowledge of the delay locations. When no statistical knowledge is available from the channel this formulation is no longer possible. It then comes naturally to use the known formulation of 6.11 and define the

correlation matrices according to the assumption of Non-sample-spaced PDP with uniformly and independently distributed tap delays τ_i over $[0, T_{med}]$. According to the derivations in appendix C.4 the CTF correlation matrix can then be given by:

$$\mathbf{R_{hh}}[k, k'] = \frac{1 - e^{-j2\pi\frac{(k-k')}{N_{fft}}T_{med}}}{j2\pi\frac{(k-k')}{N_{fft}}T_{med}}, \tag{6.30}$$

where, $\mathbf{R_{h_u h_p}}$ $\mathbf{R_{h_p h_p}}$ are subsets of $\mathbf{R_{hh}}$. $\mathbf{h}_u$ and $\mathbf{h}_p$ are respectively defined in equations 2.47 and 2.49. When no information is available on the CIR MED, and T_{med} is replaced by the duration of the CP length T_g we denote this estimate by RW_1. When the CIR MED is known to the receiver we denote the estimate by RW_2 and finally when the SNR is also known we denote the estimate by RW_3.

MSE of the Estimators

Unlike the SS scenario, it is difficult to find a general expression that includes all the studied algorithms for an NSS channel. For this reason, we will study the performance of a generic estimator such as:

$$\mathbf{h}_{est} = \mathbf{M}_{est}\mathbf{h}_{ls} \tag{6.31}$$

which includes any linear estimator that can be expressed in matrix form. With this formulation, the MSE over an NSS channel is:

$$\begin{aligned}
\overline{\mathbf{MSE}}\{\mathbf{h}_{est}\} = \tfrac{1}{N_u}\text{tr}\Big\{ & \mathbf{T}_u\mathbf{R}_{aa}\mathbf{T}_u^H \\
& -\mathbf{T}_u\mathbf{R}_{aa}\mathbf{T}_p^H\mathbf{M}_{est}^H - \mathbf{M}_{est}\mathbf{T}_p\mathbf{R}_{aa}\mathbf{T}_u^H \\
& +\mathbf{M}_{est}\mathbf{T}_p\mathbf{R}_{aa}\mathbf{T}_p^H\mathbf{M}_{est}^H + \sigma_w^2\mathbf{M}_{est}\mathbf{M}_{est}^H \Big\}
\end{aligned} \tag{6.32}$$

and the specific values of $\mathbf{M}_{est}$ for each studied algorithm are:

$$\mathbf{M}_{est} = \begin{cases}
\mathbf{F}_{um}(\mathbf{F}_{pm}^H\mathbf{F}_{pm} + \gamma_{mnra}\mathbf{I}_m)^{-1}\mathbf{F}_{pm}^H, & \text{MNRA} \\
\mathbf{T}_u(\mathbf{T}_p^H\mathbf{T}_p + \gamma_{enra}\mathbf{I}_t)^{-1}\mathbf{T}_p^H, & \text{ENRA} \\
\mathbf{T}_u(\mathbf{T}_p^H\mathbf{T}_p + \sigma_w^2\mathbf{R}_{aa}^{-1})\mathbf{T}_p^H, & \text{WF}
\end{cases} \tag{6.33}$$

6.4   Performance evaluation

In the following, the performance of the estimators discussed in section 6.3 will be studied via Monte Carlo simulations. A single-input single-output OFDM system

with physical layer parameters proposed for the downlink of UTRA LTE will be used [1]. These parameters are given in Table 6.2. QPSK modulation is used for both pilot and data symbols. Evenly spaced pilot symbols with a spacing of $\Delta_p = 6$ subcarriers are transmitted in every OFDM block.

Table 6.2: Simulation parameters

Parameter	Value
Sampling frequency	30.72 MHz
τ_s	32.552 ns
CP length	4.69 μs
Pilot spacing	6
N_{fft}	2048
Subcarrier spacing	15 KHz

In Table A.3 of appendix A, three channel power delay profiles with 20 taps are given for this simulation study. The "long SS" profile is sample spaced of length 3.711 μs, the "long NSS" profile is not sample spaced differing by 0.5 T_s from the "long SS" profile and the "short NSS" is also not sample spaced with a length of only 0.635 μs. Results for both MSE and uncoded Bit Error Rate (BER) using the studied estimators as a function of the Signal-to-Noise Ratio (SNR) will be given. The SNR will be expressed as signal-to-noise ratio per bit $(\frac{E_b}{N_0})$ [31], which in the case of QPSK modulation corresponds to:

$$\frac{E_b}{N_0}(\text{dB}) = 10 \log_{10}\left(\frac{1}{2\sigma_w^2}\right) \tag{6.34}$$

since the symbols are assumed to have unit power.

### 6.4.1 Full Bandwidth and Sample-Spaced Scenario

The performance of the different studied algorithms in a Full Bandwidth system using the "long SS" channel profile is depicted in Fig. 6.3. As can be seen in Fig. 6.3(a), the MSE results obtained by simulation correspond to the theoretical

values given in section 6.3.1. TDLS has the largest MSE among the estimators. The ML estimator performs equal to the NRA at sufficiently high SNR, and the same effect can be seen with ENRA and WF. As a general result, the MSE's of NRA and ML will always be between the ones obtained with TDLS and ENRA: for short CIRs, the MSE will approach the one of the ENRA, and it will be closer to the TDLS for long CIRs. From the BER results shown in 6.3(b), we see that the TDLS curve lies 3.5 dB from the known channel performance at $\frac{E_b}{N_0}$ =10 dB, whereas this distance is reduced to 0.25 dB for the ENRA and WF estimators.

6.4.2 Partial Bandwidth and Sample-Spaced Scenario

The effect of introducing virtual subcarriers at the band edges will be studied in the following. The simulations done for the full bandwidth scenario have been repeated with the difference that N_u=1200, as suggested in the LTE standard [1]. MSE and BER results are given in Fig. 6.4. It is noted that in this specific case the ill-conditioning of $\mathbf{F}_{pp}$ and $(\mathbf{F}_{ps}^H\mathbf{F}_{ps})$ will lead to a BER of 0.5 for TDLS and ML, and a very high MSE which is out of the range of Fig. 6.4(a). The performance of NRA, ENRA and WF is slightly deteriorated compared to Full Bandwidth as the total number of pilot subcarriers decreases due to the constant pilot spacing.

In Fig. 6.5, the MSE of the ML estimator is analyzed as a function of the assumed maximum delay of the channel (N_s) using (6.19), where different number of used subcarriers have been represented at $\frac{E_b}{N_0}$ =15 dB. When all the subcarriers are used ($N_u = 2048$), the error of the estimate grows linearly with the assumed channel length. When virtual subcarriers are introduced, however, the matrix to be inverted, $\mathbf{F}_{ps}^H\mathbf{F}_{ps}$, becomes ill-conditioned after a certain channel length, yielding a large degradation of the MSE that makes the estimator unusable. The maximum channel excess delay before the estimator becomes unstable decreases as the number of used subcarriers is reduced. Note that the same effect can be seen for the TDLS estimator, which is equivalent to the ML when the assumed CIR length is set to $(N_p - 1)\tau_s$.
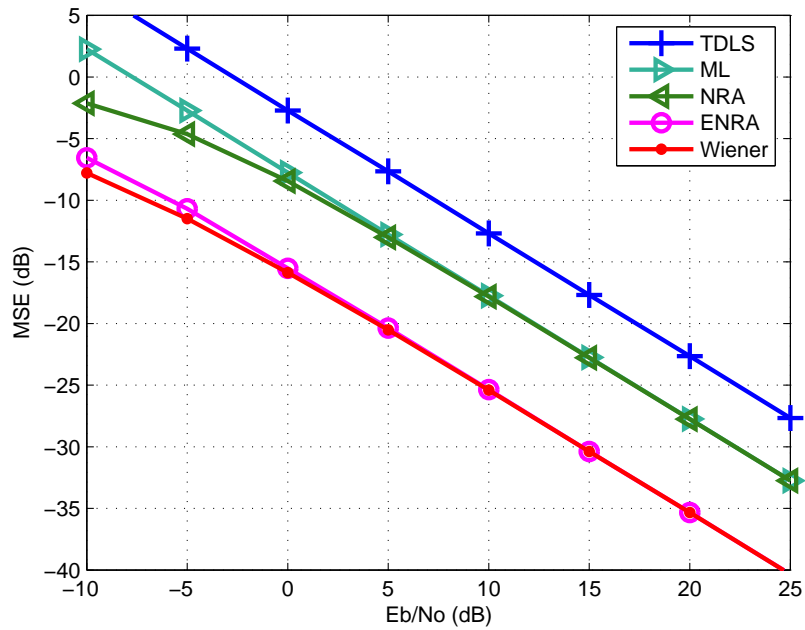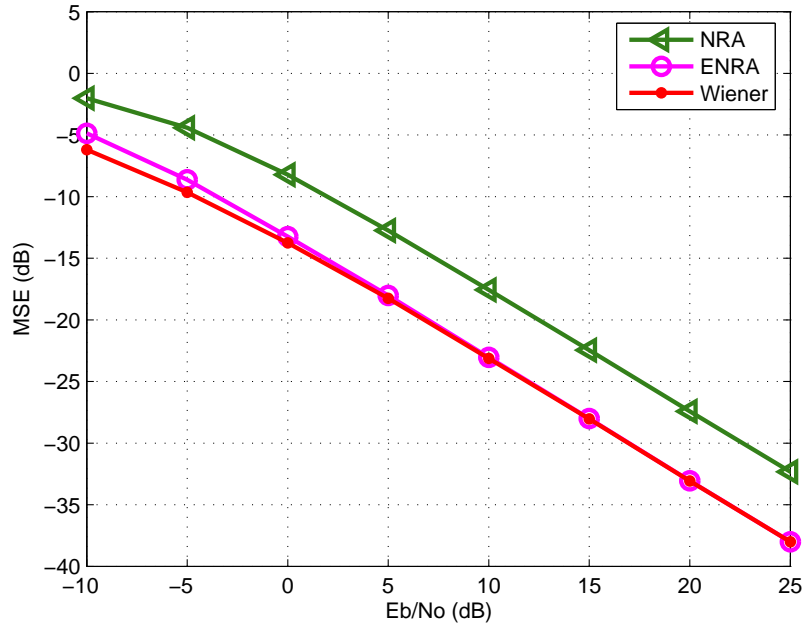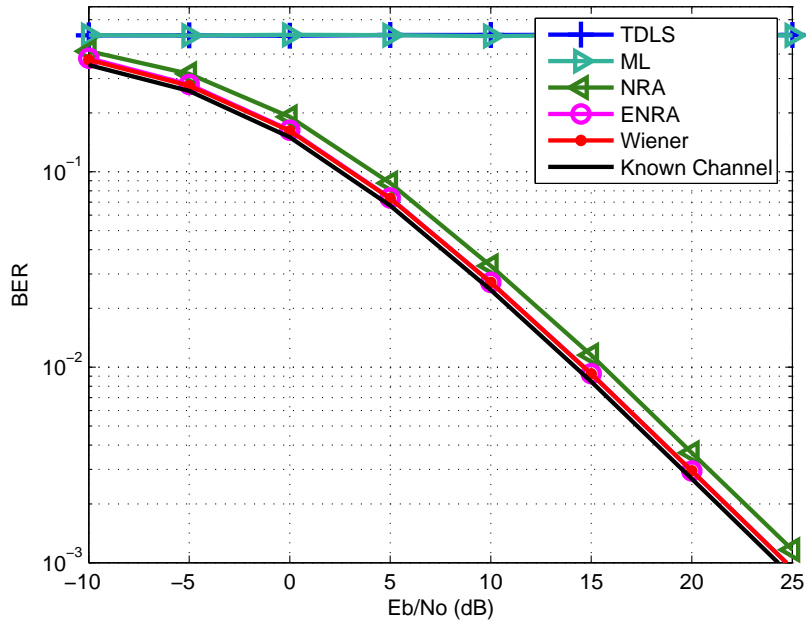
(a)
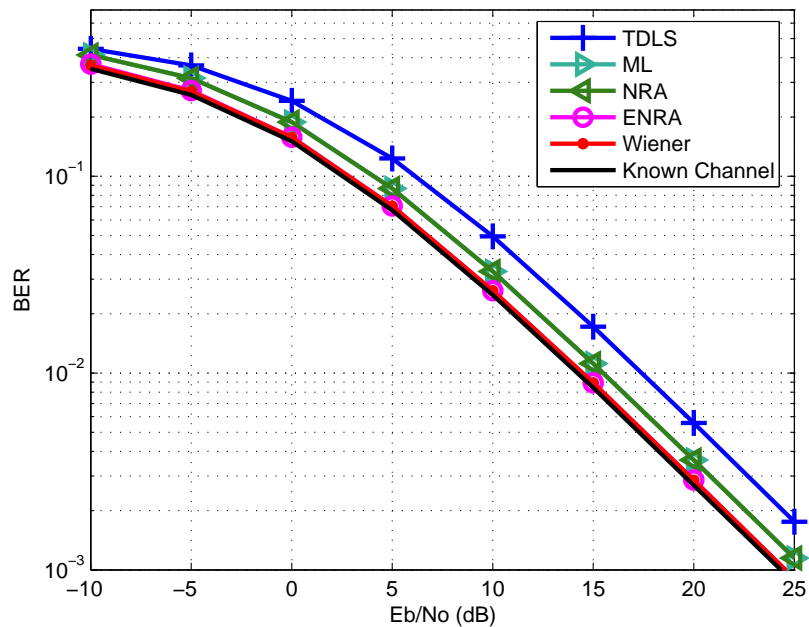
(b)

Figure 6.3: Performance of the different estimators in a Full Bandwidth OFDM system ($Nu = N_{fft} = 2048$) and a pilot spacing of 6 for the "long" SS channel. (a) MSE. (b) BER.

(a)

(b)

Figure 6.4: Performance of the different estimators in an LTE scenario with $Nu = 1200$, $N_{fft} = 2048$ and a pilot spacing of 6 for the "long" SS channel. (a) MSE. (b) BER.
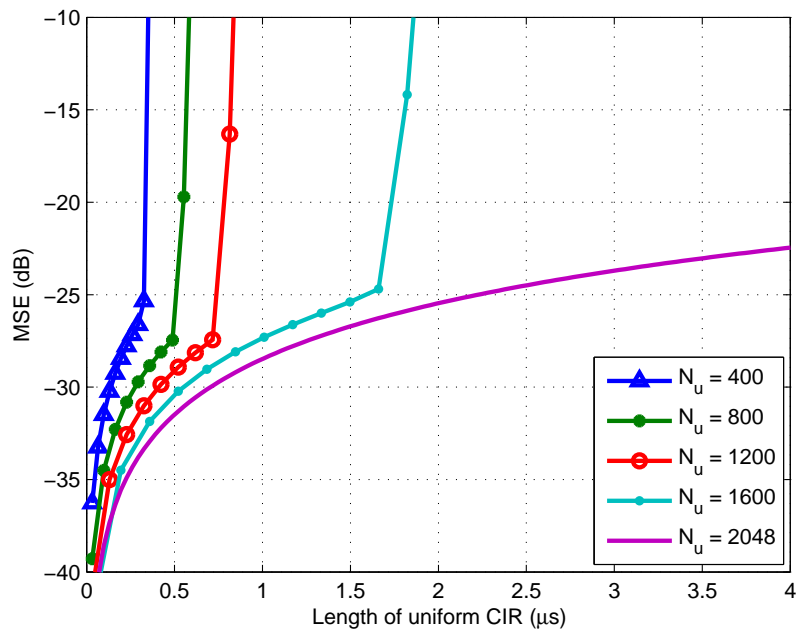
Figure 6.5: MSE of the ML estimator for varying assumed CIR length and different N_u, $N_{fft} = 2048$ and $Eb/No = 15$ dB

6.4.3 Non-Sample-Spaced Scenario

In a first step, the effect of having an NSS PDP on the classical algorithms will be studied. The MSE and BER results are given in Fig. 6.6 for the NRA, RW, ENRA and WF in the exact same scenario as for Fig. 6.4, but using the "long NSS" channel profile. It is noted that the ENRA and WF have the same performance as when employing the "long SS" PDP. The NRA, on the other hand, suffers from significant degradation for $\frac{E_b}{N_0} \geq 10$ dB in both MSE and BER. The RW used is RW$_3$ for simplicity. From these results it can be observed that the RW, ENRA and WF are not affected by the leakage effect. The knowledge of the tap delays of the PDP gives an advantage of the ENRA and WF over the RW of approx. 1dB in the studied scenario for the BER plot. It is noted that varying the PDP will influence this gain.

In Fig. 6.7 the robustness of the ENRA against delay estimation errors is studied. A random zero-mean Gaussian error with variance σ_τ^2 has been added to the delay's values to simulate imperfect delay estimates, and the MSE of the estimates has
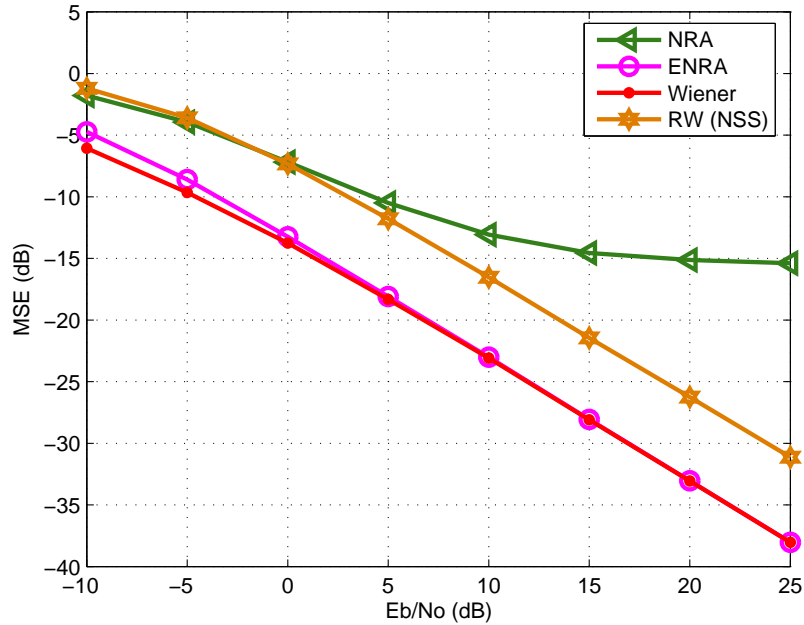
(a)
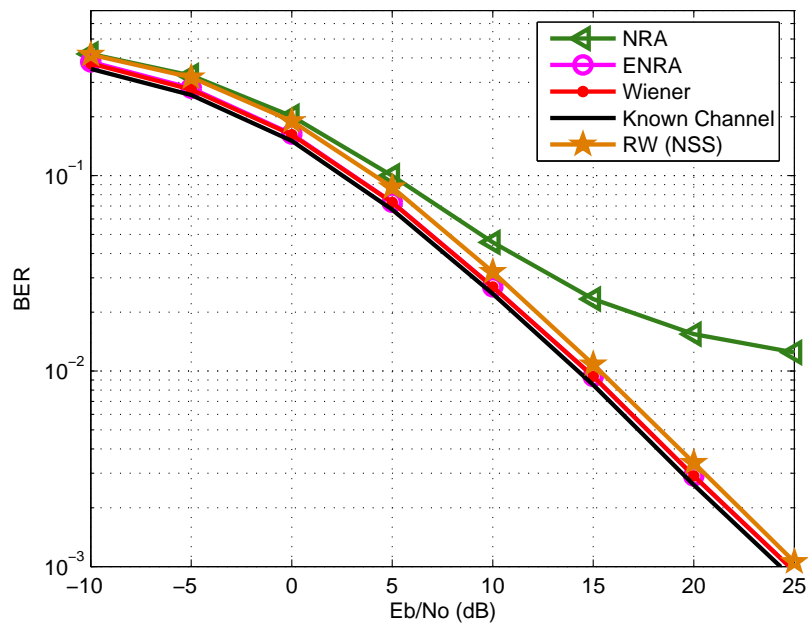
(b)

Figure 6.6: Effect of leakage on the classical algorithms in an LTE scenario with $Nu = 1200$, $N_{fft} = 2048$ and a pilot spacing of 6 for the "long" NSS channel. (a) MSE. (b) BER.
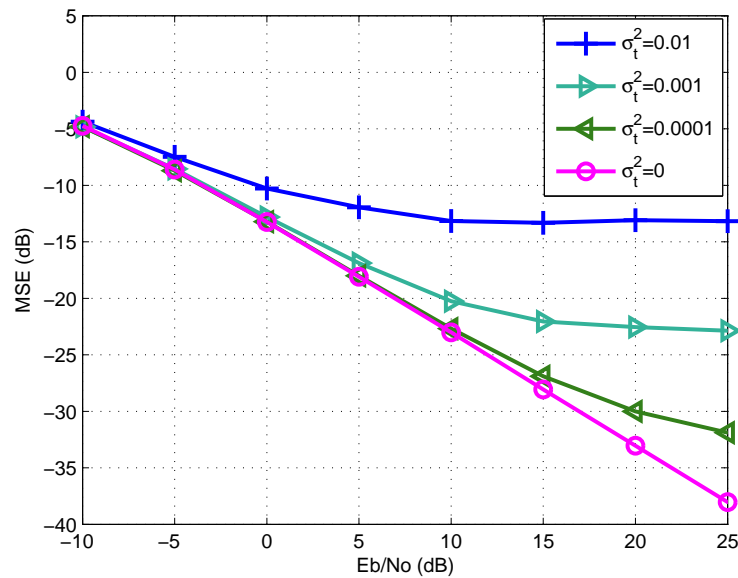
Figure 6.7: MSE of the ENRA with different delay estimation errors in an LTE scenario with $Nu = 1200$, $N_{fft} = 2048$ and a pilot spacing of 6 for the "long" NSS channel.
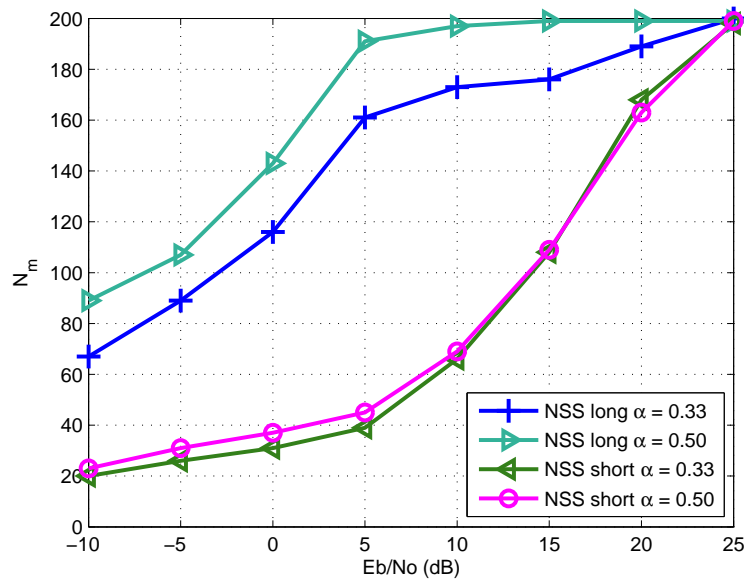

Figure 6.8: Optimal N_m for MNRA in a nLTE scenario with $Nu = 1200$, $N_{fft} = 2048$ and a pilot spacing of 6 for the "long" and "short" NSS channels.

been represented. The results show that even with small errors the ENRA suffers from severe degradation as the SNR increases. Very high accuracy in the tap delay estimates is therefore needed in order to avoid leakage.

In a second step, the ability of MNRA to cope with NSS channels will be studied. In Fig. 6.8, the optimal N_m value is given through an exhaustive search. The centering parameter α has been fixed to the values $1/2$ and $1/3$, and the values of N_m that obtain the lowest MSE have been represented as a function of $\frac{E_b}{N_0}$ for the "long NSS" and "short NSS" profiles. It is noted that the optimum N_m is larger for longer channel profiles, and increases with the SNR, reaching its maximum value $N_m = N_p$ at $\frac{E_b}{N_0} = 25$ dB.

In Fig. 6.9, we show the MSE and BER performance of the MNRA with the values of N_m of Fig. 6.8, in the case of the "long NSS" and "short NSS" PDP's, with the same simulation parameters as for Fig. 6.6. It can be noticed that $\alpha = 1/3$ performs better than $\alpha = 1/2$ for both channel profiles, and seems to be robust to the length of the channel response. Comparing the performance of MNRA in the "long NSS" channel with the classical NRA, the MSE flooring effect occurs at higher SNR and, at $\frac{E_b}{N_0} = 25$ dB, the MSE is improved by 7 dB. In BER terms, the degradation due to channel estimation with MNRA can be kept low for BER smaller than 1 %, but performance limitation is unavoidable for $\frac{E_b}{N_0} \geq 15$ dB.

6.5   Computational complexity

This section documents the complexity analysis of the frequency direction interpolation algorithms studied previously. The concept of complexity is first defined, then calculated theoretically and finally evaluated for different bandwidth and channel conditions. The different algorithm complexities are illustrated afterwards.

When dealing with computational complexity one is investigating the amount of resources required for the execution of a given algorithm. One can separate the complexity in two concepts: **time complexity** and **space complexity**. The first concept refers to the number of operations needed as a function of the input size. In our specific study case of frequency direction channel estimation in OFDM, this will
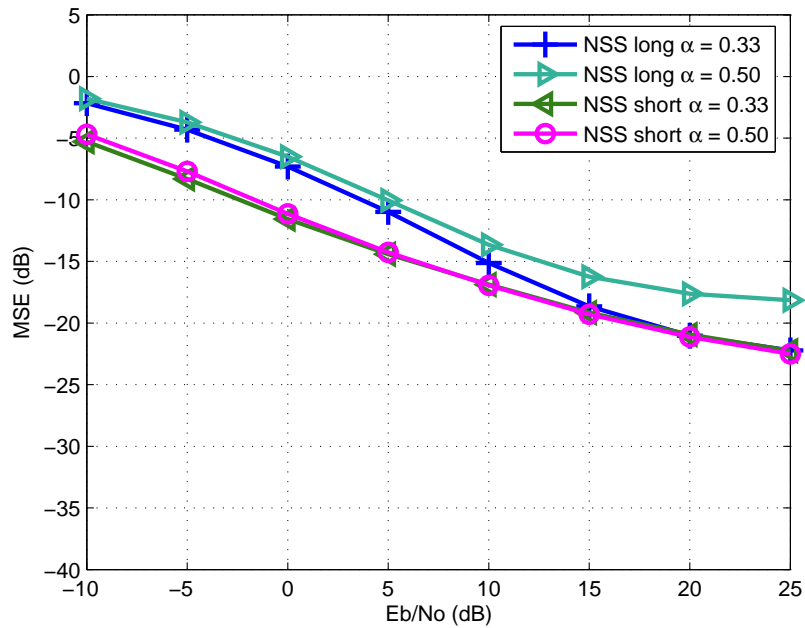
(a)
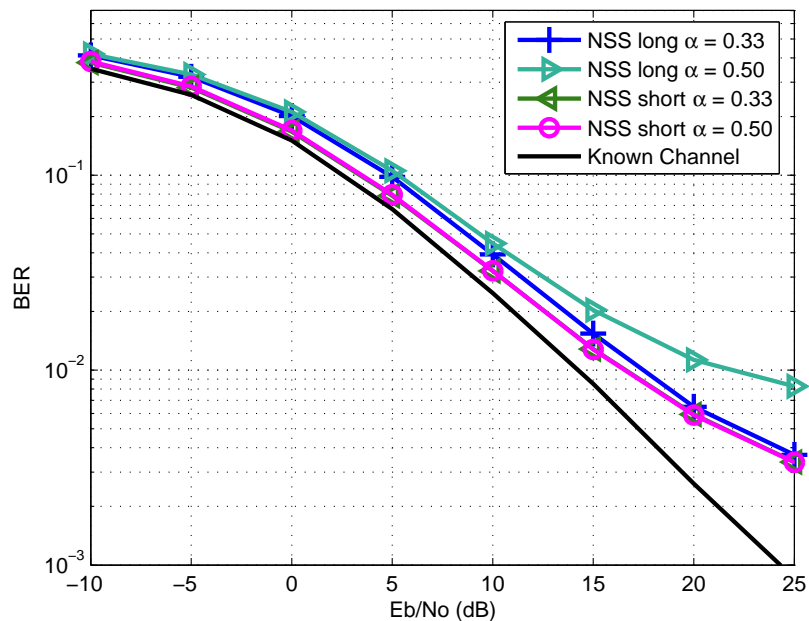
(b)

Figure 6.9: Performance of the MNRA with different α and optimal N_m in an LTE scenario with $Nu = 1200$, $N_{fft} = 2048$ and a pilot spacing of 6 for the "long" and "short" NSS channels. (a) MSE. (b) BER.

refer to the number of Complex Multiply Accumulate (CMAC) operations needed for the interpolation in each OFDM symbol containing pilots. The second concept will refer to the memory required by the studied algorithm.

In this section the focus will be restricted to **time complexity**, more specifically to the number of CMAC's needed to estimate a CTF given N_p initial least square estimates at the pilot subcarriers.

6.5.1 Theoretical complexity count

In the following the theoretical complexity will be evaluated for the different algorithms by using several implementation methods. The big O notation will be used and we will assume the operation costs given in table 6.3.

Table 6.3: Complexity for matrix and vector of dimensions $(n \cdot n)$ and (n).

Operation type	Computational cost
Matrix by Matrix multiplication	$O(n^3)$
Matrix Inverse	$O(n^3)$
Matrix by vector multiplication	$O(n^2)$

It is noted that both matrix by matrix multiplication and matrix inverse can be performed with lower order of operational cost. For example the Strassen's algorithm explained in [33] will use $O(n^{log_2(7)})$ instead of $O(n^3)$ of the classical straightforward procedure (as Gaussian elimination for the inverse). It is however rarely used in practice as it is awkward to implement and can lead to numerical stability issues. The CoppersmithWinograd algorithm [38] has asymptotic complexity of approximately $O(n^{2.376})$ however it is only interesting for very large matrices that are much larger than then ones studied for the present investigation.

The mathematical complexity is calculated directly from the equations of the different interpolation approaches. For simplicity, the CMAC's will be counted in such way that a complex addition, when followed by a complex multiplication, will count as one CMAC. The same goes for real multiplications and additions that will

also give a CMAC.

The different complexity orders of the different interpolation algorithms can be appreciated in table 6.4.

Table 6.4: Complexity order of the different algorithms

Algorithm		Complexity
TDLS	Method 1	$O(N_u \cdot N_p)$
TDLS	Method 2	$O(N_{fft} \cdot log_2(N_{fft}) + N_p^2)$
TDLS	Method 3	$O(\alpha_u \cdot N_{fft} \cdot log_2(N_{fft}) + N_p^2)$
ML/NRA	Method 1	$O(N_u \cdot N_p)$
ML/NRA	Method 2	$O(T_{med} \cdot (N_u + N_p))$
ML/NRA	Method 3	$O(\alpha_u \cdot N_{fft} \cdot log_2(N_{fft}) + T_{med} \cdot N_p)$
ENRA/WF		$O(N_t \cdot (N_u + N_t^2 + N_p))$
RWF		$O(N_u \cdot N_p)$
SVD		$O(N_e \cdot (N_u + N_e + N_p))$

It is noted that the complexity calculation assumes that the a priori information on CIR length, SNR, CIR tap delays and powers are given to the receiver and not estimated. Therefore complexity overhead due to statistics estimation has not been included in this study.

TDLS: *Method 1* is the straightforward direct matrix implementation with N_p multiplications per subcarrier. *Method 2* assumes that the $\mathbf{F}_{ps}^H$ is implemented with an IFFT of size N_{fft} with null inputs corresponding to the band edges with virtual subcarriers. *Method 3* is based on the principle of using an optimized partial-input partial-output IFFT. The operational gain is quantified by the α_u factor, which is an approximation of true gain [44, 89].

ML and NRA: *Method 1* for ML and NRA is the same as the *Method 1* for TDLS. *Method 2* takes advantage of the CIR length T_{med} where the N_p LS estimates are first multiplied with the pre-calculated $((\mathbf{F}_{ps}^H \mathbf{F}_{ps})^{-1} \mathbf{F}_{ps}^H)$ matrix and then mapped back in the Frequency domain with the $\mathbf{F}_{us}^H$ matrix. *Method 3* for the ML and NRA

is similar to *Method 3* for the TDLS algorithm where the partial-input partial-output IFFT is used again.

ENRA and WF: both methods assume the implementation used by performing the matrix-vector operations from equations 6.28 and 6.29. The complexity of both algorithms is equal if we neglect the operational cost of the additive term. It is noted here that in both cases, the matrix to invert is of dynamic size $(N_t \cdot N_t)$. However, if the equation 6.11 is followed, the size of the matrix to invert is of $(N_p \cdot N_p)$, and is static. In case of large number of pilots N_p, this would make the inversion very demanding in computations and unfeasible in practice.

RWF: complexity follows the simple Matrix-vector product from equation 6.31.

SVD of RWF: uses a linear projection matrix as given in [44] which for a small number of eigenvalues N_e leads to a great advantage over the straightforward RWF implementation. An evaluation of the Low-Rank approximation of the RWF is given in [**?**].

6.5.2   Complexity results

Figure 6.10 presents the complexity of the TDLS algorithm that doesn't depend on the channel statistics. It is setup as a reference for the other algorithms. At both studied bandwidths *Method 3* is clearly the preferred method for implementation. At 20 MHz the gain from using *Method 3* is of order 15, whereas for 1.25 MHz bandwidth this gain is only of factor 4.

Figure 6.11 also shows the complexities for 3 methods of implementation. There is a clear dependency of *Method 2* and *Method 3* on the CIR MED length. At MED of $0.9\mu s$ and $0.3\mu s$ for respectively 20MHz and 1.25MHz bandwidth, *Method 2* and *Method 3* have approximately the same complexity. This number is 40 and 4 times lower, for respectively 20 MHz and 1.25 MHz, than for *Method 1*. However at $5\mu s$, *Method 1* and *Method 2* have similar complexities and *Method 3* is clearly the best, being 16 and 3.5 times lower for 20MHz and 1.25MHz respectively.

Figure 6.12 presents the ENRA and WF complexities for 2 bandwidths. As the number of estimated CIR taps increases the complexity increases exponentially with a power of 3. For a small amount of taps the influence of the Bandwidth size is large,
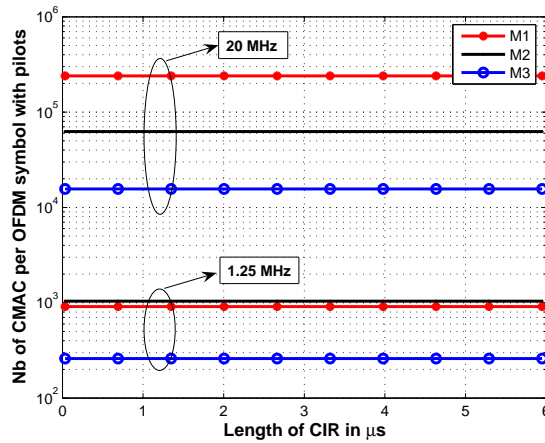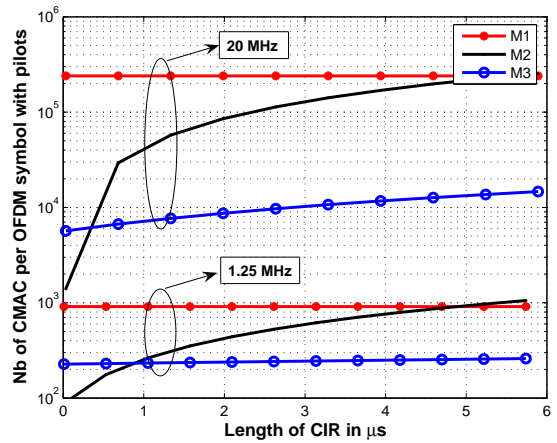
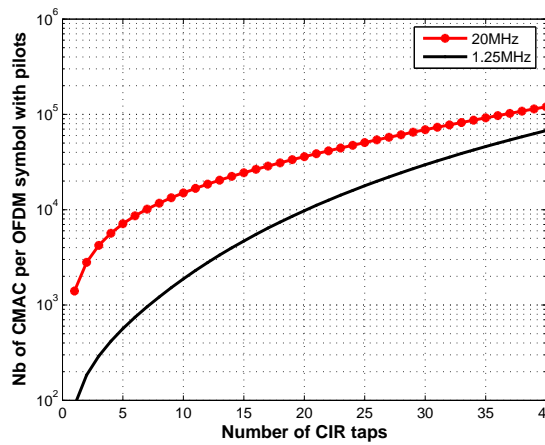Figure 6.10: TDLS

Figure 6.11: ML and NRA
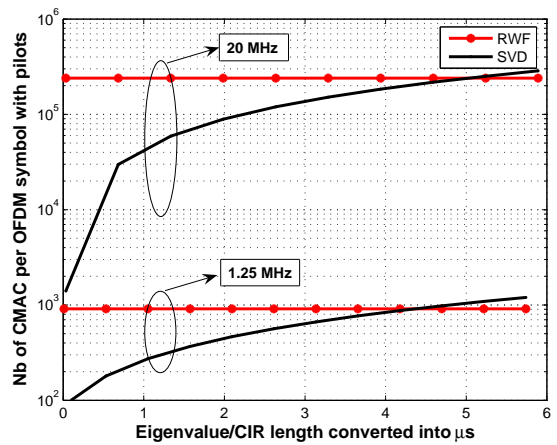

Figure 6.12: ENRA and WF

Figure 6.13: RWF and SVD

however as the number of taps increases the influence of the Bandwidth tends to be reduced.

Figure 6.13 shows the complexity gain by using an SVD approach on the RWF. The complexity gain is especially large for cases of low number of eigenvalues. When using an SVD of the RWF the number of eigenvalues is largely correlated to the CIR MED (see appendix C.6). At equivalent length of $1\mu s$, the SVD implementation is approx 6 and 3.4 times less complex than the RWF for 20MHz and 1.25MHz respectively.

6.6 Conclusion

This chapter is an in depth study of frequency direction linear PACE algorithms. A framework has been provided for a choice of interpolation algorithm in upcoming OFDM based standards. In a first step a classification has been carried out from a state of the art survey, showing that the linear solutions provided in literature can be classified into time and frequency domain approaches. They are also classified according to their a priori assumptions. A comparison of classical linear PACE OFDM algorithms using a generalized estimator formulation has been presented. It has been shown that each algorithm is a particular case of this estimator and depends on the a priori channel information taken into account. Analysis and simulation results are first given for a sample-spaced channel and Full Bandwidth, showing that the performance is improved as the amount of a priori information increases. The effects of introducing virtual subcarriers as well as a non-sample-spaced channel are then studied. When Partial Bandwidth is used, the TDLS and ML algorithms suffer from severe ill-conditioned matrices and cannot be used as such if the number of virtual subcarriers is too large.

When discarding the leakage effect due to non sample spaced CIR and when looking at SNR values in the range -10dB to 10 dB, the optimized partial-input partial-output FFT based implementation of the NRA has the lowest complexity and doesn't deteriorate the CTF estimate significantly. However, at SNR values above 10dB the leakage effect renders the NRA solution unusable and only the ENRA, WF

and RWF for non sample spaced channels should be used. The complexity of this RWF can be lowered by SVD based low rank approximation and is especially efficient for "short" channel profiles with MED in the order 1 μs. However at MED of around 4-5 μs very little computational gain can be gained by this low rank technique as the number of singular values with significant value is quite high. Therefore for larger bandwidths of 20 MHz the complexity of the RWF is fairly high.

On the other hand, the true WF and the ENRA provide lower complexities than the RWF even for channels with up to 40 taps and MED of 4-5 μs. The WF and ENRA clearly give the best performances as long as the CIR delays are accurate.

From this analysis we conclude that the WF and ENRA are the most suitable algorithms from both performance and complexity point of view as long as accurate CIR delays are provided. CIR delay tracking for OFDM has been studied in [70,75]. The accuracy and complexity of this methods depend on richness and the variability over time of the delay subspace. In practice it is therefore not trivial to determine the best solution. The RWF will "work" in all cases, within the assumptions and gives a fixed degradation from known channel performance, depending on the MED of the CIR. The ENRA/WF solutions will be able to perform up to 1-2 dB better than this depending on the channel scenario but their reliability is determined by the CIR delay estimate accuracy. In a first release of LTE the RWF solution with low rank precalculated filter is therefore recommended. For further performance improvements, low complex and accurate delay tracking will be needed.

Chapter 7

Pilot pattern and pilot density evaluation

7.1 Introduction

In order to perform coherent detection, reliable channel estimates are required. When dealing with a PACE OFDM based system, these initial estimates are obtained from transmitting known data symbols, also called pilot symbols. As previously shown in chapter 5 and chapter 6, the receiver interpolates from the initial channel information at the pilot position to obtain the channel estimate for the data signal. One of the classical problems of designing a PACE-OFDM system is to decide where and how often to insert pilot symbols. As the pilots are pure overhead consuming system resources, the spacing should be large enough not to increase this overhead too much. At the same time the spacing should be small enough to enable reliable channel estimates.

This chapter proposes several objectives. First, we propose to *investigate the different interpolation algorithms robustness against varying pilot spacing*, also in the case of aliasing due to under-sampled channels. Secondly, *a methodology to be used for pilot design is discussed* based on a tradeoff between algorithmic complexity, pilot overhead and MSE performance. Finally, a *proposal for the pilot distribution and density is made for the studied downlink LTE scenario*.

The Nyquist-Shannon sampling theorem is a fundamental result in the field of

of information theory and is commonly referred to as the sampling theorem [94]. Applied to a PACE OFDM system the minimum pilot spacings required to avoid aliasing have previously been given in equations 5.15 and 5.16. As an example for the 10 MHz bandwidth scenario of DL LTE this can be translated into the numbers of table 7.1 and table 7.2. The ITU and COST PDP radio channels used are given respectively in [16] and [46]. The minimum number of pilot symbols in frequency direction N_p in one OFDM symbol to avoid aliasing is expressed by $N_p = \lfloor \frac{N_u}{\Delta p f_{min}} \rfloor$.

Table 7.1: Minimum frequency direction sample spacing for a 10MHz bandwidth

PDP	Ind A	Ind B	Ped A	Ped B	Veh A	Veh B	TU	RA	HT
T_{med} (ns)	310	700	410	3700	2510	20000	2140	528	18016
$\Delta p f_{min}$	215	95	162,6	18	26,6	3,3	31,1	126,6	3,7
N_p	3	7	4	33	23	180	20	5	163

Table 7.2: Minimum time direction sample spacing for a 10MHz bandwidth

Speed	3 kmph	10 kmph	30 kmph	100 kmph	300 kmph
f_d(Hz)	5,55	18,52	55,6	182,2	555,6
$\Delta p t_{min}$	1260	378	126	38	13

The sampling theorem however, isn't suitable for system design as it doesn't take into consideration the interpolation algorithm used, the performance variation of the algorithms when using oversampling, and the complexity reduction possibilities when using an increased number of pilots. The different algorithm performances strongly depend on the pilot spacing versus channel characteristics. I.e. a higher amount of pilots would allow for low complexity algorithms for a given target MSE.

Before establishing an approach to meet the goals of this chapter, a state of the art is established. In 1997 Tufvesson and Maseng analyzed different pilot patterns by means of BER derived from channel statistics [54]. Their main idea was to keep

the number of pilots to a minimum and thereby reduce the system overhead. Hoeher used a rectangular equispaced pilot grid [63] in his fundamental 2D versus 2 times 1D interpolation comparison. Negi proved analytically in [71] that the optimal selection of pilot symbols was based on equispaced non-clustered pilot symbols. Here, it is noted that he assumed a full bandwidth OFDM system (with $N_u = N_{fft}$) and the TDLS algorithm for his work. In the case of partial bandwidth OFDM with virtual subcarriers (where $N_u < N_{fft}$), Morelli then showed in [79] that equispaced pilots is not an optimal distribution. He showed better MSE performance with non-uniformly spaced pilots. However this behavior is channel specific and exhaustive search is needed for each channel realization to obtain the optimal pilot spacing arrangement. Gracia proposed in [82] a novel hexagonal pilot geometry optimal in sampling efficiency. His work is limited to the case of an optimal 2D Wiener interpolator and purely relies on the sampling theorem. Zhang proposed a novel method of deciding on the number of pilots in [83]. This method is based on analytical uncoded BER calculation as a function of channel statistics and lacks effect of forward error coding (such a Turbo Coding), thereby lacking usefulness for a practical system design. Finally, Choi proposed the optimum pilot pattern that minimizes the MSE for given pilot density and channel statistics in [84]. It was demonstrated that a diamond pilot shape provides estimation performance better than any other shape. Also he stated that the optimum pilot spacing was directly a function of the PDP and Doppler spectrum.

An analytical model of the received OFDM baseband signal has been derived in section 2.2 and is used to further derive a loss model. This model separates channel estimation inaccuracy, pilot overhead and ICI losses. A classical OFDM single tap equalizer is assumed throughout this chapter. Channel estimation efficiency is therefore a tradeoff between pilot spacing and estimation accuracy and has previously been studied in OFDM with ICI [87], and advanced receivers have been derived to cope with ICI. However, these receiver types are excessively demanding in computational complexity [88]. From the above, it may be seen that there are three main mechanisms that will cause a spectral efficiency loss in the system performance:

$$L_{total} = L_{algo} + L_{pilot} + L_{ici}. \tag{7.1}$$

In 7.1 the loss is measured in dB relative to optimal performance. L_{algo} represents the loss due to the inaccuracy of the channel transfer function estimation, and depends on the algorithm as well as the pilot pattern used. L_{pilot} is the loss due to overhead of pilot symbols, which will decrease the amount of available user information symbols. L_{pilot} is solely dependent on the pilot scheme. Finally, L_{ici} is the loss due to ICI from Doppler distortion of the transmitted signal at high speeds.

In the rest of this chapter we will first establish the channel estimation strategy to be adopted in a LTE receiver based on previous work stated in the state of the art. Secondly the behavior of the frequency and time direction interpolation algorithm will be be investigated. A subset of proposed algorithms are selected for frequency direction interpolation from the early study in chapter 6 and time direction from the work in [52]. Based on this we will end up with a pilot scheme proposal for the downlink LTE SISO scenario.

7.2   Channel estimation approach

Form the results of Hoeher in [63] the 2D interpolation problem is separated into 2 times 1D successive interpolations, as the loss by adopting this method is quasi negligible and the computational complexity gains considerable. An adaptive pilot structure would lead to better performance, however such a solution is not desirable as it would lead to increased signalling complexity. Therefore, a fixed "worst-case" design is adopted with one single pilot scheme covering all channel scenarios. The optimum pilot pattern has been shown to be the "diamond" structure in [84]. Unfortunately the LTE frame structure doesn't allow such an accurate pattern. In figure 7.2 we approximate the diamond structure and use the proposed patterns for performance evaluation. As mobile PACE OFDM systems have high latency requirements, the pilot span available in time direction is considerably limited. It follows naturally to perform a stepwise interpolation by starting with the frequency direction interpolation. Then from these full bandwidth estimates at the OFDM symbols containing pilots, we interpolate in a second step in the time direction as shown in figure 7.1.
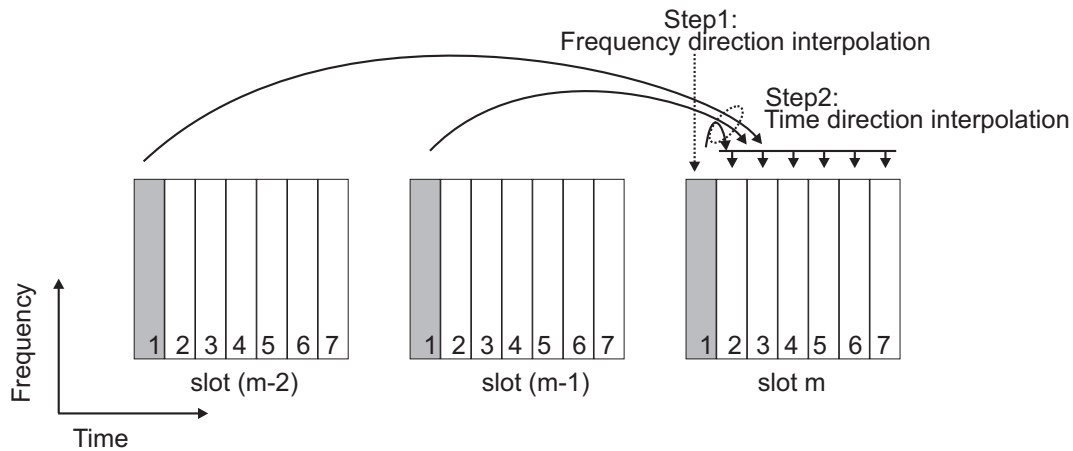
Figure 7.1: Example of the stepwise 2 times 1D interpolation

7.2.1   Frequency-direction interpolation

When receiving a time slot in downlink of LTE containing 7 OFDM symbols, the
first step in the channel estimation process is to estimate the full CTF of the OFDM
symbols containing pilot information. To perform this frequency direction interpo-
lation, a subset of the algorithms studied in chapter 6 is chosen. This subset will
consist of the RWF in the non sample spaced channel case, the ENRA and the
WF. A Linear Interpolation (LI) is also considered as this represents the simplest
interpolation method that can be implemented and has the lowest complexity. It is
included as performance lower bound at lowest complexity cost.

7.2.2   Time-direction interpolation

A requirement in modern mobile communication systems such as LTE is to allow
Discontinuous packet Transmission and Reception (DTX-DRX) as well as use of
frequency hopping on slot basis [47]. To ensure this, a limitation is introduced in
this thesis regarding the time direction interpolation as it must be performed within
the duration of one time slot of $0,5\mu s$ containing 7 OFDM symbols. This will keep
the robustness of the channel estimation algorithm against DTX-DRX and frequency
hopping. Inter-slot interpolation is therefore not considered in this thesis.

Different time direction interpolation methods exist in literature. A common
family of solutions are the polynomial based such as spline [35] and lagrange based

[34]. The simple Linear Interpolation corresponds to be the first order of these. The optimal time direction interpolation in a MMSE sense is the Wiener Filter studied by Hoeher in [63]. A subset of the different solutions performances will be studied in the subsection 7.3.2.

Five type of pilot schemes are proposed for evaluation as seen in Figure 7.2. The schemes are designated according to the number of OFDM symbols carrying pilot information in each sub-frame. The schemes all have the same frequency direction pilot spacing and, may be seen as approximations of the theoretically optimum diamond structure. They mainly differ by their time direction pilot spacing and thereby their ability to deal with the time variations of the channel that are related to the mobility of the considered receiver. For P7 no time direction interpolation is needed as pilots are present in all 7 OFDM symbols of the time slot.
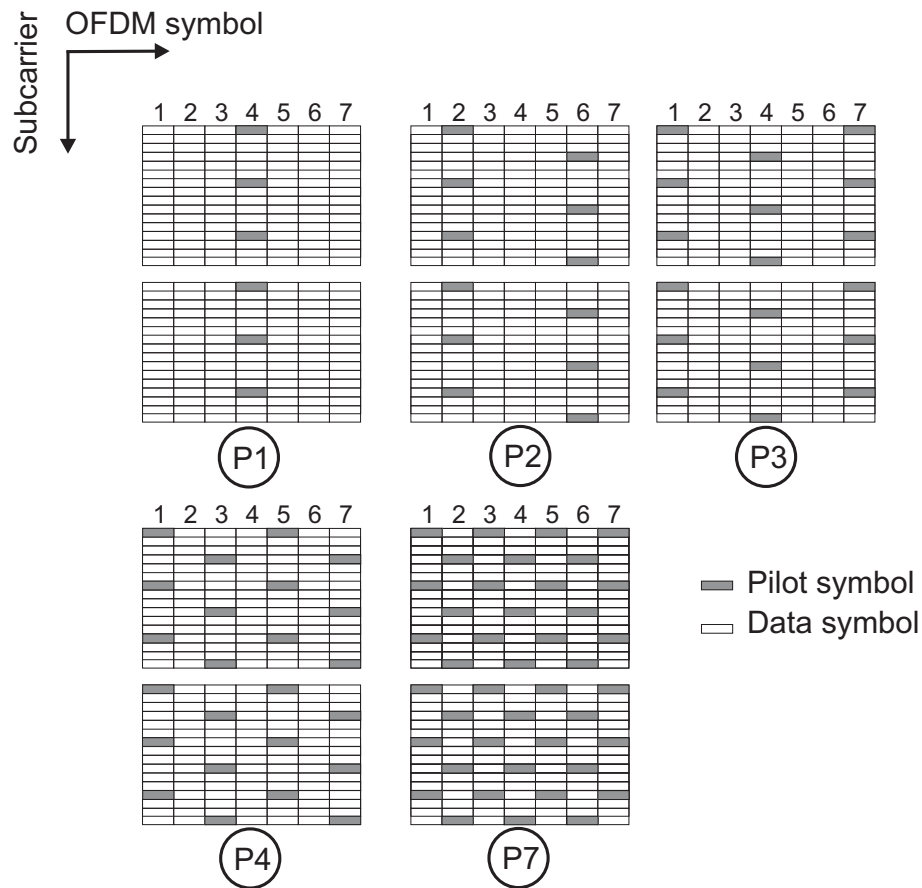

Figure 7.2: Proposed pilot schemes with different time domain spacings

7.3 Pilot spacing study for LTE

7.3.1 Simulation conditions

The simulation results are obtained by Monte Carlo simulation using the settings of the 3GPP UTRA-LTE framework. Referring to Table 7.3 the study assumes a downlink OFDM based transmission scheme using a CP duration of $4.7\mu s$ in unicast mode as well as a subcarrier spacing of 15 kHz. Each time slot duration of 0,5 ms is divided into 7 OFDM symbols of duration $71.4\mu s$ each. The bandwidth occupied by these symbols is scalable into 1.25 MHz, 2.5 MHz, 5 MHz, 10 MHz, 15 MHz and 20 MHz. This study will however only deal with a fixed bandwidth of 10 MHz. Different Modulation and Coding Sets (MCS) are chosen according to the dynamic range of the link adaptation region. The different MCS will range from QPSK ECR 1/6 to 64QAM ECR 4/5. All pilot and data symbols will have equal power in this study. Turbo decoding and interleaving following the UTRA release 6 specifications is used throughout the simulations.

Table 7.3: LTE parameters used for simulations

Parameter	Value
Carrier Frequency	2 GHz
Transmission bandwidth	10 MHz
Time slot duration	0,5 ms
Subcarrier spacing	15 kHz
Nb of OFDM symbols per time slot	7
CP length	4,69 μs
FFT size	1024
Nb of useful subcarriers	1200
MCS settings	QPSK: 1/6, 1/3, 1/2, 2/3 16QAM: 1/2, 2/3, 3/4 64QAM: 1/2, 2/3, 3/4, 4/5

7.3.2 Design method and results

In the following, a pilot spacing design method is proposed. Performance results are obtained by Monte-Carlo simulations using the simulator and the settings described in Table 7.3 . From 7.1 three types of performance degradation have been identified in channel estimation. Since we assume a simple 1 tap equalizer the ICI are not canceled and will contribute an irreducible loss. In general therefore, the trade-off is between L_{algo} and L_{pilot}. A two step procedure that minimizes the algorithmic loss is suggested. First low speed is considered and the largest frequency direction pilot spacing, for which L_{algo} is irreducible, is selected. In a second step, high speeds are considered. A worst case 300 km/h scenario is used to determine the time direction spacing that leads to the best performance.

Frequency direction pilot spacing

Low speed is taken to mean that the channel is quasi static during the transmission of one time slot. This will be 3 kmph in our study. In this state, only the pilot spacing in the frequency direction has an impact on the estimation of the CTF. The performance loss due to ICI produced by the Doppler frequency is considered negligible, $L_{ici} \approx 0$. The goal is then to find the smallest L_{pilot} for which $L_{algo} \approx 0$. From literature, a common way to determine the theoretical minimum spacing is to use the Nyquist sampling theorem. However, as performance is algorithm dependent, the results in this section will be given through simulations.

In order to evaluate the behavior of the algorithms two channel scenarios are considered for simulation. The first one uses the Indoor B profile [16], covering the case of a short MED ($T_{med} = 0, 7\mu s$). The second PDP chosen is the Pedestrian B, covering the case of a long MED ($T_{med} = 3, 7\mu s$). Note that PDP's can have much longer MED with $T_{med} = 20\mu s$ for the Vehicular B profile. The performance for this case is shown in appendix D.1, but not considered in this chapter as the probability of experiencing such long MED is relatively low in practice.

The 4 interpolation algorithms LI, RWF, ENRA and WF are evaluated by monte carlo simulations in figures 7.3, 7.4, 7.5 and 7.6, for varying frequency direction pilot spacing Δp_f in the pilot scenario P1. The modulation scheme is chosen to be 16QAM
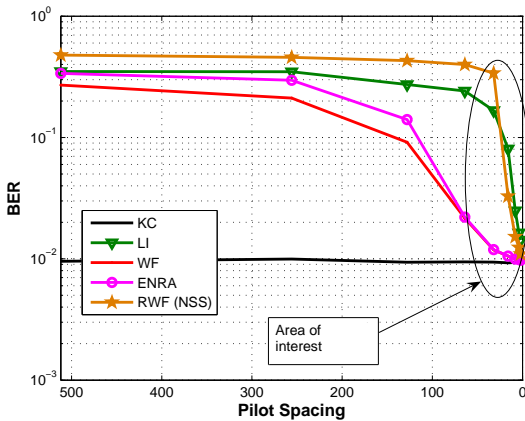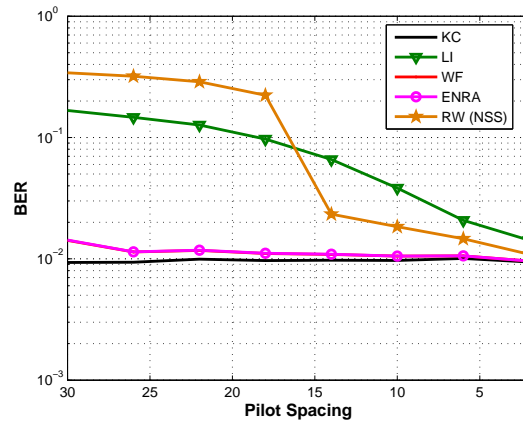
Figure 7.3: Full PedB

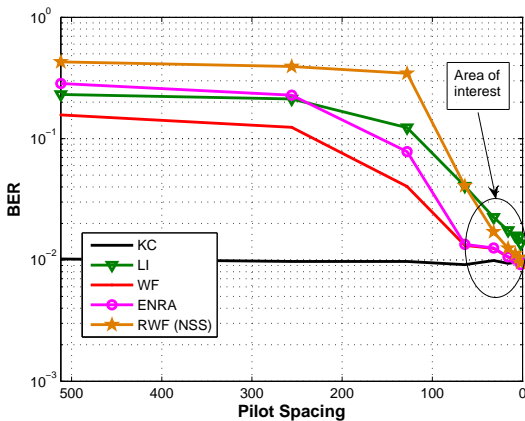Figure 7.4: Area of interest for PedB
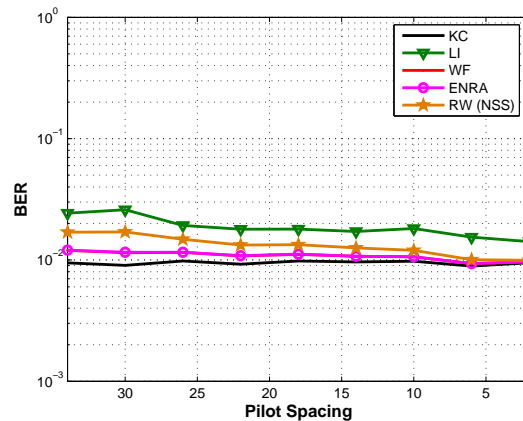

Figure 7.5: Full IndB

Figure 7.6: Area of interest for IndB

Figure 7.7: BER for different Frequency direction interpolation algorithms and varying frequency direction pilot spacing (16QAM, Eb/No = 17dB, 10 MHz bandwidth). The right hand figures are higher resolution simulations with a pilot spacing from 2 to 30 subcarriers.

and the uncoded BER versus Δpf are chosen as evaluation criterion.

The pilot spacings simulated are $\Delta p_f \in \{2, 4, 8, 16, 32, 64, 128, 256, 512\}$ in figure 7.3 and 7.5. When looking into the areas of interest with reduced performance degradation, we notice that the pilot spacing is low. The pilot spacing resolution is then increased in the area of interest for the right hand figures 7.4 and 7.6. In the case of PedB it is observed that the ENRA and WF are robust to the pilot spacing variation whereas LI and even RWF quickly degrade in BER as the pilot spacing is increased. In the case of IndB it is observed that all the algorithms seem robust to a variation of pilot spacing in the range of [2 30]. The LI has clearly the worst BER as expected. We also note that for low pilot spacing of $\Delta p_f \leq 10$, the RWF performs quasi optimally. For further results a pilot spacing of $\Delta p_f = 8$ is chosen as average value.

Time direction pilot spacing

At high velocities the channel varies significantly during the transmission of one time slot. In this state, $L_{ici} > 0$, since with a classical single tap equalizer the ICI cannot be canceled. However, by choosing pilot scheme P7, pilots will be present in each OFDM symbol and it is possible to obtain $L_{algo} \approx 0$ without the use of time direction interpolation. Consequently, by looking at Packet Error Rate (PER) we can quantify the degradation due to ICI. The PER for three different MCS and two different speeds is shown in Figure 7.8.

Assuming a link adaptation operating point at a PER of 20 %, the loss due to ICI is given in Table 7.4. At 100 kmph the loss due to ICI is minimal, whereas it can be as high as 1,5 dB at 300 kmph for 64QAM ECR 2/3.

Table 7.4: Performance loss due to ICI and estimation inaccuracy at 20 % PER

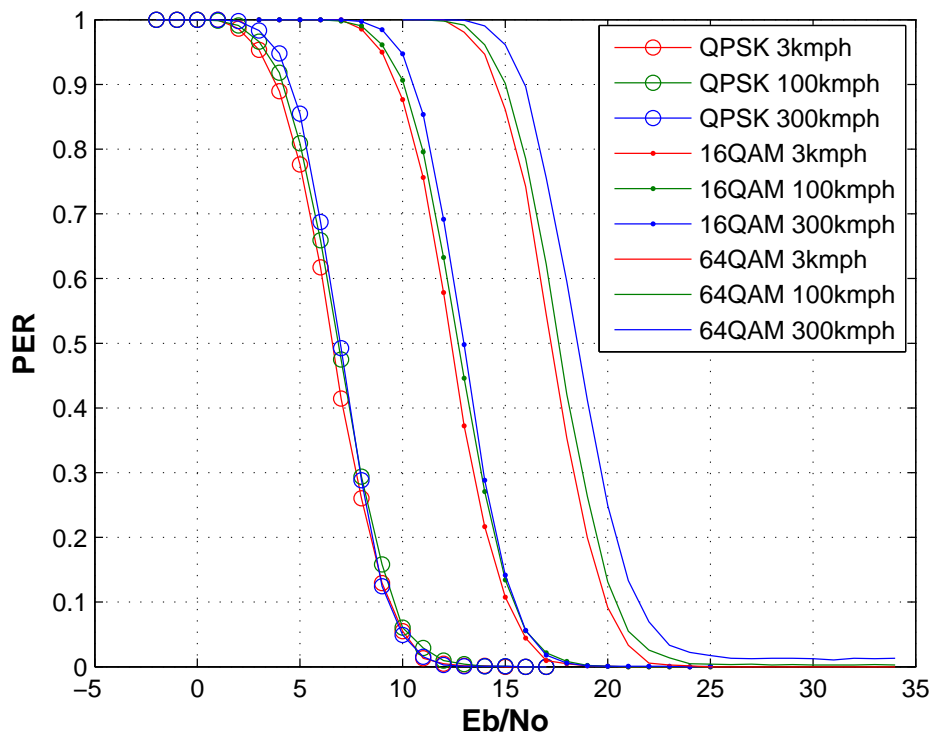| Velocity	100 kmph	300 kmph
QPSK, ECR 2/3	0,1 dB	0,3 dB
16QAM, ECR 2/3	0,4 dB	0,5 dB
64QAM, ECR 2/3	0,5 dB	1,5 dB

Figure 7.8: PER for varying G-Factor and velocity in a Typical Urban [46] profile using P7, Wiener filtering and pilot frequency set to 8

To include the loss from pilot overhead spectral efficiency results are required. The loss due the pilot overhead purely depends on the pilot scheme chosen as seen in Table 7.5 where the previous assumption of frequency direction spacing of 8 has been used.

Table 7.5: Total pilot overhead when $\Delta p_f = 8$

Scheme	P1	P2	P3	P4	P7
Overhead	1,8%	3,6%	5,4 %	7,1 %	12,5 %

In order to fully determine the performance tradeoff between pilot overhead and algorithm loss, link level simulations have been conducted for all the previously mentioned modulation and coding schemes at a range of average SNR values. Then at each SNR we have chosen the MCS leading to the highest spectral efficiency
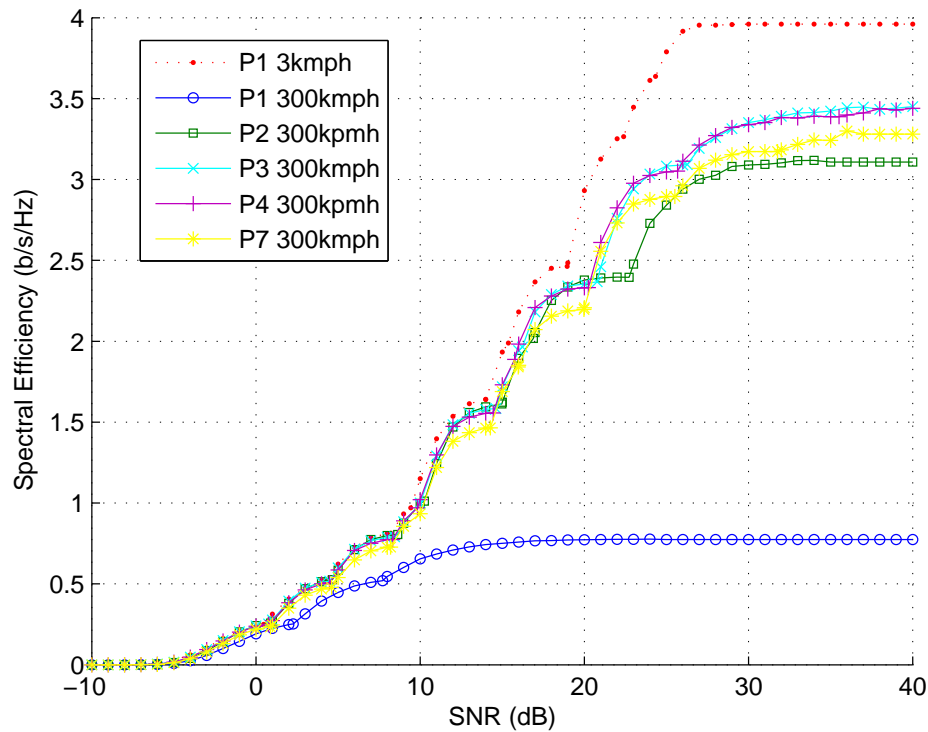
Figure 7.9: Spectral Efficiency in DL LTE, Typical Urban [46], 10MHz

so as to obtain an ideal link adaptation curve. Because of the large bandwidth assumption, which stabilizes the SNR, this result is almost identical to real time domain link adaptation as shown in [95]. The link curves for the different pilot schemes and different speeds are shown in Figure 7.9, including the low speed case with P1. This latter shows the upper performance bound achievable for a LTE system, as in this case $L_{ici} \approx 0$ and $L_{algo} \approx 0$, leaving only degradation to pilot overhead of 1.8%.

At 300 kmph there is similar Spectral Efficiency using the pilot schemes P2, P3, P4 and P7 with SNR ranging from -10 dB up to 20dB. However when going above 20 dB of SNR P2 and P7 perform with around 0,3 bits per second per Hertz less spectral efficiency. In the case of P1 at 300kmph the achievable efficiency is limited to around 17 % of the low speed performance. The choice of one single pilot scheme to cover all channel scenarios boils down to choosing between P2 and P3. P2 has a lower high speed worst case performance in the area of high SNR compared to P3. From

the requirements of [2] the LTE system should be optimized for low mobile speed but also support high mobile speed. Therefore the scheme P2 will be chosen, as it optimizes the systems at low speed by having less pilot overhead but still provides sufficient performance at high speeds. This will give a time direction spacing set to 3,5 OFDM symbols in average and with the frequency direction spacing set to 8 subcarriers, corresponding respectively to 0.25 ms and 120 kHz. The pilot overhead will be 3.6%.

7.4 Conclusion

The purpose of this chapter has been to give an estimate of performance degradation due to channel estimation as well as to propose a suitable pilot distribution in a downlink context. This work has differed from previous similar studies as it targets the UTRA-LTE context, with practical constraints considered. Notably, these are low latency, optimized low speed performance, improved spectral efficiency, low terminal complexity, and support for high mobile speed. Different objectives were proposed.

First the robustness of different interpolation algorithms against variation of pilot spacing was investigated. In the frequency direction the RWF and LI turned out to be very sensitive to minor changes in pilot spacing in the case of PDP with long delays. When the delays are short, sensitivity to varying frequency direction pilots spacing is quasi-insignificant. The ENRA and WF using a priori knowledge of tap delay location turned out to be very robust to pilot spacing variation even in the case of large PDP delays. In the time direction the importance of algorithm choice is of little relevance in the low speed scenario as the channel is quasi-static over the duration of one time slot. At very high speeds up to 300 kmph worst-case scenario, LI can still be used but leads to performance degradation at high SNR using a 64QAM modulation. The overall importance of time direction interpolation is however reduced as ICI is irreducible when using a classical OFDM 1 tap equalizer. Also DRX-DTX, and latency requirements force the estimation to be done within the duration of one time slot estimation, and inter-slot interpolation is undesirable.

Secondly, a methodology for pilot distribution design based on LTE system specific requirements has been proposed, leading to a two step strategy. Step one determines the largest frequency direction pilot spacing that keeps the estimation loss low. This is done in a low speed scenario where the channel is stationary during one time slot transmission. Step two evaluates the largest time direction pilot spacing leading to acceptable performance in a worst-case 300 kmph high speed scenario.

Thirdly, one fixed pilot pattern is proposed for downlink LTE from the previously derived method. The pilot scheme will have an overhead of 3,6 %, cover all considered channel scenarios and will have support for high mobile speeds up to 300kmph. Spectral efficiency results are shown for a wide range of proposed modulation and coding schemes going from -10 dB to +40 dB SNR, and confirm the validity of the proposed distribution.

Finally, future perspectives would be to investigate the feasibility of frequency direction interpolation algorithm using a priori tap delay knowledge, thereby allowing very low pilot overhead. Also the scenario of single frequency network MBMS transmitting continuous data would increase the importance of time averaging, filtering and predictive algorithms.

Chapter 8

Self-induced interference cancelation

8.1 Introduction

One of the main assumptions for the studies carried out in chapters 5, 6 and 7 is to assume a PDP MED duration smaller than the CP duration of the OFDM symbol. Unfortunately this assumption doesn't always hold true in which case the receiver signal quality is degraded by the resulting interference. The classical characterization of self induced interference in OFDM is modeled by Inter OFDM-Symbol Interference (ISI) and Inter Carrier Interference (ICI). The insertion of the CP cancels the interference as long as the CP is sufficiently long, but with larger fading delays, the CP can only mitigate this interference. A serious drawback of introducing a CP is the linear reduction of spectral efficiency of the system by a factor of $\frac{T_g}{T_{ofdm}}$, as the CP is pure overhead and doesn't contain any additional data information. Another source of ICI is the time variation of the radio channel when appreciable changes occur during one symbol period as studied in [22], [23] and [24]. The effect of ICI due to time variation of the radio channel will not be the focus of this chapter. Proposal of an adaptive CP length technique has been made in [98]. The downside of this proposal is the increased system signalling complexity when the solution has to adjust to different radio scenarios as the receiver experiences different radio propagation environments.

Different techniques have been studied so far to deal with the ISI and ICI resulting from a long channel MED. Kim and Stüber use the last correctly detected symbol to perform residual ISI cancelation in [97]. This technique is well suited for static slowly fading channels but doesn't deal with ICI. To mitigate long PDP's, impulse compression techniques have been studied by Melsa in [99] and by Schur [100]. The drawback of their solutions is the equalization filter length placed before the CP removal in the receiver and the related computational complexity. Also the interference is only mitigated and not completely canceled and their setup requires non-PACE based channel estimation which isn't a LTE compatible solution. Suzuki proposes in [101] a hybrid receiver where the ISI is dealt with using windowing techniques [102] and a MUD approach from Parallel Interference Cancelation (PIC) in DS-CDMA from [103] to remove the ICI. Even though this solution has practical interest the ISI is only partially removed and the computational complexity is still high.

Much research has been done on Interference Cancelation (IC) and Multiuser Detection (MUD) for CDMA [36]. As shown by our analytical model in subsection 2.2 with equation 2.24 it is possible to make an analogy between OFDM and CDMA receivers. Thereby MUD based techniques can be adapted to OFDM. When the CIR is known the interference matrices $\mathbf{C1}_{m-1}$ and $\mathbf{C0}_m$ from equation 2.24 can be determined and inverted. Unfortunately the direct computation of the matrix inverses is not appropriate due to the high computational complexity when a large number of subcarriers is used. Therefore there is a need for efficient interference cancelation techniques applied to OFDM. The aim of this chapter is first to *give an estimate of the spectral efficiency degradation when the CP has a fixed length shorter than the MED in a LTE context*, then *different IC techniques should be elaborated*, and finally *an improved IC scheme is to be proposed with tractable complexity as a function of the desired performance.* In this chapter **we propose a pre-study on the possibility to improve the performance of a LTE based system when the CP length is to short to compensate for all excess delays of the CIR, by applying CMDA-MUD based techniques to OFDM**. Put in an other way, we propose an algorithmic study to enable shorter CP length design and improved

interference reduction in OFDM systems, by means of IC in the receiver.

Section 8.2 sets the scene by introducing ISI and ICI problematic, as well as showing the impact of a long MED channel profiles on spectral efficiency in a short CP scenario. Different classical IC techniques are also presented and performance is given in a LTE context. Section 8.3 discusses the novel LCIC algorithm. Section 8.4 evaluates the feasibility of the LCIC algorithm in LTE through a complexity analysis. Finally section 8.5 discusses the obtained results.

8.2   Analysis

As stated in chapter 4, it is beneficial to only have one fixed CP length in a OFDM system. Thereby reducing the system signalling complexity and the related information overhead to be transmitted instead of data information. When only one CP length is to be chosen for a system, it is not possible both to have a short CP to reduce the CP overhead, and a long CP to limit the interference created by long PDP delays. A tradeoff solution must be chosen. In figure 8.1 the spectral efficiency versus SNR is shown in the case of three channel PDP, namely Typical Urban (TU), Vehicular B (VehB) and Hilly Terrain (HT) (presented in Appendix A). The ICI and ISI resulting from a channel MED longer than the CP length of $4,69\mu s$ degrades tremendously the achievable performance. At low SNR the degradation is not so significant, however at high SNR a performance floor is observed for VehB and HT, where the spectral efficiency is limited to 1,9 and 2,4 Bit/s/Hz respectively.

The idea is to apply DS-CDMA MUD principles to OFDM when interference such as ISI and ICI corrupts the signal. In a first step we recall, from section 2.2, equation 2.24:

$$\mathbf{z}_m = \mathbf{C0}_m\mathbf{d}_m + \mathbf{C1}_{m-1}\mathbf{d}_{m-1} + \tilde{\mathbf{\Psi}}_m^H\mathbf{w}_m$$

and equation 2.25:

$$\mathbf{z}_m = \mathbf{z}_{\mathrm{S},m} + \mathbf{z}_{\mathrm{ICI},m} + \mathbf{z}_{\mathrm{ISI},m} + \tilde{\mathbf{\Psi}}_m^H\mathbf{w}_m.$$

The dimensions of $\mathbf{C0}_m$ are $(N_u.N_u)$, which gives for a LTE 20MHz scenario, $N_u = 1200$. The inversion of such a large matrix is computationally prohibitive
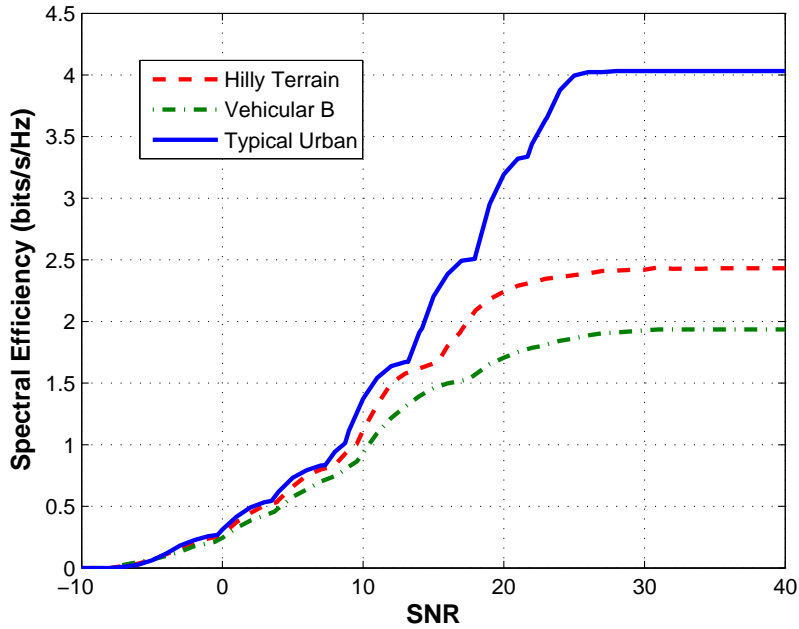
Figure 8.1: Spectral efficiency for different PDP with $T_g = 4, 69\mu s$, with a classical OFDM Linear Equalizer in a 10 MHz bandwidth

in a mobile terminal. However methods such a Parallel Interference Cancelation (PIC), Sequential Interference Cancelation (SIC) and Ordered Sequential Interference Cancelation (OSIC) do not rely on matrix inversion and will be investigated in this section.

8.2.1   Parallel Interference Cancelation

The proposed PIC scheme is depicted on figure 8.2(a). First an initialization phase is run in order to get the initial values necessary for the main loop to start. The ISI $\mathbf{z}_{\mathrm{ISI},m}$ is removed in a one shot process from the $\mathbf{z}_m^{(0)}$ vector. The $\mathbf{z}_{\mathrm{ISI},m} = \mathbf{C1}_{m-1}\mathbf{d}_{m-1}$ vector is calculated from the data symbols $\mathbf{d}_{m-1}$ detected from the $(m-1)^{th}$ OFDM symbol. Then data detection is done with the simple OFDM specific Linear Equalizer (LE) also called Maximal Ratio Combining (MRC). Other methods could be used such as Equal Gain Combining (EGC) or MMSE Combining (MMSEC), however for simplicity we only focus on the classical OFDM equalizer LE. The last step in the initialization is then to evaluate the initial ICI $\mathbf{z}_{\mathrm{ICI},m}^{(0)}$.

Once the initialization is complete the iterative phase can start. In a first step, the ICI $\mathbf{z}_{\text{ICI},m}^{(s)}$ is removed from the ISI free received signal $\mathbf{z}_m$. In a second step, the symbol detection is performed using the LE with known $\mathbf{C0}_{\text{S},m}$ (containing the diagonal elements of $\mathbf{C0}_m$) equivalent to the CTF. In a third step, symbol decision is performed based on minimal Euclidean distance. Finally the fourth step, tests if the number of iterations s is larger than the maximal number of iterations $\mathbf{S}$. If $s \geq \mathbf{S}$ the loop ends and the latest updated $\mathbf{d}_m^{(s)}$ is used as detected data symbols, else if $s < \mathbf{S}$ the loop continues and the ICI is updated with newly detected symbol vector $\mathbf{d}_m^{(s)}$.

8.2.2   Sequential Interference Cancelation

The proposed SIC scheme is depicted on figure 8.2(b). The initialization phase for both SIC and OSIC schemes is the same as for the PIC scheme. The iterative phase is however different. It is built as two concatenated loops. The inner loop removes ICI $\mathbf{z}_{\text{ICI},m}^{(s)}[k]$ row by row considering only one subcarrier at the time for each iteration k. At each inner iteration a new symbol detection is performed giving $\mathbf{d}_m^{(s)}[k]$. This symbol is then used to update the ICI if the symbol has changed from the previous outer iteration. This entire procedure is repeated until the iteration counter k is incremented to N_u. When $k = N_u$ the outer loop iteration counter s is incremented by 1. This procedure is then repeated until the outer loop counter is equal to $\mathbf{S}$, where both loops end and the latest updated $\mathbf{d}_m^{(s)}$ is used as detected data symbols.

The proposed OSIC scheme is depicted on figure 8.2(c). The OSIC scheme is almost identical with the SIC scheme with the difference that it orders the sequence of received signal subcarriers $\mathbf{z}_{\text{ICI},m}^{(s)}[k]$ at the beginning in each iteration of the outer loop. Then at the end of both loops the original subcarrier order is restored.
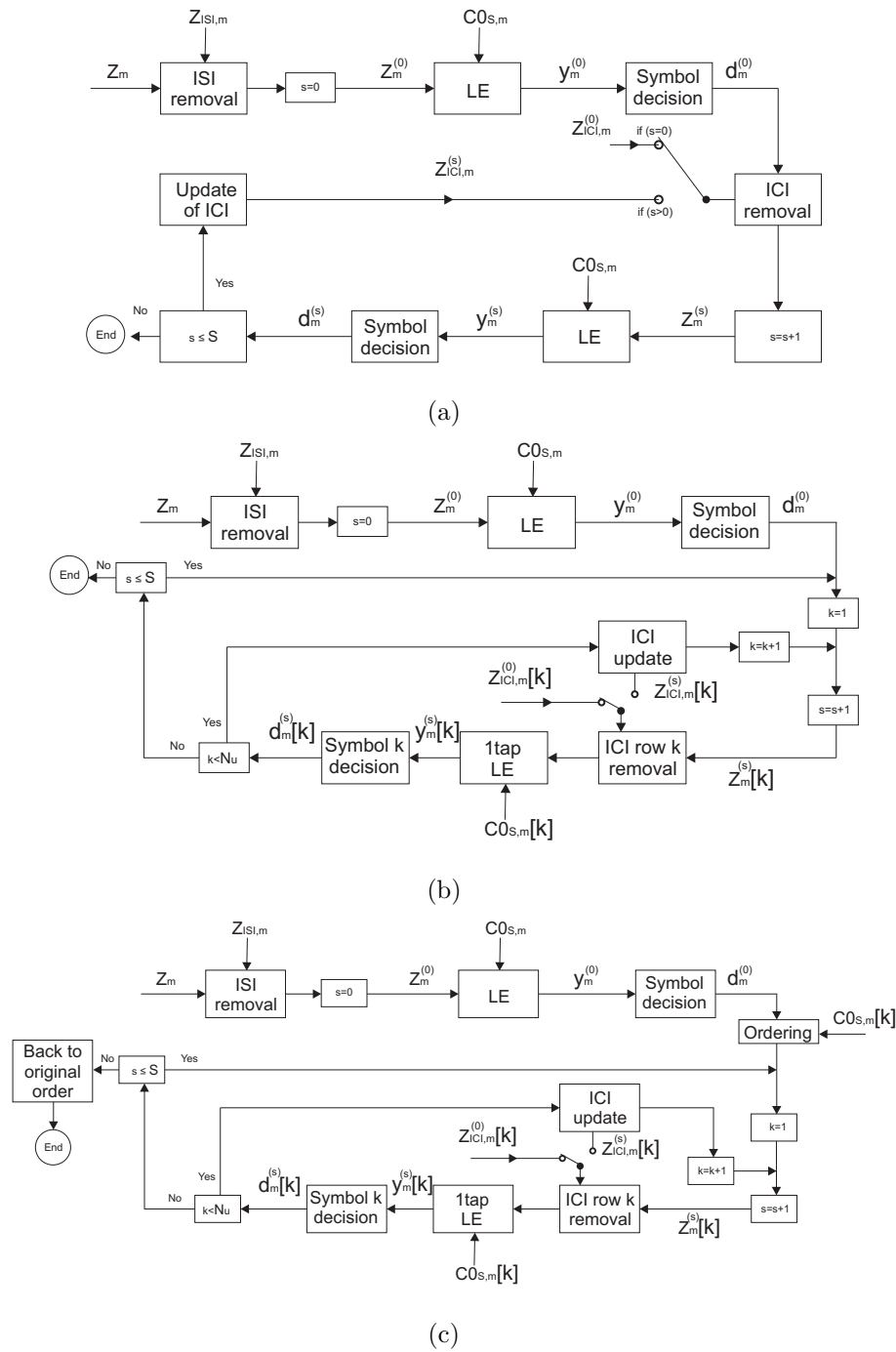
Figure 8.2: Interference cancelation schemes: (a) PIC, (b) SIC and (c) OSIC

8.2.3 Performance analysis

In order to evaluate and compare the performance of the three proposed classical IC schemes, a simulation scenario of $N_{fft} = 512$, $T_s = 7,68ns$, QPSK modulation scheme and a VehB PDP is proposed in figure 8.7. In a first step the effect of varying the length of the CP on the uncoded BER when using a simple Linear Equalizer (LE) is given on figure 8.3. As the CP length increases, the uncoded BER is lowered until it achieves the theoretical bound where no interference is present $(T_g > T_{med})$. Figures 8.4, 8.5 and 8.7 correspond respectively to PIC, SIC and OSIC, where the simulations are conducted with a very short CP of $T_g = 0,13\mu s$. For all three schemes there is a large BER gain already at $\mathbf{S} = 1$. However even at $\mathbf{S} = 4$ the optimal performance isn't achieved. In figure 8.8 the convergence rate of the three classical schemes is studied. The difference between PIC, SIC and OSIC is that OSIC has almost reached is optimal point after only $\mathbf{S} = 2$, whereas PIC and SIC need $\mathbf{S} = 4$ iterations. Also the OSIC has a lower performance bound than PIC and SIC.

All three schemes have the same initialization with the simple low complex LE. This initialization could be improved with more advanced solutions such as ZF or MMSE. Unfortunately such approaches are too computationally expensive . Another way of improving the initial estimate would be to slightly increase the CP length up to a reasonable value of $1\mu s$ or $2\mu s$.
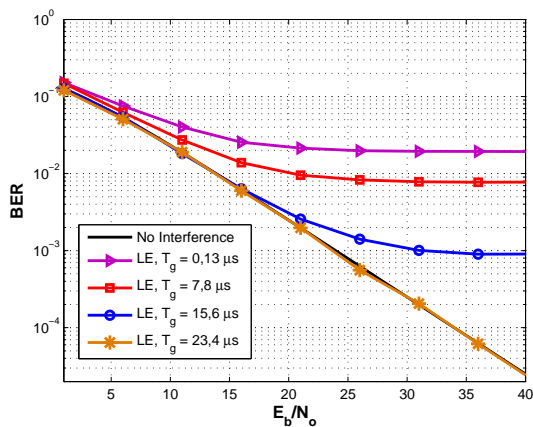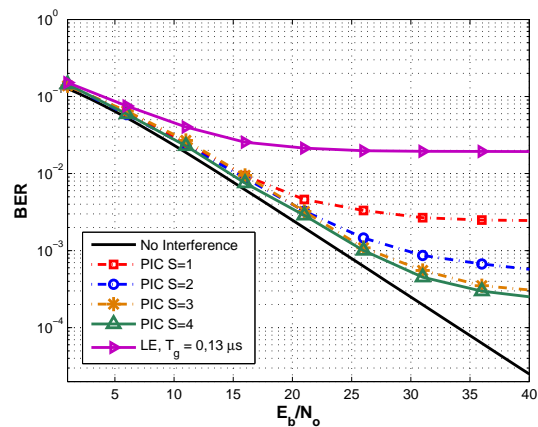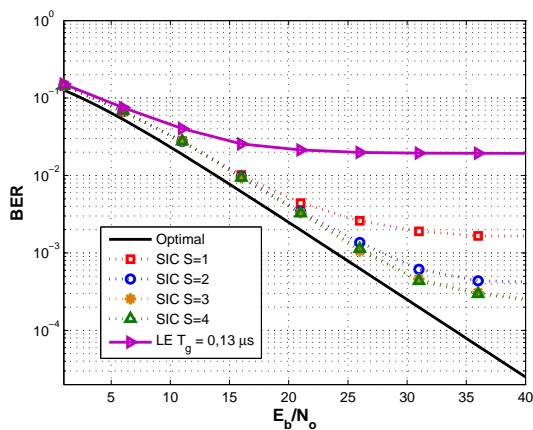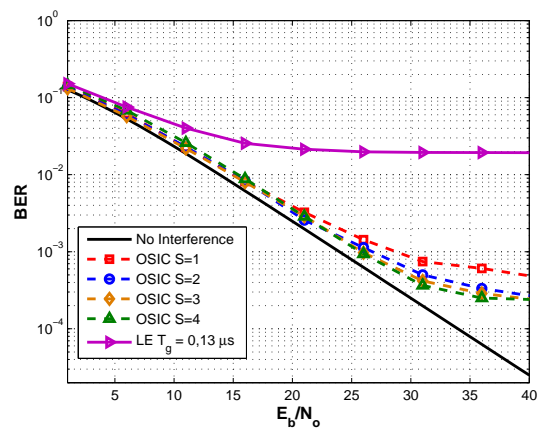
Figure 8.3: LE

Figure 8.4: PIC

Figure 8.5: SIC

Figure 8.6: OSIC

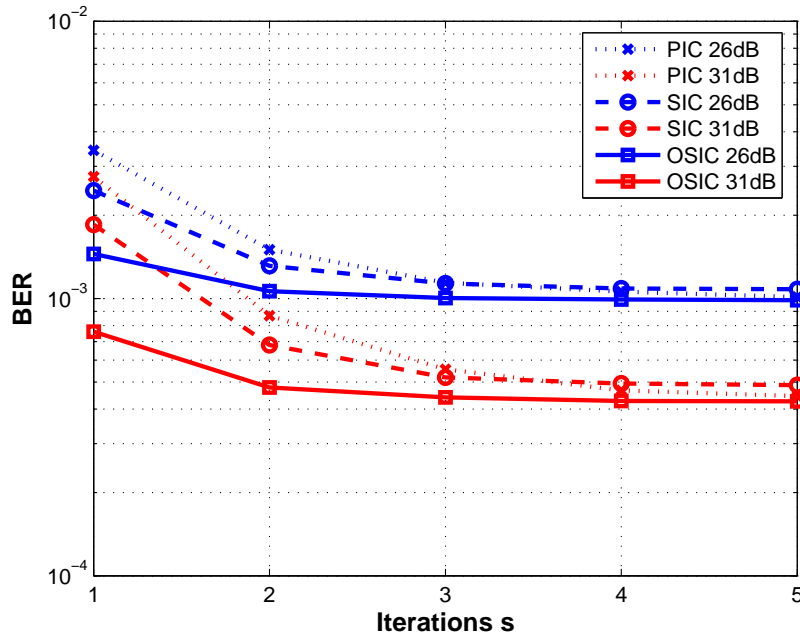Figure 8.7: Uncoded BER vs. Eb/No with $T_s = 7,68ns$, $N_u = N_{fft} = 512$, VehB

Figure 8.8: BER comparison of classical schemes for increasing iterations s

8.3 The LCIC algorithm

The OSIC scheme has the best performance of the three previously studied IC cancelation schemes. However at each outer iteration s, N_u^2 complex operations are required to cancel the ICI as well as N_u^2 complex operations are required at the initialization to cancel the ISI. When looking closer at the correlation matrices $\mathbf{C0}_m$ and $\mathbf{C1}_m$ in figure 8.13, where a 2D and 3D representation of $log(arg(\mathbf{C0}_m[k', k]))$ and $log(arg(\mathbf{C1}_m[k', k]))$ give a snapshot example of the interference distribution within the given matrices, $\{k', k\} \in [1, 128]^2$ and $\{k', k\} \in \mathbb{N}^2$.

The figure can be interpreted as: strong interference comes from nearby subcarriers, whereas distant subcarriers only interfere little the desired signal. The strongest components are mostly to be found in the diagonal of $\mathbf{C0}_m$.

From these practical observations it would makes sense only to consider a limited amount of subcarriers for IC, namely the ones with the strongest variance. By choosing the $\mathbf{I}^{th}$ closest subcarriers the complexity can be reduced by a factor $\frac{N_u}{\mathbf{I}}$. The LCIC algorithms pseudo code is given in the following.
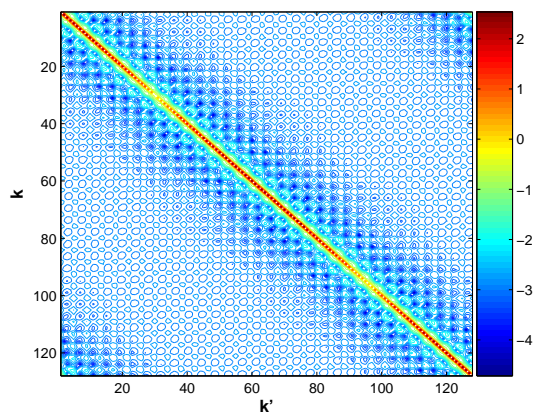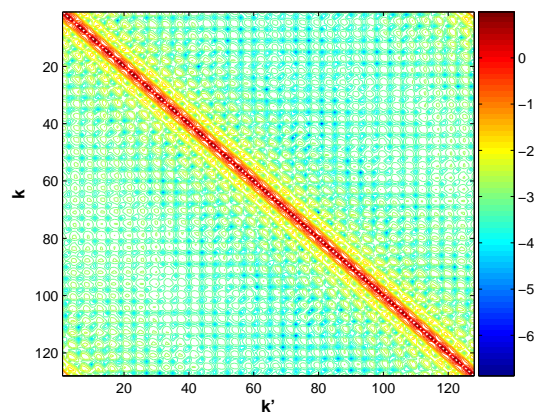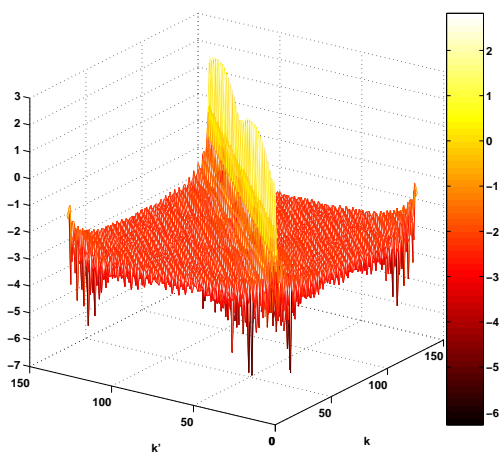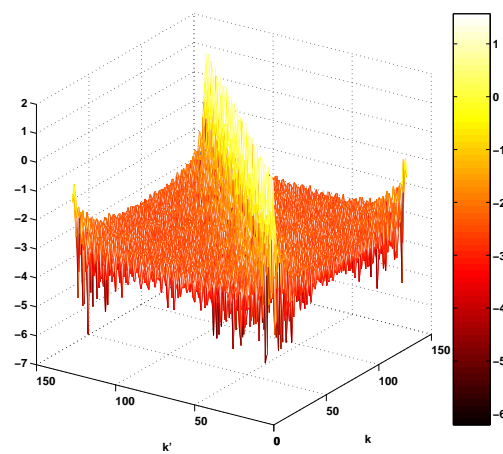
Figure 8.9: 2D contour plot of $\mathbf{C0}_m$

Figure 8.10: 2D contour plot of $\mathbf{C1}_m$

Figure 8.11: 3D mesh plot of $\mathbf{C0}_m$

Figure 8.12: 3D mesh plot of $\mathbf{C1}_m$

Figure 8.13: Snapshot example of the log of the argument of the correlation matrices

<div align="center">**LCIC pseudo code:**</div>

Initialization phase :

$$s = 0$$

$$\mathbf{z}_m^{(0)} = \mathbf{z}_m - \mathbf{C1}_{\text{band},m-1}\mathbf{d}_{m-1}$$

$$\mathbf{y}_m^{(0)} = \mathbf{C0}_{\text{S},m}^{-1}\mathbf{z}_m^{(0)}$$

$$\mathbf{d}_m^{(0)} = csgn\{\mathbf{y}_m^{(0)}\}$$

Iterative phase :

Step1 : Matrix-Vector Ordering

Step2 : $k = 1$

Step3 : $s = s + 1$

$$\mathbf{d}_m^{(s)} = \mathbf{d}_m^{(s-1)}$$

Step4 : $while(k \leq N_u)$

$$\mathbf{z}_m^{(s)}[k] = \mathbf{z}_m^{(s-1)}[k] - \mathbf{C0}_{\text{band},m}[k,(k-\mathbf{I},...,k+\mathbf{I})]\mathbf{d}_m^{(s)}[k-\mathbf{I},...,k+\mathbf{I}]$$

$$\mathbf{y}_m^{(s)}[k] = \mathbf{C0}_{\text{S},m}^{-1}[k,k]\mathbf{z}_m^{(s)}[k]$$

$$\mathbf{d}_m^{(s)}[k] = csgn\{\mathbf{y}_m^{(s)}[k]\}$$

$$k = k + 1$$

$$endwhile$$

**Step5** : $if(s \leq \mathbf{S})goto$ **Step2**

$else$ Reorder $\mathbf{d}_m^{(s)}$ and $\mathbf{y}_m^{(s)}$

$$endif$$

A graphical explanation of the initial ISI removal phase and a single iteration of ICI canceling in **Step 4** of the LCIC algorithm is given in figure 8.14. From this pseudo code and figure the data flow of the LCIC unfolds naturally. When comparing this targeted interference removal tot the graphical representation of $\mathbf{C0}_m$ and $\mathbf{C1}_m$ in figure 8.13, the complexity reduction becomes straightforward.

The performance of the LCIC for varying initial estimate qualities is given in figure 8.15. Both sub-figures show that the the steepness of the uncoded BER curve is highest for rather small values of $\mathbf{I}$. Also the performance gain by increasing the CP
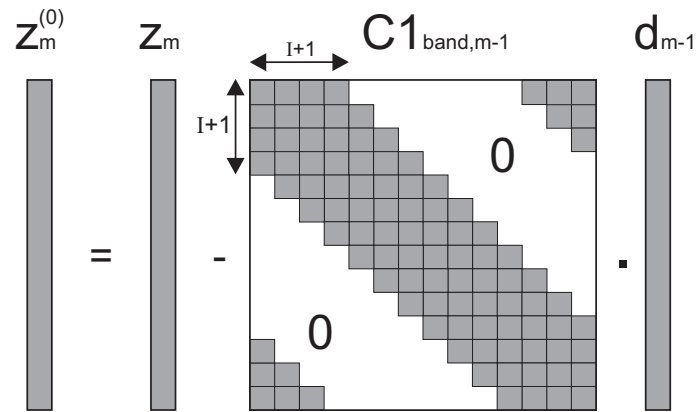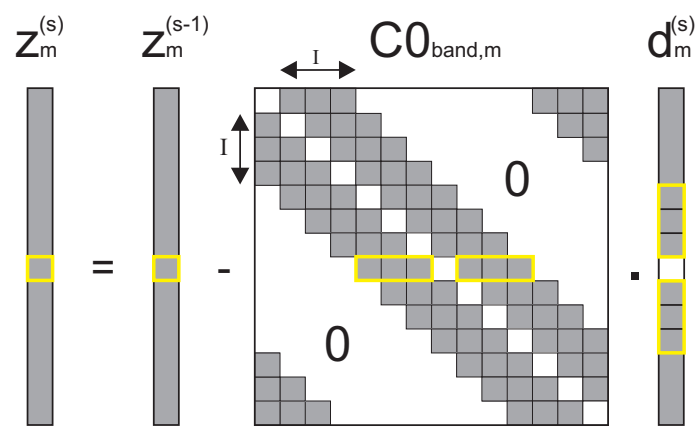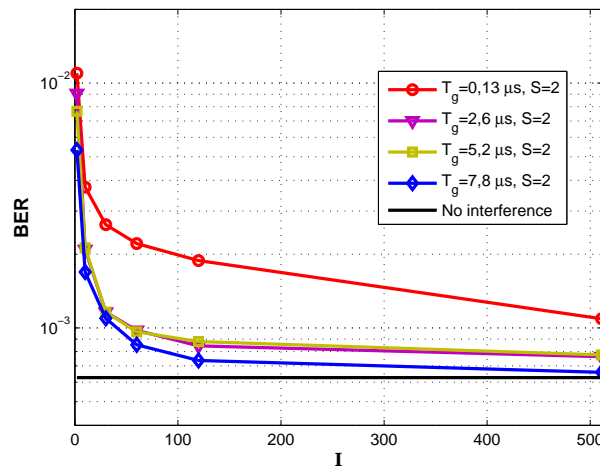
Figure 8.14: Matrix-vector illustration of two key steps in the LCIC algorithm: (a) Initial one shot ISI removal, (b) Inner iteration k with ICI row removal

length is significant, showing the importance of having good quality initialization. The optimal "No-interference" bound is not reached but the LCIC approximates it with a CP of $T_g = 7, 8\mu s$ (approximately a third of the MED).

(a)
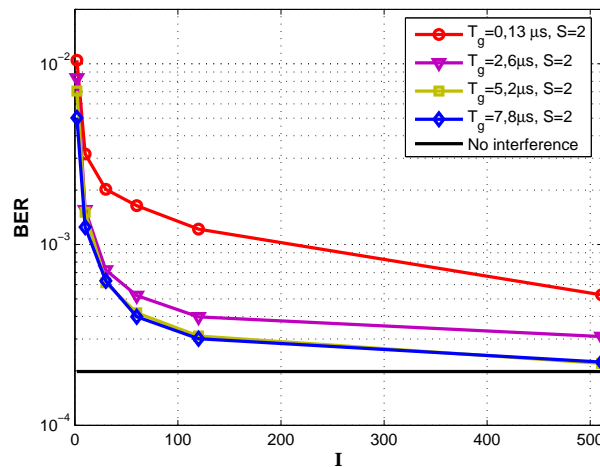
(b)

Figure 8.15: LCIC with different CP lengths for varying **I** and **S** = 2: (a) SNR=25dB, (b) SNR=31dB

8.4   Complexity and implementation

In this section the computational complexity of the different studied interference cancelation algorithms will be studied. In slowly fading channels the matrices $\mathbf{C0}_m$

and $\mathbf{C1}_m$ don't need to be updated frequently. Yet, as speed increases these ISI and ICI matrices need to be updated more frequently. The evaluation of the banded version of these matrices for the LCIC algorithm highly depend on the CIR instantaneous estimate. The calculation of their computational complexity could be very high if calculated in an straightforward brute force manner. However smart filtering based on lookup tables with delay dependent correlation could be investigated. Nevertheless this is a quite large topic and is not the focus of this section. Therefore the ISI and ICI matrices are assumed to be known and their complexity is not evaluated in this section.

The calculation of the complexity of the different IC methods follows the same guideline as the one given in section 6.5. Big O notation is used and from this follows that minor operations such as sorting and counter incrementations are not included in the counting. When observing figure 8.2 the orders of complexity of the PIC, SIC and OSIC schemes are equivalent and will be referred to as "classical" IC schemes complexity.

The amount of CMAC needed for the interference cancelation process for data detection of one OFDM symbol will be determined. The different complexity orders are given in table 8.1.

Table 8.1: Complexity order for the studied IC schemes

Algorithm	Complexity
Classical	$O((\mathbf{S}+1)N_u^2)$
LCIC	$O((\mathbf{S}+1)2\mathbf{I}N_u)$

Figure 8.16 depicts the number of CMACs needed per OFDM symbol as a function of the number of iterations $\mathbf{S}$. Also the gain of using the LCIC versus the classical schemes is shown. For small values of $\mathbf{I}$, the gain can be up to a factor 100.
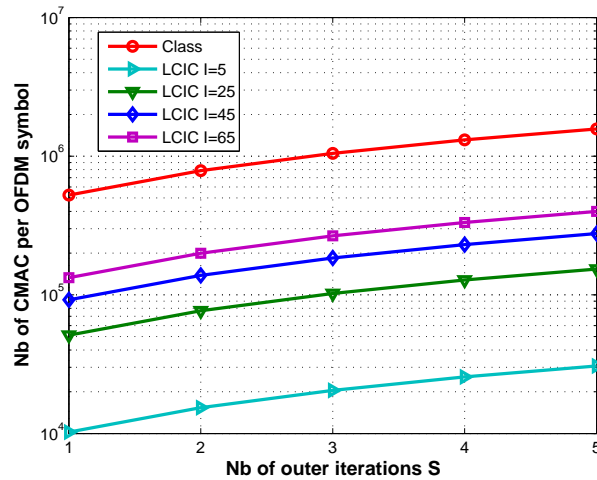
(a)
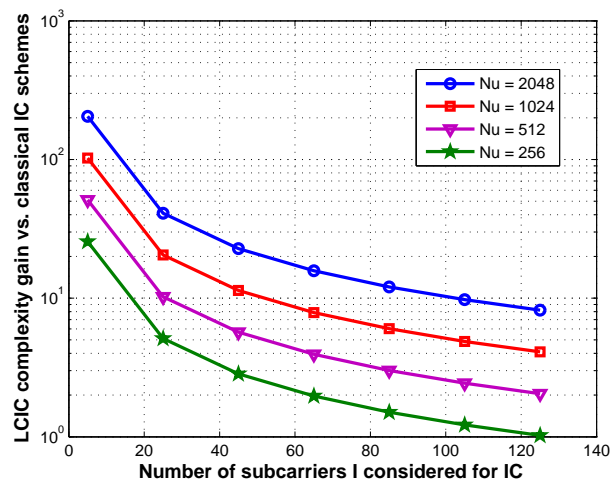
(b)

Figure 8.16: Complexity of the LCIC vs. the classical IC schemes for different I values: (a)Evaluation for Nu=512 (b) LCIC gain for different NU

8.5   Conclusion

In this chapter, it was shown how IC schemes could deal with short CP lengths. Classical IC schemes were analyzed and led to the development of a novel reduced complexity IC algorithm: the Low Complex Interference Cancelation scheme. The use of the LCIC enables a considerable shortening of the CP length, and presents itself as a tradeoff between affordable computational complexity and desired performance.

Further investigations shall however be done before practical implementation could be considered. Smarter evaluation of the ICI and ISI matrix bands is highly relevant, as direct brute force computation would create a complexity bottleneck. The interaction with channel estimation should also be investigated, more specifically an iterative joint channel estimation and IC would be of high relevance. The estimation of the CIR tap phases, amplitudes and delays are a necessity to evaluate $\mathbf{C0}_m$ and $\mathbf{C1}_m$.

Finally, the developed analytical model of the received signal after the FFT has been restricted to one single user using the full OFDM signal bandwidth. Yet, it could be extended to a multiuser scenario using a similar approach as the LCIC. In this case the algorithm would help in removing interference from an asynchronous interferer and not from a to short CP. This could potentially be very beneficial, increasing the frequency reuse of a system by lowering interference form other cells.

Chapter 9

Conclusions

9.1 Thesis summary

In this thesis a deep and careful study was carried out, based on mathematical analysis and simulations using Matlab, to understand the interaction between OFDM parameter design and receiver algorithm choice.

This study was conducted in a physical layer, SISO OFDM, downlink LTE generic frame structure context. As a result a CP length was proposed, two channel estimation algorithms recommended for LTE UE receivers, a pilot scheme suggested and a low complex interference cancelation algorithm developed.

The influence of CP length on SISO OFDM system capacity with LTE based parameters was studied. The results showed that if only one CP length is to be chosen, then a good tradeoff value would be in the range 4 to 5 μs. The received SNR increased the sensitivity of the Capacity to the CP length. On the other hand, higher other-cell interference will decrease the sensitivity to CP and its length could be reduced. The useful OFDM symbol should be as long as the system design allows. It was shown that the RMS delay spread of a PDP turns out not to be a sufficient statistic to determine the optimal CP length as large variations of optimal CP length can be observed for different PDPs having equal RMS delay spread. Thereby, the whole PDP of the channel shall be considered when conducting CP design.

A framework has been provided for a choice of PACE frequency direction interpolation algorithm in upcoming OFDM based standards. A classification has

been carried out from a state of the art survey, showing that the linear solutions provided in literature can be grouped into time and frequency domain approaches, and categorized according to their a priori assumptions. A generalized estimator formulation for linear PACE OFDM was derived, showing that each algorithm is a particular case of this estimator and depends on the a priori channel information taken into account. The effects of introducing virtual subcarriers as well as a non-sample-spaced channel are studied and show that when Partial Bandwidth is used, the TDLS and ML algorithms suffer from severe ill-conditioned matrices and cannot be used as such if the number of virtual subcarriers is too large. From a complexity point of view the FFT based algorithms showed their benefits compared to RW, ENRA and WF. However the leakage effect due to non-sample-spaced channels renders them unusable at higher SNRs than 10 dB. From the studied algorithms, only the RW, ENRA an WF are robust to this leakage effect. We conclude that the WF and ENRA are the most suitable algorithms from both performance and complexity point of view as long as accurate CIR delays are provided. The accuracy and complexity of this methods depend on richness and the variability over time of the delay subspace. In practice it is therefore not trivial to determine the best solution. The RWF will work in all cases, within the assumptions and gives a fixed degradation from known channel performance, depending on the MED of the CIR. The ENRA/WF solutions will be able to perform up to 1-2 dB better than this depending on the channel scenario but their reliability is determined by the CIR delay estimate accuracy. Therefore, in a first release of LTE, the RWF solution with low rank precalculated filter is recommended. If better performance is needed, the ENRA should then be considered with optimized delay tracking. The WF is not that interesting, as the ENRA gives almost same performance without having to track the different CIR tap powers.

A suitable pilot distribution for downlink LTE has been proposed by simulation approach taking into considerations the practical constraints that this implies. First the robustness of different interpolation algorithms against variation of pilot spacing was investigated. In the frequency direction the RWF and LI turned to be very sensitive to minor changes in pilot spacing in the case of CIR with long delays.

When the CIR delays are short, sensitivity to varying frequency direction pilots spacing is quasi-insignificant. The ENRA and WF using a priori knowledge of tap delay location, turned to be very robust to pilot spacing variation even in the case of large CIR delays. In the time direction the importance of algorithm choice is little relevant in the low speed scenario as the channel is quasi-static over the duration of one time slot. The overall importance of time direction interpolation is however reduced as ICI is irreducible when using a classical OFDM1 tap equalizer. Also DRX-DTX, and latency requirements force the estimation to be done within the duration of one time slot estimation, and inter-slot interpolation is undesirable. One fixed pilot pattern is proposed for downlink LTE from the derived method. The pilot scheme will have an overhead of 3,6%, cover all considered channel scenarios and will have support for high mobile speeds up to 300kmph. Spectral efficiency results are shown for a wide range of proposed modulation and coding schemes going from -10 dB to 40 dB SNR, and confirm the validity of the proposed distribution.

Finally, it was shown how IC schemes could deal with scenarios where the CIR tap delays are longer than the CP length. Classical IC schemes were analyzed and led to the development of a novel reduced complexity IC algorithm: the LCIC scheme. The use of the LCIC enables a considerable shortening of the CP length, and presents itself as a tradeoff between affordable computational complexity and desired performance.

9.2 Future work

Regarding PACE, future perspectives would be to investigate the feasibility of frequency direction interpolation algorithm using a priori tap delay knowledge such as ENRA, thereby enhancing the BLER performance and allowing lower pilot overhead than in current PSAM OFDM systems. More specifically low complex and accurate tap delay tracking in UE terminals would be the key for this to be done. The scenario of single frequency network MBMS transmitting continuous data would increase the importance of time averaging, filtering and predictive algorithms. Adaptive PACE algorithms in UE terminals supporting both one shot estimators and averaging esti-

mators should be investigated. The correlation properties in MIMO channels should be used for further improvements of channel estimation accuracy and complexity reduction.

Regarding the LCIC algorithm, further investigations shall be done before practical implementation could be considered. Smart computation and estimation of the ICI and ISI matrix bands is highly relevant, as direct brute force computation would create a complexity bottleneck. The interaction with channel estimation should also be elaborated, more specifically an iterative joint channel estimation and IC would be of high relevance. The estimation of the CIR tap phases, amplitudes and delays are a necessity to evaluate C0m and C1m. The developed analytical model of the received signal after the FFT has been restricted to one single user using the full OFDM signal bandwidth. Yet, it could be extended to a multiuser scenario using a similar approach as the LCIC. In this case the algorithm would help in removing interference from an asynchronous interferer and not from a to short CP. This could potentially be very beneficial, increasing the frequency reuse of a system by lowering interference form other cells.

As a final comment to this thesis, one is lead to observe following. Standardization of future mobile wireless systems will most likely continue to have requirements on increasing spectral efficiency and in the same time on limiting terminal computational complexity and power consumption. These requirements work against each other and even though technical solutions exist for increasing the spectral efficiency, these can't be to expensive. Thereby one can state that solutions to increase system spectral efficiency must be cheap from a computational complexity and the related power consumption.

Bibliography

[1] 3GPP TR 25.814 V2.0.0 (2006), "Physical Layer Aspects for evolved Universal Terrestrial Radio Access (UTRA)"

[2] 3GPP TR 25.913 V7.3.0 (2006-03), "Requirements for Evolved UTRA (E-UTRA) and Evolved UTRAN (E-UTRAN)"

[3] 3GPP TR 25.892 V6.0.0 (2004). "Feasability Study for Orthogonal Frequency Division Multiplexing (OFDM) for UTRAN enhancement"

[4] 3GPP TS 36.201 V0.2.0 (2006-11), "Technical Specification Group Radio Access Network; LTE Physical Layer - General Description (Release 8)"

[5] 3GPP TS 36.211 V1.1.0 (2007-05), "Technical Specification Group Radio Access Network; Physical Channels and Modulation (Release 8)"

[6] 3GPP TS 36.212 V0.2.1 (2006-11), "Technical Specification Group Radio Access Network; Multiplexing and channel coding (Release 8)"

[7] 3GPP TSG RAN WG1 Meeting 41 R1-050386 (May 2005), "Views on OFDM Parameter Set for Evolved UTRA Downlink"

[8] ANSI/IEEE Std 802.11, 1999 Edition (R2003) Information technology - Telecommunications and information exchange between systems - Local and metropolitan area networks - Specific requirements. Part 11: Wireless LAN Medium Access Control (MAC) and Physical Layer (PHY) Specifications

[9] IEEE Std 802.11a-1999(R2003) Supplement to IEEE Standard for Information technology - Telecommunications and information exchange between systems -

Local and metropolitan area networks - Specific requirements. Part 11: Wireless LAN Medium Access Control (MAC) and Physical Layer (PHY) Specifications. High-speed Physical Layer in the 5 GHz band.

[10] IEEE Std 802.11g^{TM}-R2003 IEEE Standard for Information technology - Telecommunications and information exchange between systems - Local and metropolitan area networks - Specific requirements. Part 11: Wireless LAN Medium Access Control (MAC) and Physical Layer (PHY) Specifications. Further Higher Data Rate Extension in the 2.4 GHz band.

[11] Final draft ETSI EN 300 401 v1.4.1 (2006-01) Radio Broadcasting Systems; Digital Audio Broadcasting (DAB) to mobile, protable and fixed receivers.

[12] ETSI EN 300 744 V1.5.1 (2004-11) Digital Video Broadcasting (DVB);Framing structure, channel coding and modulation for digital terrestrial television

[13] ETSI EN 302 304 V1.1.1 (2004-11) Digital Video Broadcasting (DVB);Transmission System for Handheld Terminals (DVB-H)

[14] IEEE Std 802.16-2004 (Revision of IEEE Std 802.16-2001) IEEE Standard for Local and Metropolitan Area Networks Part 16: Air Interface for Fixed Broadband Wireless Access Systems

[15] 802.16e-2005 and IEEE Std 802.16-2004/Cor1-2005 IEEE Standard for Local and metropolitan area networks Part 16: Air Interface for Fixed and Mobile Broadband Wireless Access Systems Amendment 2: Physical and Medium Access Control Layers for Combined Fixed and Mobile Operation in Licensed Bands and Corrigendum 1

[16] Recommendation ITU-R M.1225, "Guidelines for evaluation of radio transmission technologies for IMT-2000," 1997

[17] G. E. Moore, "Cramming more components onto integrated circuits" McGraw-Hill, Electronics Magazine, Volume 38, Number 8, April 19, 1965

[18] R.W. Chang , Synthesis of Band-Limited Orthogonal Signals for Multichannel Data Transmission, Bell System Technical Journal, 45, pp. 1775-1796, 1966

[19] L.J. Cimini, Analysis and Simulation of a Digital Mobile Channel Using Orthogonal Frequency-Division Multiplexing, IEEE Transactions on Communications, 33, 7, pp. 665-675, 1985

[20] J. A. C. Bingham, "Multicarrier Modulation for Data Transmission: An Idea Whose Time Has Come," *IEEE Commun. Mag.* vol. 31, pp 5-14, May 1990.

[21] C. Rom, T.B. Sørensen, P.E. Mogensen and B. Vejlgaard, "Impact of Cyclic Prefix length on OFDM system Capacity", *Proceedings of the WPMC'05* Vol.3, pp. 1871-1875, 18-22 September 2005

[22] H. Steendam, M. Moenclaey, "Analysis and Optimization of the Performance of OFDM on Frequency-Selective Time-Selective Fading Channels," *IEEE Trans. Commun.* vol. 47, pp. 1811-1819, dec. 1999

[23] J. Li, M. Kavehrad, Effect of Time Selective Multipath Fading on OFDM Systems for Broadband Mobile Applications, *IEEE Com. Letters*, vol. 3, no. 12, Dec. 1999.

[24] M. Russel, G. L. Stüber, Interchannel Interference Analysis of OFDM in a Mobile Environment, Proc. VTC 95, p. 820, 1995.

[25] S.R. Searle, *Matrix Algebra Useful for Statistics.* New York: Wiley, 1982.

[26] L. Hanzo, M. Mnster, B. J. Choi, T. Keller, *OFDM and MC-CDMA for Broadband Multi-User Communications, WLANs and Broadcasting*, Wiley, 2003

[27] R. Van Nee, R. Prasad, *OFDM for Wireless Multimedia Communications*, Artech House, 2000

[28] A. R. S. Bahai, B. R. Saltzberg, M. Ergen, *Multi-Carrier Digital Communications Theory and Applications of OFDM, Second Edition*, Springer, 2004

[29] A. V. Oppenheim and R. W. Schafer, *Discrete-Time Signal Processing (2nd Edition)*, Prentice Hall, 1999, ISBN-13: 978-0-137-54920-7

[30] J. D. Parsons, *The mobile radio propagation channel (2nd Edition)*, Wiley, 2000, ISBN-13: 978-0-471-98857-1

[31] J. Proakis, *Digital Communications (4th edition)*, Mc Graw Hill, 2001, ISBN-10: 0072321113

[32] T. Moon, W. Stirling, "Mathematical Mehtods and Algorithms for Signal Processing". Prentice Hall, 2000

[33] Thomas H. Cormen, Charles E. Leiserson, Ronald L. Rivest, and Clifford Stein, "Introduction to Algorithms". Second Edition, MIT Press and McGraw-Hill, 2001. ISBN 0-262-03293-7

[34] Harold Jeffreys and Bertha Jeffreys, " Methods of Mathematical Physics (Third Edition)" Cambridge University Press, 1999, ISBN: 0521664020

[35] J. Harold. Ahlberg, "The Theory of Splines and Their Applications ", Academic Pr (June 1967), ISBN: 0120447509

[36] Sergio Verdu, "Multiuser detection", Cambridge University Press, 1998, ISBN 0-521-59373-5

[37] Na Wei, "MIMO Techniques in UTRA Long Term Evolution", Ph.D. thesis, Department of Electronic Systems, Aalborg University, Denmark, June 2007.

[38] D. Coppersmith and S. Winograd. "Matrix multiplication via arithmetic progressions." *In Proc. Nineteenth ACM Symp. Theory of Computing*, pages 1-6, 1987

[39] Kaare Brandt Pedersen and Michael Syskind Pedersen, "The Matrix Cookbook." Version: Fbruary 16, 2006

[40] Max Welling, "The Kalman Filter," Lecture Note.

[41] 3GPP TR 25.848, Physical Layer Aspects of UTRA High Speed Downlink Packet Access.

[42] S. M. Alamouti, "A simple transmit diversity technique for wireless communication" IEEE Journal on *Selected Areas in Communications*, Volume 16, Issue 8, Oct. 1998 Page(s):1451 - 1458

[43] G. J. Foschini, "Layered Space-Time Architecture for Wireless Communication in a Fading Environment When Using Multiple Antennas" Bell Labs Technical Journal, Vol. 1, No. 2, Autumn 1996, pp 41-59.

[44] C. Rom, C. N. Manchón, T.B. Sørensen, P.E. Mogensen and Luc Deneire, "Analysis of Time and Frequency Domain PACE Algorithms for OFDM with Virtual Subcarriers" *Personal, Indoor and Mobile Radio Communications, 2007 IEEE 18th International Symposium* Sept. 2007 Pages: 1-5

[45] L. Schumacher, J. P. Kermoal, F. Frederiksen, K. I. Pedersen, A. Algans and P. E. Mogensen, MIMO Channel Characterisation, IST Project IST- 1999-11729 METRA Deliverable 2, February 2001.

[46] 3GPP TR 25.943, Deployment aspects.

[47] 3GPP TS 36.300, v8.2.0 (2007-09), "E-UTRA and E-UTRAN Overall descrtiption, stage2"

[48] H. Holma and A. Toskala, Eds., WCDMA for UMTS, Radio Access For Third Generation Mobile Communications, Wiley, Chichester, UK, second edition, 2002.

[49] T. E. Kolding, F. Frederiksen, P. E. Mogensen, Performance aspects of WCDMA systems with High Speed Downlink Packet Access (HSDPA), VTC Fall, July, 2002.

[50] P. O. Vidal, "Analysis of OFDM for UTRAN enhancement," Master thesis for Aalborg University, Institute of Electronic Systems, Departement of Communication Technology, Cellular Systems.

[51] G. Monghal and Y. Malidor, "PSAM-Based Channel Estimation applied on a novel OFDM Downlink Equalization technique", Master thesis for Aalborg University, Institute of Electronic Systems, Departement of Communication Technology, Cellular Systems, June 2005

[52] C. N. Manchón, "Next Generation of Mobile Systems: The Channel Estimation Problematic in Downlink OFDM", Master Thesis, Department of Communication Technology, Aalborg University, May 15, 2006

[53] H. Yaghoobi, "Scalable OFDMA Physical Layer in IEEE 802.16 Wireless MAN," Intel Technology Journal, Volume8, Issue3, 2004

[54] F. Tufvesson, T. Maeseng "Optimization of Sub-Channel Bandwidth for mobile OFDM systems," MMT'97, Melbourne, Australia, dec. 1997

[55] J. L. Seoane, S. K. Wilson, S. Gelfand, "Analysis of Intertone and Interblock Interference in OFDM when the length of the Cyclic Prefix is shorter than the length of the Channel Impulse Response," *Globecom 97*, Pheonix Arizona, Nov 1997.

[56] M. Batariere, K. Braum, T. P. Krauss "Cyclic Prefix Length Analysis for 4G OFDM Systems," VTC'04, Los Angeles, USA, sept. 2004

[57] C. Lim, Y. Chang, J. Cho, P. Joo, H. Lee, "Novel OFDM Transmission Scheme to Overcome ISI Caused by Multipath Delay Longer than Cyclic Prefix," VTC'05, Stockholm, Sweeden, May. 2005.

[58] K. L. Baum, T. A. Kostas, P. J. Sartori, B. K. Classon, "Performance Characteristics of Cellular Systems with Different Link Adaptation Strategies," *IEEE Trans. Vehicular Technology*, Vol. 52, No. 6, November 2003.

[59] L.J. Cimini, Jr., Analysis and Simulation of a Digital Mobile Channel Using Orthogonal Frequency-Division Multiplexing. IEEE Trans. Commun., vol.33, no.7, pp. 665-675, July 1985.

[60] R. Gonzlez and F. Bader "Time-Frequency Spacing Design for PACE in OFDM Systems," IST 14th Summit, Dresden 19-23 June 2005

[61] S. Coleri, M. Ergen, A. Puri and A. Bahai, "Channel estimation techniques based on pilot arrangement in OFDM systems," *IEEE Trans. Broadcasting,* vol 48, pp. 223-229, Sept. 2002.

[62] K. F. Lee and D. B. Williams, "Pilot-symbol-assisted channel estimation for space-time coded OFDM systmes," *EURASIP J. Applied Signal Process.*, vol. 5, pp. 507-516, May 2002.

[63] P. Hoeher,S. Kaiser and I. Robertson, "Two-dimensional pilot-symbol-aided channel estimation by wiener filtering," in *Proc. Int. Conf. Acoustics Speech and Signal Processing (ICASSP)*, 1997, pp. 1845-1848.

[64] P. Hoeher, S. Kaiser and I. Robertson, "Pilot-symbol-aided channel estimation in time and frequency", in Proc. Sixth Communication Theory Mini-Conference in conjunction with IEEE GLOBECOM 97, Phoenix, Arizona, pp. 90-96, November 1997

[65] P. Hoeher, "TCM on frquency-selective land-mobile fading channels," in *International Workshop on Digital Communications*, (Tirrenia, Italy), pp. 317-328, September 1991.

[66] J.-J. van de Beek,O. Edfors, M. Sandell, S. K. Wilson and P.O. Borjesson "On channel estimation in OFDM systems," in *Proc. IEEE VTC'96,*, Nov. 1996, pp. 815-819.

[67] O. Edfors, M. Sandell, J. van de Beek, S. K. Wilson, and P. O. Borjesson, "OFDM channel estimation by singular value decomposition," in *Proceedings of Vehicular Technology Conference*, vol. 2, (Atlanta, GA USA) pp. 923-927, April-May 1996

[68] O. Edfors, M. Sandell, J. van de Beek, S. K. Wilson, and P. O. Borjesson, "OFDM channel estimation by singular value decomposition," in *IEEE Trans. Commun.*, vol. 46, pp. 931-939, July 1998

[69] Igor A. Tolochko, "Channel estimation for OFDM systems with transmitter diversity", Doctor of Philosophy, Centre for Telecommunications and Micro-Electronics, Victoria University of Technology, August 2005

[70] O. Simeone, Y. Bar-Ness, U. Spagnolini, "Pilot-Based Channel Estimation for OFDM Systems by Tracking the Delay-Subspace" in *IEEE Trans. Wireless. Comm.*, vol. 3, no. 1, jan 2004

[71] R. Negi and J. Cioffi, "Pilot tone Selection for channel estimation in a mobile OFDM system," in *IEEE Trans. Consumer Electron.*, vol. 44, pp. 1122-1128.

[72] L. Deneire, P. Vandenameele, L. van der Pierre, B. Gyselinckx, and M. Engels "A low Complexity ML channel estimator for OFDM," in *IEEE Trans. Commun*, vol. 51, no.2, pp 135-140, February 2003.

[73] H. Schmidt, V. Khn, K.D. Kammeyer, R. Rueckriem, and S. Fechtel, "Channel tracking in wireless OFDM systems," in *SCI 2001*, Orlando, Florida, USA, 22-25 July 2001.

[74] M.H. Hsieh and C.H. Wei, "Channel estimation for OFDM systems based on comb-type pilot arrangement in frequency selective fading channels," *IEEE Trans. Consumer Electronics*, vol.44, pp. 217-225, Feb. 1998.

[75] B. Yang, K.B. Letaief, R.S. Cheng and Z. Cao, "Channel estimation for OFDM transmission in multipath fading channels based on parameteric channel modelling," in *IEEE Trans. Commun.*, vol. 49, pp. 467-479, March 2001.

[76] D. Schafhuber, G. Matz and F. Hlawatsch "Adaptive Wiener Filters for Time-Varying Channel Estimation in OFDM Systems" *2003 IEEE International Conference on Acoustics, Speech, and Signal Processing, (ICASSP '03),* vol.4, pp. 688-91, 6-10 April 2003

[77] G. Auer, S. Sand and A. Dammann, "Comparison of Low Complexity OFDM Channel Estimation Techniques" *In Proc. of Int OFDM Workshop*, Hamburg, Germany, September 2003

[78] Y. Li, L. J. Cimini, and N. R. Sollenberger, "Robust channel estimation for OFDM systems with rapid dispersive fading," in *IEEE Trans. Commun.*, vol. 46, pp. 902-915, July 1998

[79] M. Morelli and U. Mengali, "A Comparison of Pilot-Aided Channel Estimation Methods for OFDM Systems," in *IEEE Trans. Signal Proc.*, vol. 49, pp. 3065-3073, December 2001

[80] F. Tufvesson, M. Faulkner, and T. Maseng, "Pre-Compensation for Rayleigh Fading Channels in Time Divisoin Duplex OFDM Systems," in *Proceedings of 6th International Workshop on Intelligent Signal Processing and Communication Systems,* (Melbourne, Australia), pp. 57-33, IEEE, November 5-6 1998.

[81] A. Tikhonov and V. Arsenin, *Solutions of Ill-Posed Problems.* Washington: Winston, 1977.

[82] M.J. Frenandez-Getino Garcia, S. Zazo and J.M. Paez-Borrallo, "Pilot patterns for channel estimation in OFDM" *Electronic Letters*, Vol.36, No.12 ,pp. 1049-1050, 8th of June 2000

[83] W. Zhang, X.G. Xia, P.C. Ching and W.K. Ma, "On the number of pilots for OFDM system in multipath fading channels" *ICASSP 2004*, Volume 4, 17-21 May 2004 Page(s):iv-381 - iv-384

[84] J.W. Choi and Y.H. Lee, "Desing of the Optimum Pilot Pattern for Channel Estimation in OFDM Systems," *Global Telecommunications Conference, 2004, GLOBECOM04*, pp. 3661- 3665 Vol.6, IEEE, 29 Nov.-3 Dec. 2004.

[85] H. Nyquist, "Certain topics in telegraph transmission theory", Trans. AIEE, vol. 47, pp. 617-644, Apr. 1928

[86] E. Al-Susa and R. Ormondroyd "A Predictor-Based Decision Feedback Channel Estimation Method for COFDM with High Resilience to Rapid Time-Variations," in *Proceedings of Vehicular Conference,* vol. 1, (Amsterdam, Netherlands), pp. 273-278, IEEE, September 19-22 1999

[87] A. Stamoulis, S.N. Diggavi, N. Al-Dhahir, "Intercarrier interference in MIMO OFDM", in IEEE Transactions, vol. 50, issue 10, pp 2451-2464 Oct. 2002

[88] P. Schniter, "Low-Complexity Equalization of OFDM in Doubly Selective Channels", IEEE Trans. On Signal Processing, Vol. 52, No. 4, apr. 2004

[89] T. V. Sreenivas adn P. V. S. Rao, "High-Resolution Narrow-Band Spectra by FFT Prunning," in *IEEE Trans. on Acoustics Speech and Signal Processing*, vol. assp-28, pp. 254-257, No.2, April 1980

[90] B. Lu and X. Wang, "Bayesian Blind Turbo Reciever for Coded OFDM Systems with Frequency Offset and Frequency-Selective Fading," *IEEE Journal on Selected Areas in Communications,* vol. 19, pp. 2516-2527, December 2001.

[91] Chengyang Li and Sumit Roy, "Subspace-Based Blind Channel Estimation for OFDM by Explointing Virtual Carriers," in *IEEE Trans. Commun.*, vol. 2, pp. 141-150, Jan 2003

[92] Marc C. Necker and Gordon L. Stuber "Totally Blind Channel Estimation for OFDM on Fast Varying Mobile Radio Channels" in *IEEE Trans. Commun.*, vol. 3, pp. 1514-1524

[93] M Munster and L. Hanzo "Second-order channel parameter estimation assisted cancellation of channel variation-induced inter-subcarrier interference in OFDM systems," EURCON 2001, Volume 1, 4-7 July 2001 Page(s):1 - 5

[94] A. J. Jerri. "The Shannon sampling theoremIts various extensions and applications: A tutorial review" *Proceedings of the IEEE*, Volume 65, Issue 11, Nov. 1977 Page(s):1565 - 1596

[95] N. Wei, A. Pokhariyal, C. Rom, B.E. Priyanto, F. Frederiksen, C. Rosa, T. B. Srensen, T. Kolding, P.E. Mogensen, "Baseline E-UTRA Spectral Efficiency Evaluation," IEEE Vehic. Technol. Conf., Montreal, Canada, October 2006

[96] "Matlab, The Language of Technical Computing", version 7.0.4.365 (R14), Service Pack 2. Copyright 1984-2005, the Mathworks, Inc.

[97] D. Kim, G. L. Stuber, Residual ISI Canccllation for OFDM with Application to HDTV Broadcasting, *IEEE J. Select. Areas in Conim.*, vol. 16, no. 8, Oct. 1998.

[98] C. Lim, Y. Chang, J. Cho, P. Joo, H. Lee, Novel OFDM Transmission Scheme to Overcome ISI Caused by Multipath Delay Longer than Cyclic Prefix, *VTC05*, Stockholm, Sweeden, May. 2005

[99] P. J. W. Melsa, R. C. Younce, C. E. Rohrs, "Impulse response shortening for discrete multitone transceivers," *IEEE Trans. Commun.*, vol. 44, no.12, pp. 1662-1672, Dec. 1996.

[100] R. Schur, Impulse Compression for OFDM Transmission over Time-Varying Multipath Channels, *Proc. IEEE VTC 2002-fall*, vol.2, pp.1074-1076, September 2002.

[101] N. Suzuki, H. Uehara, M. Yokoyama, A New OFDM Demodulation Method with Variable Length Effective Symbol and ICI Canceller., *IEICE Trans Fundamentals*, vol.E85-A, no.12, December 2002.

[102] N. Suzuki, T. Shibata, N. Itoh and M. Yokoyama, "OFDM demodulation method with variable effective symbol duration",*IEICE Trans. Fundamentals*, vol. E85-A, no.7, pp. 1665-1674, July 2002.

[103] Y. C. Yoon, R Kohno and H. Imai, "A spread-spectrum multiacces system with cochannel interference cancellation for mulitpath fading channels", *IEEE Journal Sel. Areas Commun.*, vol.11, no.7, pp.1067-1075, Sep. 1993

[104] R4-071135, Agreed LTE UE demodulation performance simulation assumptions, Motorola

[105] R4-071297 LTE UE demodulation results, Ericsson

[106] R4-071325 Ideal simulations results for E-UTRA PDSCH with Rel-7 coding chain, NEC

Appendix A

Channel Power Delay Profiles

Table A.1: ITU channel PDP's considered

Indoor B		Pedestrian B		Vehicular B	
Delay	Power	Delay	Power	Delay	Power
0	0	0	0	0	-2,5
100	-3,6	200	-0,9	300	0
200	-7,2	800	-4,9	8900	-12,8
300	-10,8	1200	-8,0	12900	-10,0
500	-18,0	2300	-7,8	17100	-25,2
700	-25,2	3700	-23,7	20000	-16,0
$\tau_{rms} = 100$		$\tau_{rms} = 630$		$\tau_{rms} = 4000$	

Table A.2: Hilly Terrain channel PDP

PDP characteristics		
Tap Number	Delay (μs)	Power (dB)
1	0	-3,6
2	0,356	-8,9
3	0,441	-10,2
4	0,528	-11,5
5	0,546	-11,8
6	0,609	-12,7
7	0,625	-13,0
8	0,842	-16,2
9	0,916	-17,3
10	0,941	-17,7
11	15000	-17,6
12	16,172	-22,7
13	16,492	-24,1
14	16,876	-25,8
15	16,882	-25,8
16	16,978	-26,2
17	17,615	-29,0
18	17,827	-29,9
19	17,849	-30,0
20	18,016	-30,7
$\tau_{rms} = 3000$		

Table A.3: Channel Power Delay Profiles

i	"long SS"		"long NSS"		"short NSS"		
	τ_i (T_s)	$\approx \tau_i$ (ns)	τ_i (T_s)	$\approx \tau_i$ (ns)	τ_i (T_s)	$\approx \tau_i$ (ns)	Pow (dB)
0	0	0	0.5	16.3	0.5	16.3	0
1	6	195	6.5	212	1.5	48.8	-1
2	12	391	12.5	407	2.5	81.4	-2
...	...	...	...	...	...	...	...
18	108	3516	108.5	3532	18.5	602	-18
19	114	3711	114.5	3727	19.5	635	-19

Appendix B

Validation of simulations

In RAN4, meeting #43bis and AdHoc were held to discuss LTE UE demodulation requirements, where the main focus was on the PDSCH. It was agreed to carry out deal simulations for the PDSCH. The assumptions for these simulations were summarized in [104], see table B.1. In this appendix we present ideal simulation results for PDSCH in the agreed conditions from the different participating companies. The results for QPSK with 1/3 coding rate are given in Figure B.1. Similarly the results for 16QAM with R = 1/2 and 64QAM with R = 5/6 are shown in figure B.2 and B.3, respectively.

In general the results are well aligned. With the exception of the results presented by Ericsson [105] and possibly also the results presented by NEC [106]. The offset of the results from Ericsson [105] is due to an error in calculating the bandwidth which results in a 2.3 dB offset. If the results are corrected, these results are also aligned with the rest of the results.

Table B.1: Main link simulation assumption

Paramter	Assumption
Carrier Frequency	2GHz
Bandwidth	10 MHz
CP length	Normal ($\Delta_f = 15$ KHz)
Propagation channel	Extended Typical Urban
Max nb tx H-ARQ process	4
RV sequence	$\{0, 1, 2, 3\}$ for QPSK, 16QAM and 64QAM
ACK/NACK error rate	0%
Nb UE antennas	2 (Fully uncorrelated)
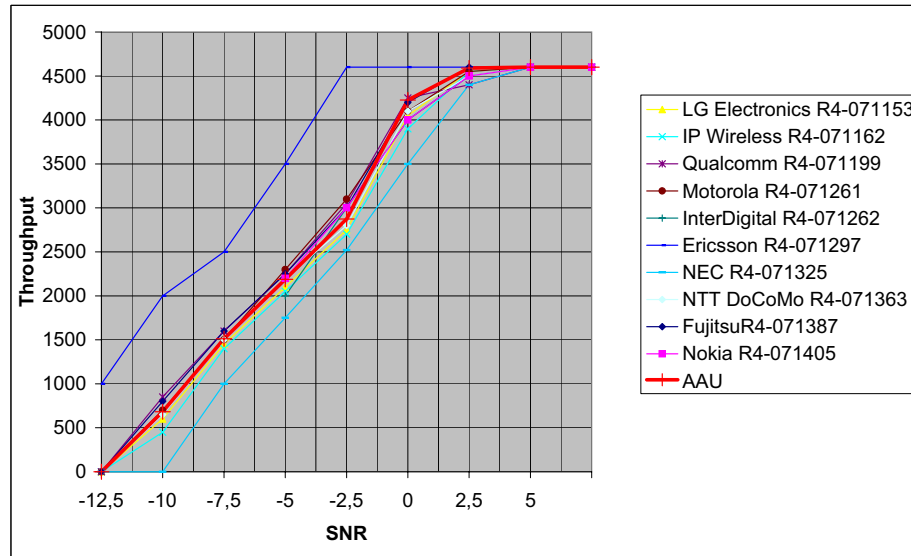
Figure B.1: QPSK ECR 1/3
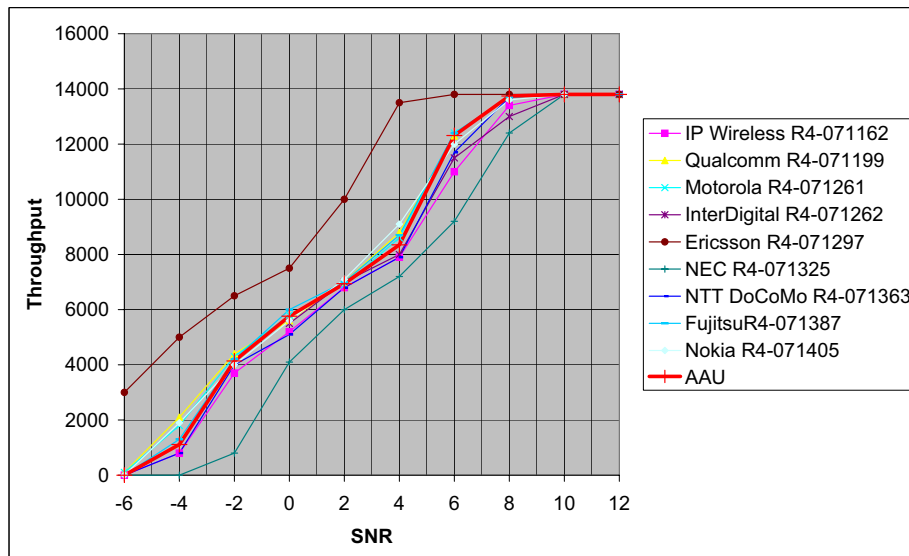
Figure B.2: 16QAM ECR 1/2
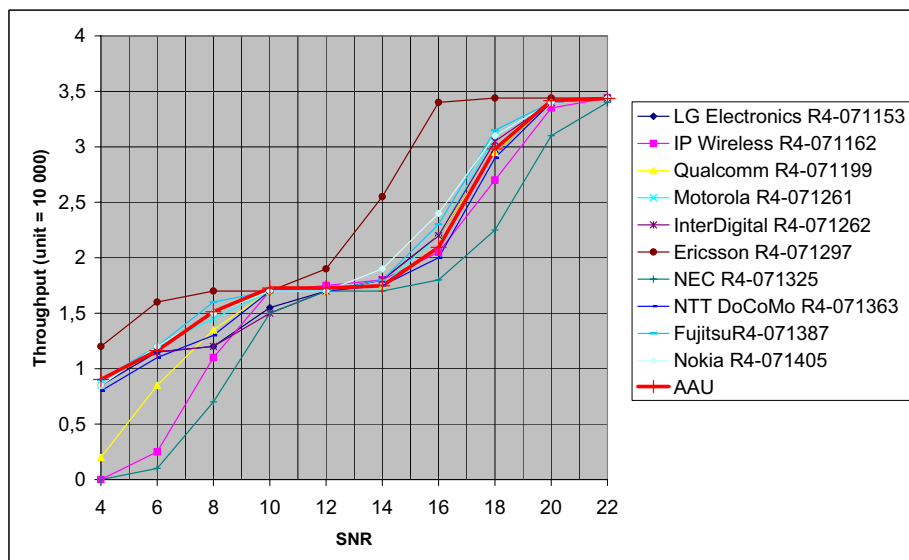
Figure B.3: 64QAM ECR 5/6

June 18, 2008

Appendix C

On Frequency direction interpolation

C.1 Time-frequency equivalence of NRA and the Sample Spaced Robust Wiener filter

According to equation 6.9, the NRA estimator is given by:

$$\mathbf{h}_{nra} = \mathbf{F}_{us}(\mathbf{F}_{ps}^H\mathbf{F}_{ps} + \gamma_{nra}\mathbf{I}_s)^{-1}\mathbf{F}_{ps}^H\mathbf{h}_{ls}. \qquad \text{(C.1.1)}$$

Using the Woodbury Identity [39, 40], with $\mathbf{P}$ and $\mathbf{R}$ positive definite, we have:

$$(\mathbf{P}^{-1} + \mathbf{B}^H\mathbf{R}^{-1}\mathbf{B})^{-1}\mathbf{B}^H\mathbf{R}^{-1} = \mathbf{P}\mathbf{B}^H(\mathbf{B}\mathbf{P}\mathbf{B}^H + \mathbf{R})^{-1}, \qquad \text{(C.1.2)}$$

and replacing $\mathbf{P} = \mathbf{I}_s$, $\mathbf{B} = \mathbf{F}_{ps}$ and $\mathbf{R} = \gamma_{nra}\mathbf{I}_p$, we obtain:

$$\mathbf{h}_{nra} = \mathbf{F}_{us}\mathbf{I}_s\mathbf{F}_{ps}^H(\mathbf{F}_{ps}\mathbf{I}_s\mathbf{F}_{ps}^H + \gamma_{nra}\mathbf{I}_p)^{-1}\mathbf{h}_{ls}. \qquad \text{(C.1.3)}$$

The NRA estimator can then also be written as:

$$\mathbf{h}_{nra} = \mathbf{F}_{us}\mathbf{F}_{ps}^H(\mathbf{F}_{ps}\mathbf{F}_{ps}^H + \gamma_{nra}\mathbf{I}_p)^{-1}\mathbf{h}_{ls}. \qquad \text{(C.1.4)}$$

Recalling the expression of the WF from equation 6.11, we have:

$$\mathbf{h}_{wf} = \mathbf{R}_{\mathbf{h}_u\mathbf{h}_p}(\mathbf{R}_{\mathbf{h}_p\mathbf{h}_p} + \sigma_w^2\mathbf{I}_p)^{-1}\mathbf{h}_{ls}. \qquad \text{(C.1.5)}$$

Assuming a Sample Spaced Channel and uniformly distributed channel power delays we can simplify the correlation matrices with:

$$\mathbf{R_{h_u h_p}} = \mathrm{E}\{\mathbf{h}_u \mathbf{h}_p^H\} = \mathbf{F}_{us}\mathrm{E}\{\mathbf{g}_s \mathbf{g}_s^H\}\mathbf{F}_{ps}^H = \frac{1}{N_s}\mathbf{F}_{us}\mathbf{F}_{ps}^H \tag{C.1.6}$$

and

$$\mathbf{R_{h_p h_p}} = \mathrm{E}\{\mathbf{h}_p \mathbf{h}_p^H\} = \mathbf{F}_{ps}\mathrm{E}\{\mathbf{g}_s \mathbf{g}_s^H\}\mathbf{F}_{ps}^H = \frac{1}{N_s}\mathbf{F}_{ps}\mathbf{F}_{ps}^H. \tag{C.1.7}$$

Replacing the expressions C.1.6 and C.1.7 in C.1.5 we obtain the sample spaced robust wiener espression:

$$\mathbf{h}_{ssrw} = \mathbf{F}_{us}\mathbf{F}_{ps}^H(\mathbf{F}_{ps}\mathbf{F}_{ps}^H + \sigma_w^2 N_s \mathbf{I}_p)^{-1}\mathbf{h}_{ls}. \tag{C.1.8}$$

By comparing equation C.1.4 with C.1.8, we can observe that the NRA estimator and the sample spaced RWF are equivalent if $\gamma_{nra} = \sigma_w^2 N_s$.

C.2 MSE evaluation for the NRA

According to the formulation in 6.17 applied to the NRA algorithm, the MSE per subcarrier can be evaluated for different channel PDP's. The MSE per subcarrier for the Indoor A, Typical Urban and Pedestrian B profiles are respectively presented in Figures C.1, C.2 and C.3. As the pilot spacing is diminished the total number of pilot subcarriers is increased, thereby the average MSE is decreased as the CIR MED remains constant. One can observe that the MSE is especially high at band edges when the subcarrier index is above 200 or below -200. This is true for all 3 studied PDP's, where the MSE shapes vary form PDP to PDP.

In figure C.4 the idea is to keep the total amount of pilot subcarriers constant by varying the pilot spacing according to N_u. The smaller the occupied bandwidth the smaller the MSE. It is noted that for full bandwidth (where $N_u = N_{fft}$), the MSE is independent of the subcarrier index, and no band edge effect is observed.

Finally figure C.5 shows the MSE per subcarrier in a LTE context with a fixed pilot spacing of 6. It is noted that the MSE is increased as N_u decreases.
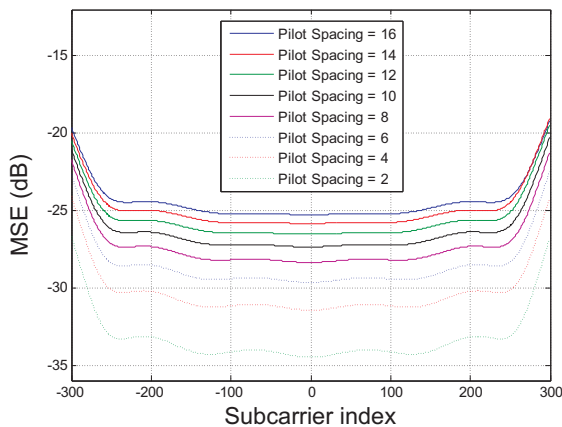
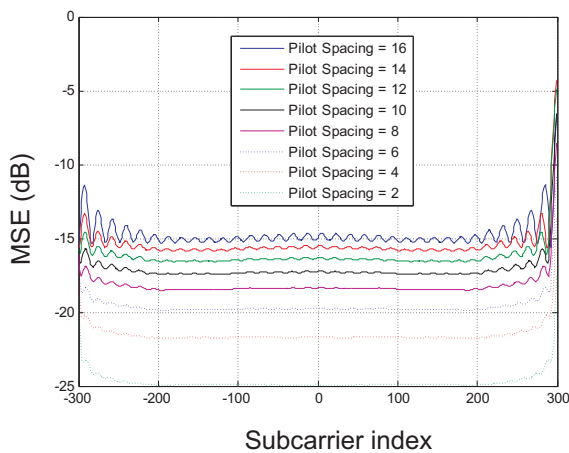Figure C.1: IndoorA
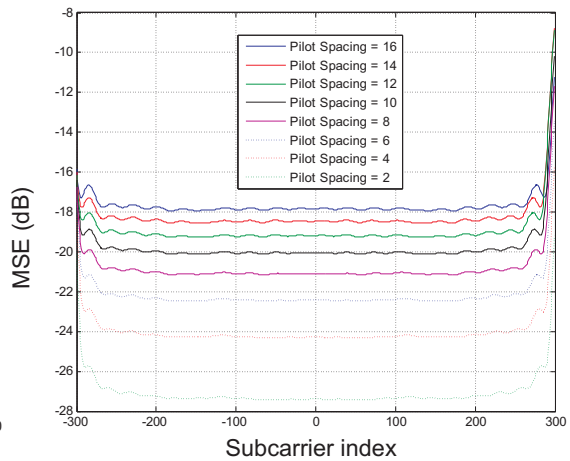
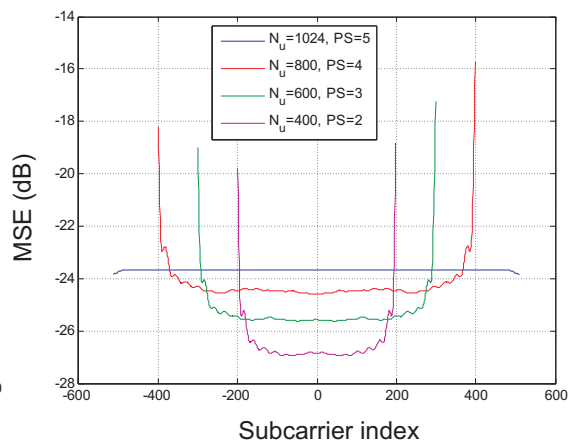Figure C.2: Typical Urban

Figure C.3: Pedestrian B

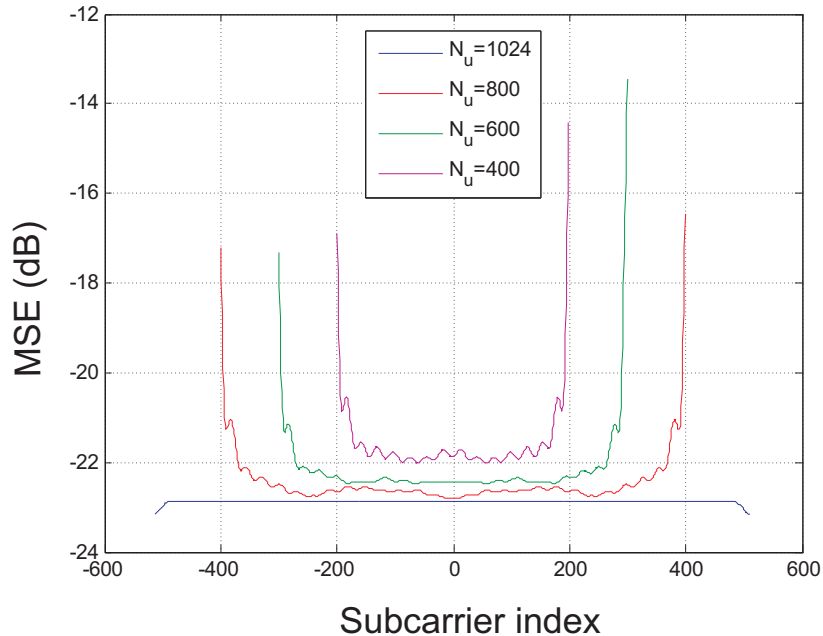Figure C.4: Typical Urban, Quasi-fixed Nb of pilot subcarriers

Figure C.5: MSE in dB per subcarrier for the NRA algorithm in the case of an Typical Urban profile for a fixed pilot spacing PS=6

C.3 On the ML $(\mathbf{F}_{ps}^{H}\mathbf{F}_{ps})$ Matrix invertibility

From theory, the $(\mathbf{F}_{ps}^{H}\mathbf{F}_{ps})$ matrix is always full rank and thus invertible due to the Vandermonde structure of the sub-DFT matrix structure of $\mathbf{F}_{ps}$. However the matrix can become ill conditioned. In this appendix we evaluate the "numerical rank" by using the Matlab 7.0 function *rank* [96]. In the rest of this section we refer to the estimated rank of this Matlab 7.0 *rank* function. Floating point computation of the rank of a given matrix can be performed in several ways. One classical method would be to use an SVD. The numerical determination of rank requires a criterion for deciding when a value, such as singular value from the SVD, should be treated as zero. This is a practical choice which depends on both the matrix and the application targeted.

For an FFT size of $N_{fft} = 1024$, a number of used sub-carriers $N_u = 600$, and without considering the DC carrier as virtual sub-carrier, the rank of the $(\mathbf{F}_{ps}^{H}\mathbf{F}_{ps})$
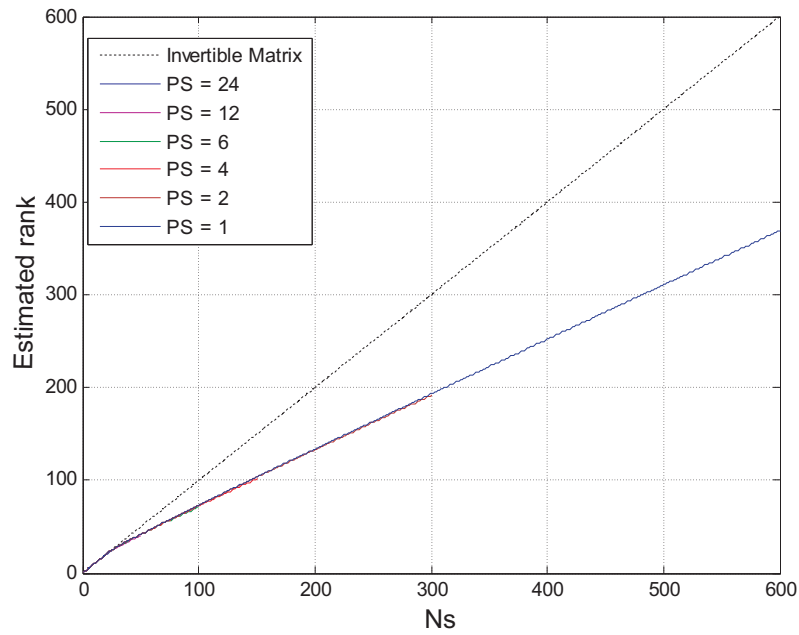
Figure C.6: Estimated rank of $(\mathbf{F}_{ps}^H \mathbf{F}_{ps})$

matrix is shown in Figure C.6 for different pilot spacings. It seems like the number
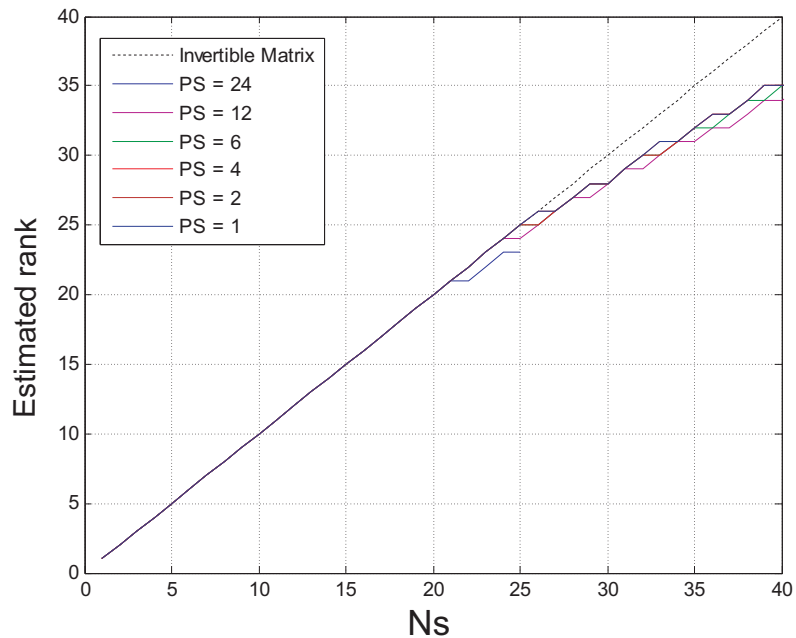
Figure C.7: Zoom on the region of interest for Figure C.6

of pilot symbols used does not significantly influence the effective rank of the matrix. Figure C.7 is a zoom on Figure C.6 where the focus is set on the region where the estimated rank of the matrix starts to be lower than N_s. This point is around a CIR of length 25 samples for all pilot spacings (PS). If the number of pilots is sufficiently bigger than 25, there is almost no influence, whereas we can see that for a PS=24 (total of 25 pilots), the matrix is already non-invertible for $N_s = 21$. However, it should be noted that this difference is due to the MATLAB *rank* function precision.
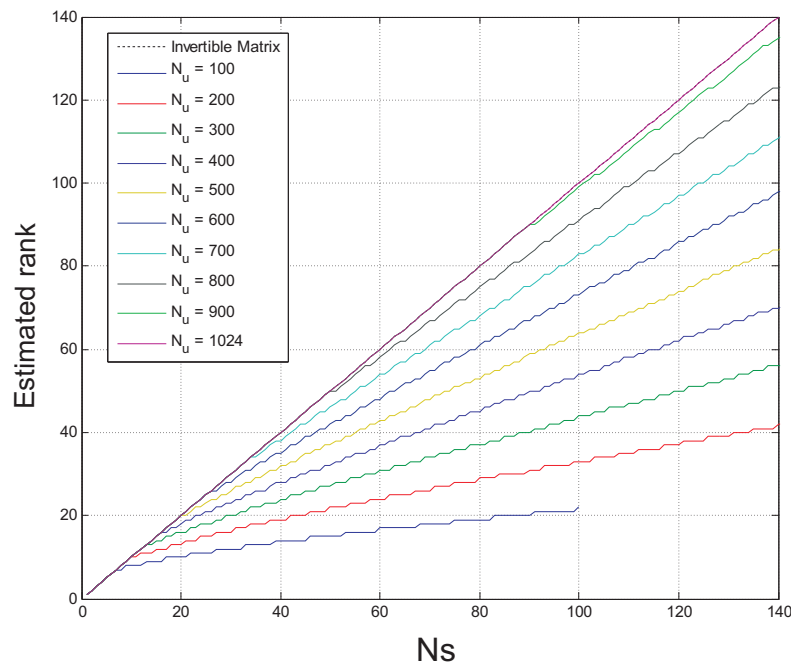
Figure C.8: Estimated rank of $(\mathbf{F}_{ps}^H \mathbf{F}_{ps})$, $N_{fft} = 1024$, PS=1 and varying N_u

Assuming that the rank of the matrix does not depend on the pilot spacing used, the impact of the number of sub-carriers used from the full FFT size will be studied. The results for a size of $N_{fft} = 1024$, a pilot spacing of $PS = 1$ and varying number of used sub-carriers N_u are shown in Figure C.8.

The matrix $(\mathbf{F}_{ps}^H \mathbf{F}_{ps})$ is always full rank when all the sub-carriers are used, but the rank falls rapidly when the number of used sub-carriers N_u is decreased. In order to obtain a better idea of the dependence of the matrix rank on the parameter N_u , the maximum N_s for which the matrix is invertible depending of the number
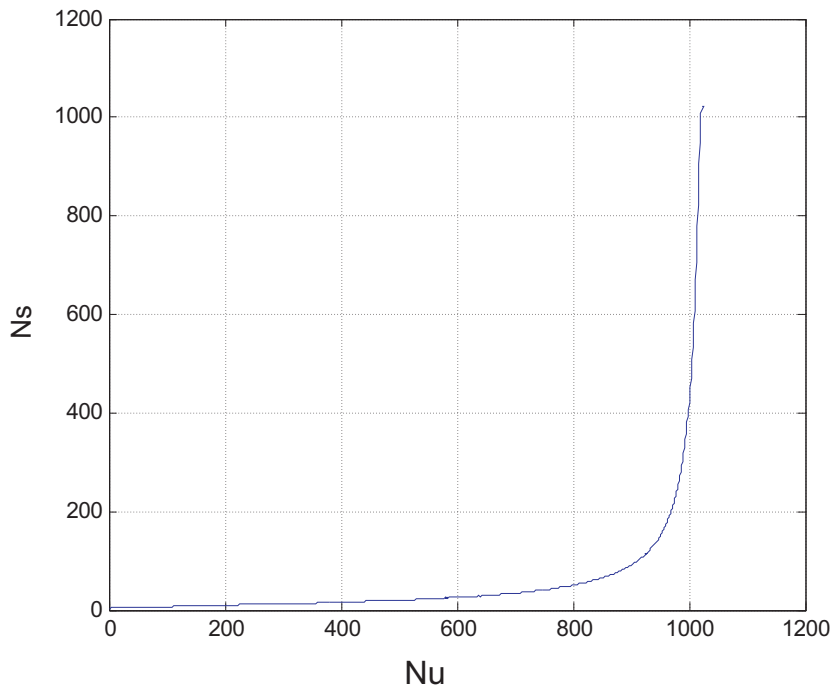
Figure C.9: Maximum N_s for which the estimated rank of $(\mathbf{F}_{ps}^H \mathbf{F}_{ps})$ is equal to N_s

of used subcarriers has been plot in Figure C.9 for $N_{fft} = 1024$ and pilot spacing $PS = 1$. Figure C.9 shows that the maximum N_s increases slowly for N_u of up to 800 subcarriers. Thereafter the slope increases in an exponential manner as N_u is close to the maximum of 1024.

C.4 CTF auto-correlation matrix for the Robust Wiener filter

Considering the physical channel to be constant over the duration of one OFDM symbol, the CIR can be expressed independently from the time parameter t, as:

$$g(\tau) = \sum_{i=0}^{N_t-1} a_i \delta(\tau - \tau_i) \tag{C.4.9}$$

If the delays τ_i are uniformly and independently distributed over $[0, T_{med}]$ we have:

$$E\{a_n a_{n'}^*\} = \begin{cases} \frac{1}{N_t} & , n = n' \\ 0 & n \neq n' \end{cases} \tag{C.4.10}$$

The CTF is defined as:

$$\mathbf{h}[k] = \sum_{i=0}^{N_t-1} a_i e^{-j2\pi \frac{k}{N_{fft}}\tau_i} \tag{C.4.11}$$

The CTF auto-correlation matrix is expressed as:

$$\mathbf{R_{hh}}[k,k'] = \mathrm{E}\{\mathbf{h}[k]\mathbf{h}^*[k']\} \tag{C.4.12}$$

$$= \mathrm{E}\{\sum_{i1=0}^{N_t-1} a_{i1} e^{-j2\pi \frac{k}{N_{fft}}\tau_{i1}} \sum_{i2=0}^{N_t-1} a_{i2}^* e^{j2\pi \frac{k'}{N_{fft}}\tau_{i2}}\} \tag{C.4.13}$$

$$= \frac{1}{N_t} \sum_{i=0}^{N_t-1} \mathrm{E}\{e^{-j2\pi \frac{(k-k')}{N_{fft}}\tau_i}\} \tag{C.4.14}$$

We observe that the probability density function of τ_i is:

$$f(\tau_i) = \begin{cases} \frac{1}{T_{med}} & , \tau_i \in [0, T_{med}] \\ 0 & , else. \end{cases} \tag{C.4.15}$$

It follows,

$$\mathbf{R_{hh}}[k,k'] = \frac{1}{N_t} \sum_{i=0}^{N_t-1} \int_0^{T_{med}} \frac{e^{-j2\pi \frac{k-k'}{N_{fft}}\tau_i}}{T_{med}} d\tau_i \tag{C.4.16}$$

$$= \frac{1}{N_t} \sum_{i=0}^{N_t-1} \left[\frac{-N_{fft} e^{-j2\pi \frac{k-k'}{N_{fft}}\tau_i}}{j2\pi(k-k')T_{med}}\right]_0^{T_{med}} \tag{C.4.17}$$

$$= \frac{1}{N_t} \sum_{i=0}^{N_t-1} \left[\frac{-N_{fft} e^{-j2\pi \frac{k-k'}{N_{fft}}T_{med}}}{j2\pi(k-k')T_{med}} + \frac{N_{fft}}{j2\pi(k-k')T_{med}}\right] \tag{C.4.18}$$

$$= \frac{N_{fft}}{j2\pi(k-k')T_{med}}(1 - e^{-j2\pi \frac{k-k'}{N_{fft}}T_{med}}) \tag{C.4.19}$$

$$\tag{C.4.20}$$

Finally we have:

$$\mathbf{R_{hh}}[k,k'] = \frac{1 - e^{-j2\pi \frac{(k-k')}{N_{fft}}T_{med}}}{j2\pi \frac{(k-k')}{N_{fft}}T_{med}}. \tag{C.4.21}$$

C.5 On the optimal choice of γ for the NRA

According to the formulation of equation 6.9 we have:

$$\mathbf{h}_{nra} = \mathbf{F}_{us}(\mathbf{F}_{ps}^H \mathbf{F}_{ps} + \gamma \mathbf{I}_s)^{-1}\mathbf{F}_{ps}^H \mathbf{h}_{ls}. \tag{C.5.22}$$

When $N_u = N_{fft}$, the γ value that minimizes the MSE of the NRA is $\gamma = N_s\sigma_w^2$ as shown by equation 6.20.

When $N_u < N_{fft}$, the γ value that optimizes the NRA depends ont the channel PDP and on the number of used subcarriers N_u.

Figure C.10 shows the average MSE int the case of a varying N_u. The optimal value of γ decreases as N_u decreases. However as the gradient in the area of interest is flat, the MSE augmentation by misadjusting the γ value remains low.
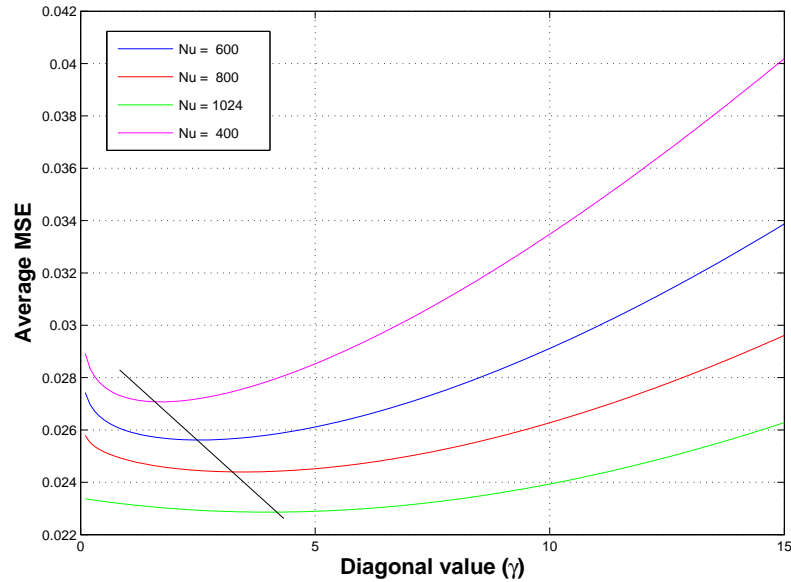
Figure C.10: Average MSE for the NRA for a varying value of γ and different number of used subcarriers

C.6 Evaluation of the Low-Rank approximation of the Robust Wiener filter for different PDPs

The Singular Value Decomposition of the channel auto-covariance matrix $\mathbf{R_{hh}}$ of the RWF from equation 6.30 is given by:

$$\mathbf{R_{hh}} = \mathbf{U\Lambda U}^H, \tag{C.6.23}$$

with $\mathbf{U}$ being an $(N_{fft} \cdot N_{fft})$ unitary matrix containing the singular vectors. The Λ diagonal matrix of dimension $(N_{fft} \cdot N_{fft})$ contains the singular values $\lambda_1 \geq \lambda_2 \geq \lambda_3 ... \geq \lambda_{N_{fft}}$ of $\mathbf{R_{hh}}$.

The rank-e estimator from [68] is given by:

$$\mathbf{h}_{svd}^{(e)} = \mathbf{U}\Delta_e\mathbf{U}^H\mathbf{h}_{ls}. \tag{C.6.24}$$

Δ_e is a diagonal matrix with entries given by:

$$\Delta_e[n, n'] = \begin{cases} \frac{\lambda_n}{\lambda_n + \beta\sigma_{\mathbf{w}}^2} & \{n = n'\} \wedge \{n = 1, 2, ..., N_e\} \\ 0 & \{n = n'\} \wedge \{n \geq N_e + 1\} \\ 0 & n \neq n', \end{cases} \tag{C.6.25}$$

where β is modulation dependent (i.e. for 16QAM $\beta = \frac{17}{9}$), and λ_n is the nth singular value.

The complexity of this rank-e estimator is of the order $O(N_e \cdot (2N_{fft} + N_e))$ however in a system with N_u used subcarriers and N_p pilot subcarriers this becomes $O(N_e \cdot (N_u + N_e + N_p))$. This shows a strong dependency on the rank N_e chosen for the estimator.

In order to quantify the rank order to be chosen, different CIR MED length are chosen for the RWF. The magnitude of the ordered singular values of $\mathbf{R_{hh}}$ are depicted in Figures C.11 and C.12.

The blue circles represent the CIR MED length in samples. It is clear to see a strong drop of the singular values as soon as the index n is slightly larger than the CIR MED.
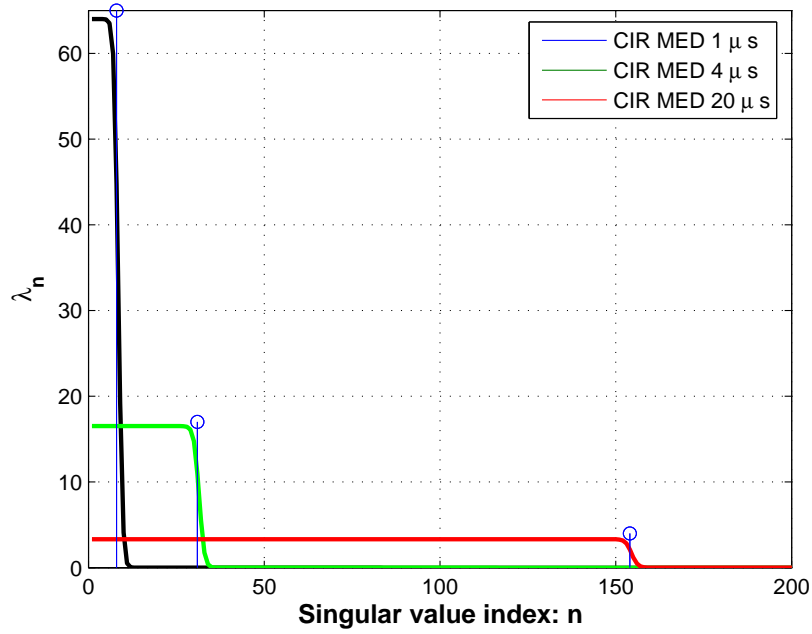
Figure C.11: Singular Value analysis as a function of the CIR MED for a 5MHz bandwidth using a linear scale
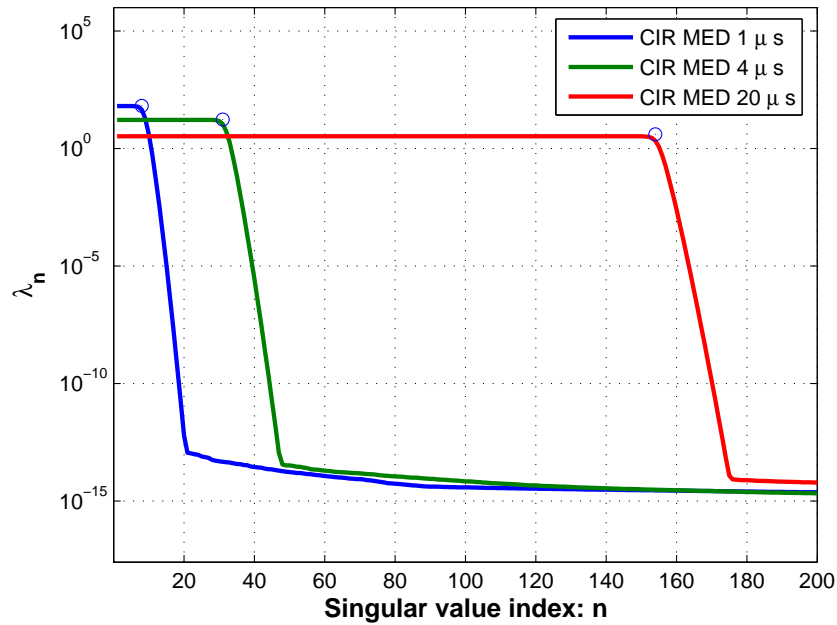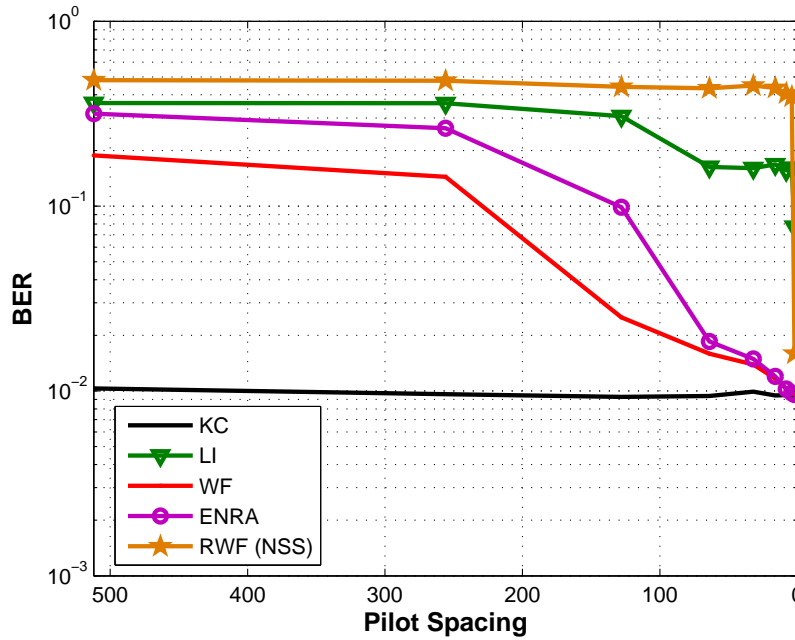

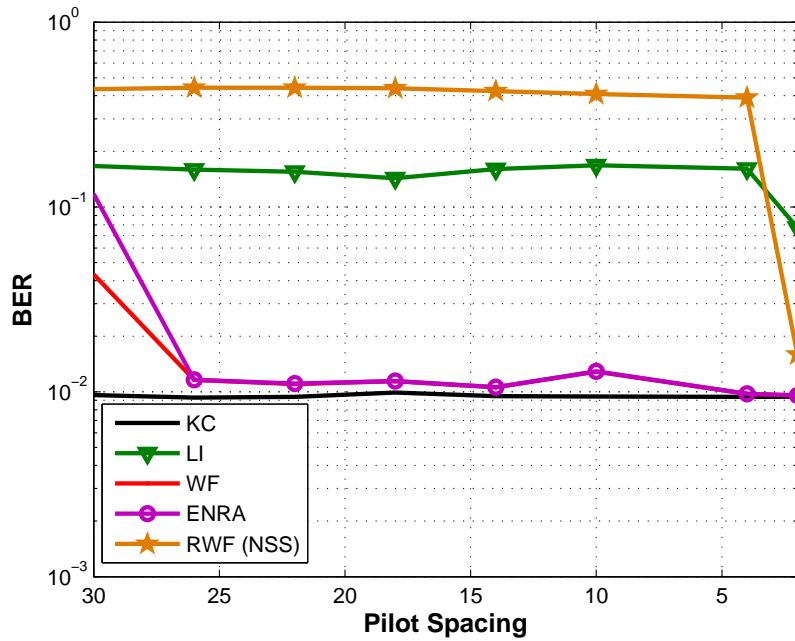Figure C.12: Singular Value analysis as a function of the CIR MED for a 5MHz bandwidth using a logaritmic scale

June 18, 2008

Appendix D

On pilot density evaluation

D.1   Channel estimation with varying pilot spacing for Vehicular B profile

(a)

(b)

Figure D.1: BER for different Frequency direction interpolation algorithms and varying frequency direction pilot spacing (16QAM, Eb/No = 17dB, 10 MHz bandwidth, Vehicular B).

D.2   Spectral Efficiency evaluation for different pilot schemes
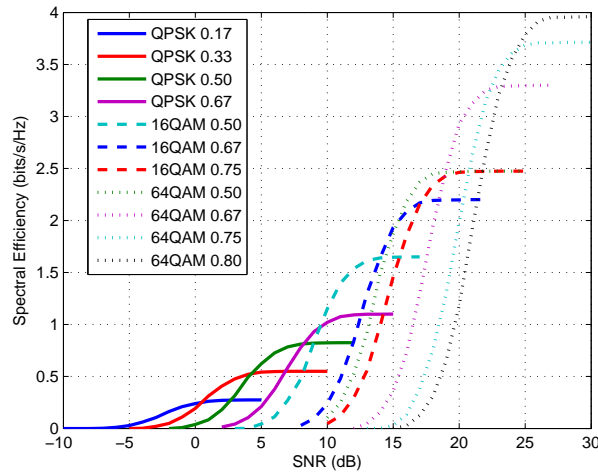
Figure D.2: Spectral efficiency for a 10 MHz bandwidth, Typical Urban PDP, different ECR, Pilot scheme P1 at 3kmph, WF in frequency direction and LI in time direction interpolation
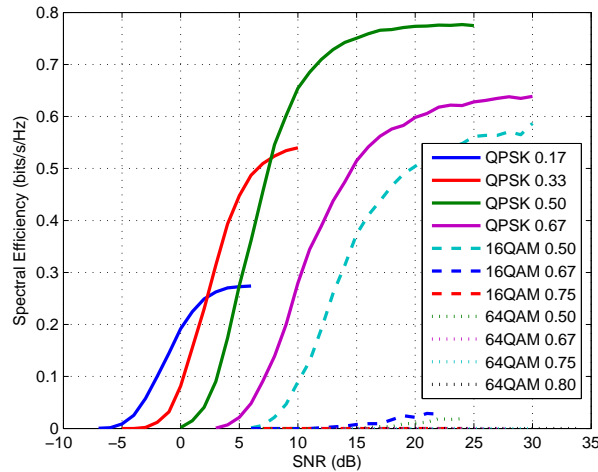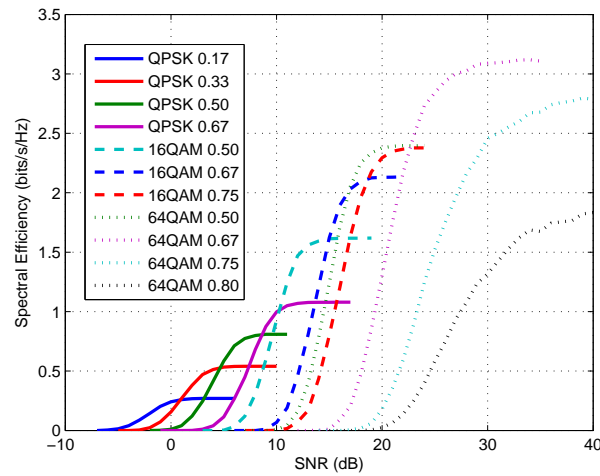

Figure D.3: Spectral efficiency for a 10 MHz bandwidth, Typical Urban PDP, different ECR, Pilot scheme P1 at 300kmph, WF in frequency direction and LI in time direction interpolation

Figure D.4: Spectral efficiency for a 10 MHz bandwidth, Typical Urban PDP, different ECR, Pilot scheme P2 at 300kmph, WF in frequency direction and LI in time direction interpolation
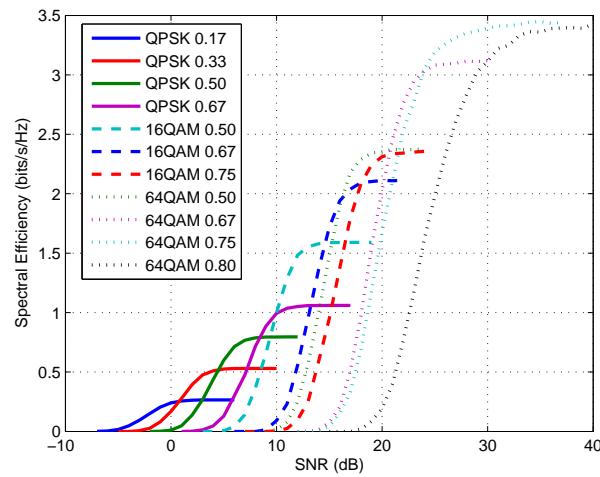

Figure D.5: Spectral efficiency for a 10 MHz bandwidth, Typical Urban PDP, different ECR, Pilot scheme P3 at 300kmph, WF in frequency direction and LI in time direction interpolation
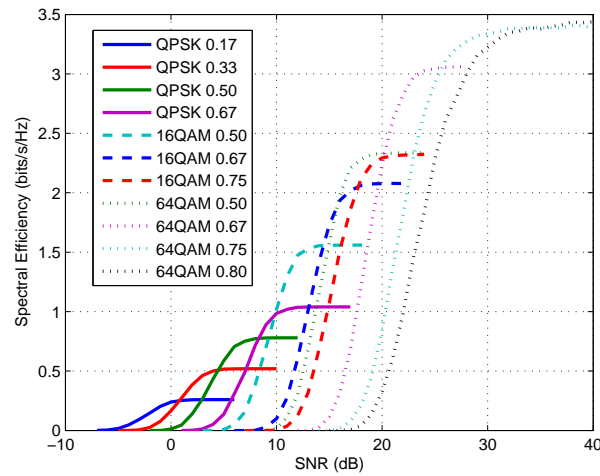
Figure D.6: Spectral efficiency for a 10 MHz bandwidth, Typical Urban PDP, different ECR, Pilot scheme P4 at 300kmph, WF in frequency direction and LI in time direction interpolation
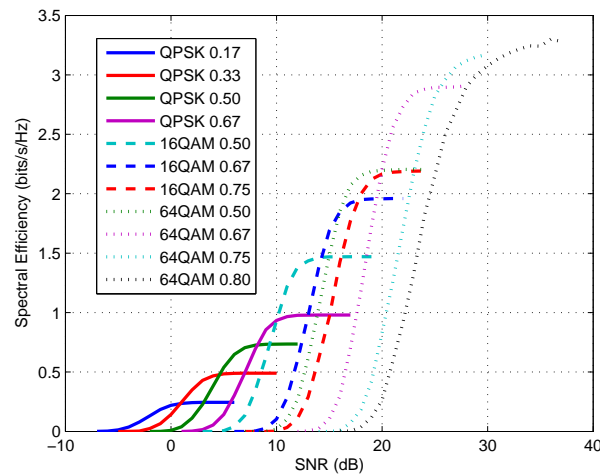

Figure D.7: Spectral efficiency for a 10 MHz bandwidth, Typical Urban PDP, different ECR, Pilot scheme P7 at 300kmph, WF in frequency direction and LI in time direction interpolation